Dear Reviewers,

First of all, we would like to thank you for your detailed comments that helped to improve the manuscript. We think we have addressed all of them. You will find the new version of the manuscript, with changes highlighted attached to this letter, along with a clean version of the manuscript.

To comment on a few points:

One of the main comments we adressed is the sensitivities of $\delta^{11}B_{carbonate}$ to $\delta^{11}B_{borate}$, >1 for *G. ruber* and *T. sacculifer*. We acknowledge that the sensitivities are not statistically different from published literature. When doing the bootstrap analysis on all compiled data, the regression for *G. ruber* was similar to Raitzsch et al., (2018), with a sensitivity of 0.46 ± 0.34 (updated table 3) compared to 0.45 ± 0.16 for Raitzsch et al., (2018) and the sensitivity was of 0.83 ± 0.48 for *T. sacculifer* in line with Martinez-Boti et al., (2015b) and Raitzsch et al., (2018). We also take into account the pCO_2 based $\delta^{11}B$ reconstructions against the Vostok pCO_2 record as pointed out. We also have clearly written that possible sensitivities of >1 are speculative.

Another major change is the reconstruction of microenvironment pH for each species (Figure 8) which we believe are in line with results of a study of photosynthesis/symbiont density from Takagi et al., (2019) for different species. This also helps to explain a possible light-limiting threshold for calibrations. We have also added discussion around symbionts-host interactions of different species.

We do observe changes in calcification depth with thermocline depth for most of the deeper-dwelling species (*G. ruber*, *T. sacculifer*) which might be problematic for future reconstructions over periods when there is evidence for changes in stratification. However, our data are too limited to derive a robust trend.

We understand that our discussion on the Western Equatorial Pacific in the earlier draft was limited as it was based on a single site. In order to strengthen the discussion, we added two other sites, ODP Sites 806A and 807A. The data record similar, low values to what we reported for site WPO7, and add to our confidence in the results.

Also, a reviewer pointed out a potential issue with the circularity of some of the calculations presented in the last manuscript. In order to address this issue, we recalculate for each species a calibration that excludes results for a single site, and then use the modified calibration that contains a subset of calibration data to reconstruct vertical profiles of carbonate chemistry as shown in Figure 9. What Fig. S5 shows is the comparison of vertical profiles using these two approaches, which yield consistent results. On average, the difference in $\delta^{11}B$ is 0.8% for $^{11}B_{borate}$, 0.2% for pH and 5% for pCO_2. The fact that using a subset of the calibration data and all of the calibration data yields similar results validates the work.

Reviews are adressed in the commented version of the manuscript and in our response to reviewers. We thank you for your time.

Best Regards,

Seawater pH reconstruction using boron isotopes in multiple planktonic foraminifera species with different depth habitats and their potential to constrain pH and pCO_2 gradients

Maxence Guillermic[1,2], Sambuddha Misra[3,4], Robert Eagle[1,2], Alexandra Villa[2,5], Fengming Chang[6], Aradhna Tripati [1,2]

[1] Department of Earth, Planetary, and Space Sciences, Department of Atmospheric and Oceanic Sciences, Institute of the Environment and Sustainability, UCLA, University of California – Los Angeles, Los Angeles, CA 90095 USA
[2] Laboratoire Géosciences Océan UMR6538, UBO, Institut Universitaire Européen de la Mer, Rue Dumont d'Urville, 29280, Plouzané, France
[3] Indian Institute of Science, Centre for Earth Sciences, Bengaluru, Karnataka 560012, India
[4] The Godwin Laboratory for Palaeoclimate Research, Department of Earth Sciences, University of Cambridge, UK
[5] Department of Geology, University of Wisconsin-Madison, Madison, WI 53706 USA
[6] Key Laboratory of Marine Geology and Environment, Institute of Oceanology, Chinese Academy of Sciences, Qingdao 266071, China

Submitted to Biogeosciences

*Corresponding author:
E-mail address: maxence.guillermic@gmail.com

ABSTRACT

Boron isotope systematics of planktonic foraminifera from core-top sediments and culture experiments have been studied to investigate the sensitivity of $\delta^{11}B$ of their calcite tests to seawater pH. However, our knowledge of the relationship between $\delta^{11}B$ and pH remains incomplete for many taxa. Thus, to expand the potential scope of application of this proxy, we report $\delta^{11}B$ data for 7 different species of planktonic foraminifera from sediment core-tops. We utilize a method for the measurement of small samples of foraminifera and calculate the $\delta^{11}B$-calcite sensitivity to pH for *Globigerinoides ruber*, *Trilobus sacculifer* (sacc or w/o sacc), *Orbulina universa*, *Pulleniatina obliquiloculata*, *Neogloboquadrina dutertrei*, *Globorotalia menardii* and *Globorotalia tumida*, including for unstudied core-tops and species. The sensitivity of $\delta^{11}B_{carbonate}$ to $\delta^{11}B_{borate}$ (eg. $\Delta\delta^{11}B_{carbonate}/\Delta\delta^{11}B_{borate}$) in core-tops is consistent with previous studies for *T. sacculifer* and *G. ruber* and close to unity for *N. dutertrei*, *O. universa* and combined deep-dwelling species. Deep-dwelling species closely follow the core-top calibration for *O. universa*, which is attributed to respiration-driven microenvironments, likely caused by light limitation and/or symbiont/host interactions. These taxa have diverse ecological preferences and are from sites that span a range of oceanographic regimes, including some that are in regions of air-sea equilibrium and others that are out of equilibrium with the atmosphere. Our data support the premise that utilizing boron isotope measurements of multiple species within a sediment core can be utilized to constrain vertical profiles of pH and pCO_2 at sites spanning different oceanic regimes, thereby constraining changes in vertical pH gradients and yielding insights into the past behavior of the oceanic carbon pumps**.**

1. Introduction

The oceans are absorbing a substantial fraction of anthropogenic carbon emissions resulting in declining surface ocean pH (Fig. 1; IPCC, 2014). Yet there is a considerable uncertainty over the magnitude of future pH change in different parts of the ocean and the response of marine biogeochemical cycles to physio-chemical parameters (T, pH) caused by climate change (Bijma et al., 2002; Ries et al., 2009). Therefore, there is an increased interest in reconstructing past seawater pH (Hönisch and Hemming, 2005; Liu et al., 2009; Wei et al., 2009; Douville et al., 2010), in understanding spatial variability in aqueous pH and carbon dioxide (pCO_2) (Foster et al., 2008; Martinez-Boti et al., 2015b; Raitzsch et al., 2018), and in studying the response of the biological carbon pump utilizing geochemical proxies (Yu et al., 2007, 2010, 2016).

Although proxies for carbon cycle reconstruction are complex in nature (Pagani et al., 2005; Tripati et al., 2009, 2011; Allen and Hönisch, 2012), the boron isotope composition of foraminiferal tests is emerging as one of the more robust candidates (Hönisch et al., 2005, 2009; Ni et al., 2007; Foster et al., 2008, 2012; Bartoli et al., 2011; Henehan et al., 2013; Martinez-Boti et al., 2015b; Chalk et al., 2017). The study of laboratory cultured foraminifera has demonstrated a systematic dependence of the boron isotope composition of tests on ambient pH (Sanyal et al., 1996, 2001; Henehan et al., 2013, 2016). Core-top measurements on globally distributed samples also show a $\delta^{11}B$ sensitivity to pH with taxa-specific offsets from the theoretical fractionation line of borate ion (Rae et al., 2011; Henehan et al., 2016; Raitzsch et al., 2018).

Knowledge of seawater pH, in conjunction with constraints on one other carbonate system parameter (Total Alkalinity (TA), DIC (dissolved inorganic carbon), $[HCO_3^-]$, $[CO_3^{2-}]$), can be utilized to constrain aqueous pCO_2. Application of empirical calibrations for boron isotopes, determined for select species of foraminifera from core-tops and laboratory cultures, has resulted in accurate reconstructions of pCO_2 utilizing downcore samples from sites that are in quasi-equilibrium with the atmosphere at present. $\delta^{11}B_{carbonate}$ based reconstructed values of pCO_2 are analytically indistinguishable from ice core CO_2 records (Hönisch et al., 2005, 2009; Foster et al., 2008; Henehan et al., 2013; Chalk et al., 2017).

Therefore, the last decade has produced several studies aiming at reconstructing past seawater pH using boron isotopes to constrain atmospheric pCO_2 in order understand the changes in the global carbon cycle (Hönisch et al., 2005, 2009; Foster et al., 2008, 2012, 2014; Seki et al., 2010; Bartoli et al., 2011; Henehan et al., 2013; Martinez-Boti et al., 2015a, 2015b; Chalk et al., 2017). In addition to reconstructing atmospheric pCO_2, in a few studies, the $\delta^{11}B$ proxy has been applied to mixed-layer planktonic foraminifera at sites out of equilibrium with the atmosphere to constrain past air-sea fluxes (Foster et al., 2014; Martinez-Boti et al., 2015b). A small body of work has examined whether data for multiple species in core-top (Foster et al., 2008) and down-core samples could be used to constrain vertical profiles of pH through time (Palmer et al., 1998; Pearson and Palmer, 1999).

In this study, we make critical additions to the emerging pool of boron isotope data of core-top planktonic foraminifera from different oceanographic regimes, including data for species that have not previously been examined. We utilize a low-blank (15 pg B to 65 pg B), high precision (2sd on the international standard JCP-1 is 0.20 ‰, n=6) $\delta^{11}B_{carbonate}$ analysis method (down to ~250 µg $CaCO_3$), modified after Misra et al. (2014), to study multiple species of planktonic foraminifera from sediment core-tops that span a range of oceanographic regimes, including open-ocean oligotrophic settings and marginal seas. We constrain calibrations for different species, and compare results to published work (Foster et al., 2008; Henehan et al., 2013; Henehan

et al., 2016; Martinez-Boti et al., 2015b; Raitzsch et al., 2018). We also test whether these data support the application of boron isotope measurements of multiple species within a sediment core as a proxy for constraining vertical profiles of pH and pCO_2.

2. Background

2.1 Planktonic foraminifera as archives of seawater pH

Planktonic foraminifera are used as archives of past environmental conditions within the mixed layer and thermocline, as their chemical composition is correlated with the physio-chemical parameters of their calcification environment (Ravelo and Fairbanks, 1992; Elderfield and Ganssen, 2000; Dekens et al., 2002; Anand et al., 2003; Sanyal et al., 2001; Ni et al., 2007; Henehan et al., 2013, 2015, 2016; Howes et al., 2017; Raitzch et al., 2018). The utilization of geochemical data for multiple planktonic foraminifera species with different ecological preferences to constrain vertical gradients has been explored in several studies. The framework for such an approach was first developed using modern samples of planktonic foraminifera for oxygen isotopes, where it was proposed as a tool to constrain vertical temperature gradients and study physical oceanographic conditions during periods of calcification (Ravelo and Fairbanks, 1992).

Because planktonic foraminifera species complete their lifecycle in a particular depth habitat due to their ecological preference (Ravelo and Fairbanks, 1992; Farmer et al., 2007), it is theoretically possible to reconstruct water column profiles of pH using data from multiple taxa (Palmer and Pearson, 1998; Anagnostou et al., 2016). The potential use of an analogous approach to reconstruct past profiles of seawater pH was first highlighted by Palmer and Pearson (1998) on Eocene samples to constrain pH-depth gradients. However, in these boron isotope-based studies, it was assumed that boron isotope offset from seawater and foraminiferal carbonate were constant, which is an assumption not supported by subsequent studies (e.g., Hönisch et al., 2003; Foster et al., 2008; Henehan et al., 2013, 2016; Raitszch et al., 2018; Rae, 2018). Furthermore, $\delta^{11}B$ differences between foraminifera species that inhabit waters that are the same pH makes the acquisition of more core-top and culture data essential for applications of the proxy.

2.2 Boron systematics in seawater

Boron is a conservative element in seawater with a long residence time (τ_B ~ 14 Myr) (Lemarchand et al., 2002a). In seawater, boron exists as trigonal boric acid $B(OH)_3$ and tetrahedral borate ion $B(OH)_4^-$ (borate). The relative abundance of boric acid and borate ion is a function of the ambient seawater pH. At standard open ocean conditions (T = 25 °C and S = 35), the dissociation constant of boric acid is 8.60 (Dickson, 1990), implying that boron mainly exists in the form of boric acid in seawater. Since the pK_B and seawater pH (e.g., ~8.1, NBS) values are similar, it implies that small changes in seawater pH will induce strong variations in the abundance of the two boron species (Fig. 2).

Boron has two stable isotopes, ^{10}B and ^{11}B, with average relative abundances of 19.9 and 80.1 %, respectively. Variations in B isotope ratio are expressed in conventional delta (δ) notation:

$$\delta^{11}B\ (‰) = 1000 \times \left(\frac{^{11}B/^{10}B_{Sample}}{^{11}B/^{10}B_{NIST\ 951\text{-}a}} - 1\right) \quad (1)$$

where positive values represent enrichment in the heavy isotope ^{11}B, and negative values enrichment in the light isotope ^{10}B, relative to the standard reference material. Boron isotope values are reported versus the NIST SRM 951 (Cantazaro et al., 1970).

$B(OH)_3$ is enriched in ^{11}B compared to $B(OH)_4^-$ with a constant offset between the two chemical species, within the range of physio-chemical variation observed in seawater, given by the fraction factor (α). The fractionation (ε) between $B(OH)_3$ and $B(OH)_4^-$ of 27.2 ± 0.6 ‰ has been empirically determined by Klochko et al., (2006) in seawater. Note, Nir et al., (2015) calculate this fractionation, using an independent method, to be 26 ± 1 ‰, which is within the analytical uncertainty of the Klochko et al., (2006) value.

2.3 Boron isotopes in planktonic foraminifera calcite

Many biogenic carbonate-based geochemical proxies are affected by "vital effects" or biological fractionations (Urey et al., 1951). The $\delta^{11}B_{carbonate}$ in foraminifera exhibits species-specific offsets (see Rae et al., 2018 for review) compared to theoretical predictions for the boron isotopic composition of $B(OH)_4^-$ (α=1.0272, Klochko et al., 2006). As the analytical and technical aspects of boron isotope measurements have improved (Foster et al., 2008; Rae et al., 2011; Misra et al., 2014; Lloyd et al., 2018), evidence for taxonomic differences have not been eliminated, but have become increasingly apparent (Foster et al., 2008, 2018; Henehan et al 2013, 2016; Noireaux et al., 2015; Foster et al., 2016; Rae et al., 2018; Raitzsch et al., 2018).

At present, culture and core-top calibrations have been published for several planktonic species including *Trilobatus sacculifer*, *Globigerinoides ruber*, *Globigerina bulloides*, *Neogloboquadrina pachyderma*, *Orbulina universa* (Foster et al., 2008; Henehan et al., 2013; Henehan et al., 2015; Sanyal et al., 1996; Sanyal et al., 2001). Although the boron isotopic composition of several species of foraminifera are now commonly used tools for reconstructing surface seawater pH, for other species, there is a lack of data constraining boron isotope sensitivity between foraminiferal carbonate and borate ion in seawater.

2.4 Origin of biological fractionations in foraminifera

Perforate foraminifera are calcifying organisms that maintain a large degree of biological control over their calcification space, and thus, mechanisms of biomineralization may be of significant importance in controlling the $\delta^{11}B$ of the biogenic calcite. The biomineralization of foraminifera is based on seawater vacuolization (Erez, 2003; de Nooijer et al., 2014) with parcels of seawater being isolated by an organic matrix thereby creating a vacuole filled with seawater. Recent work has also demonstrated that even if the chemical composition of the reservoirs is modified by the organism, seawater is directly involved in the calcification process with vacuoles formed at the periphery of the shell (de Nooijer et al., 2014). Culture experiments by Rollion-Bard and Erez., (2010) have proposed that the pH at the site of biomineralization is elevated to an upper pH limit of ~9 for the shallow-water, symbiont-bearing benthic foraminifera *Amphistegina lobifera*, which would support a pH modulation of a calcifying fluid in foraminifera. We acknowledge this is speculative as it is based upon benthic foraminifer experiments.

For taxa with symbionts, the microenvironment surrounding the foraminifera is chemically different from seawater due to photosynthetic activity (Jorgensen et al., 1985; Rink et al., 1998; Köhler-Rink and Kühl, 2000). Photosynthesis by the symbionts elevates the pH of the microenvironment (Jorgensen et al., 1985; Rink et

al., 1998; Wolf-Gladrow et al., 1999; Köhler-Rink and Kühl, 2000), while calcification and respiration decrease it (Equation 2 and 3).

$$Ca^{2+} + 2HCO_3^- \leftrightarrow CaCO_3 + H_2O + CO_2 \text{ or } Ca^{2+} + CO_3^{2-} \leftrightarrow CaCO_3 \quad \text{[calcification]} \quad (2)$$

$$CH_2O + O_2 \leftrightarrow CO_2 + H_2O \quad \text{[respiration/photosynthesis]} \quad (3)$$

$\delta^{11}B$ in foraminifera is primary controlled by seawater pH, but is also dependent of the pH alteration of microenvironments due to calcification, respiration and symbiont photosynthesis. $\delta^{11}B$ should therefore reflect the relative dominance of these processes and may account for species-specific $\delta^{11}B$ offsets. Theoretical predictions from Zeebe et al. (2003) and foraminiferal data from Hönisch et al., (2003) highlighted the dominance of microenvironment pH in $\delta^{11}B$ signature of foraminifera. Their work also suggested that for a given species, there should be a constant offset observed between the boron isotope composition of foraminifera and borate ion over a large range of pH, imparting confidence in utilizing species-specific boron isotope data as a proxy for seawater pH.

Comparison of boron isotope data for multiple planktonic foraminiferal species indicate that taxa with high levels of symbiont activity such as *T. sacculifer* and *G. ruber* show higher $\delta^{11}B$ values than the $\delta^{11}B$ of ambient borate (Foster et al., 2008, Henehan et al., 2013, Raitzsch et al., 2018). The sensitivities ($\Delta\delta^{11}B_{carbonate}/\Delta\delta^{11}B_{borate}$ referred to as the slope) of existing calibrations suggest a different species-specific sensitivity for these species compared to other taxa (Sanyal et al., 2001; Henehan et al., 2013; Henehan et al.,2015; Raitzsch et al., 2018). For example, *Orbulina universa* exhibits a lower $\delta^{11}B$ than *in situ* $\delta^{11}B$ values of borate ion (Henehan et al., 2016), consistent with the species living deeper in the water column characterized by reduced photosynthetic activity.

It is possible that photosynthetic activity by symbionts might not be able to compensate for changes in calcification and/or respiration, leading to an acidification of the microenvironment. It is interesting to note that for *O. universa* the slope determined for the field-collected samples is not statistically different from unity (0.95 ± 0.17) (Henehan et al. 2016), while culture experiments report slopes of ≤ 1 for multiple species including *G. ruber* (Henehan et al., 2013), *T. sacculifer* (Sanyal et al., 2001), and *O. universa* (Sanyal et al., 1999). More core-top and culture calibrations are needed to fully understand why different slopes are observed, which is part of the motivation for this study.

2.5 Planktic foraminifera depth and habitat preferences

The preferred depth habitat of different species of planktonic foraminifera depends on their ecology, which in turn relies on the hydrographic conditions. For example, *G. ruber is* commonly found in the mixed layer (Fairbanks and Wiebe, 1980; Dekens et al., 2002; Farmer et al., 2007) during the summer (Deuser et al., 1981) whereas *T. sacculifer* is present in the mixed layer until mid-thermocline depths (Farmer et al., 2007) during spring and summer (Deuser et al., 1981, 1989). Specimens of *P. obliquiloculata* and *N. dutertrei* are abundant during winter months (Deuser et al., 1989), with an acme in the mixed layer (~60m) for *P. obliquiloculata*, and at mid-thermocline depths for *N. dutertrei* (Farmer et al., 2007). In contrast, *O. universa* tends to record annual average conditions within the mixed layer. Specimens of *G. menardii* calcify within the seasonal thermocline (Fairbanks et al., 1982, Farmer et al., 2007, Regenberg et al., 2009), and in some regions in

the upper thermocline (Farmer et al., 2007), and records annual temperatures. *G. tumida* is found at the lower thermocline or below the thermocline and records annual average conditions (Fairbanks and Wiebe, 1980; Farmer et al., 2007, Birch et al., 2013).

3. Materials and Methods

3.1 Localities studied

Core-top locations were selected to span a broad range of seawater pH, carbonate system parameters, and oceanic regimes. Samples from Atlantic Ocean (CD107-A), Indian Ocean (FC-01a and FC-02a), Arabian Sea (FC-13a and FC-12b) and Pacific Ocean (WP07-01, A14, and Ocean Drilling Program 806A and 807A) were analyzed; characteristics of the sites are summarized in Table 1 and S7, Fig. 3, and Fig. 4.

Atlantic site CD107-a (CD107 site A) was drilled in 1997 by the Benthic Boundary Layer program (BENBO) (K.S. Black et al., 1997 - cruise report RRS Charles Darwin Cruise 107). Arabian Sea sites FC-12b (CD145 A150) and FC-13a (CD145 A3200) were retrieved by the *Charles Darwin* in the Pakistan Margin in 2004 (B.J. Bett et al., 2003 - cruise report n°50 RRS Charles Darwin Cruise 145). A14 was recovered by box corer in the southern area of the South China Sea in 2012. Core WP07-01 was obtained from the Ontong Java Plateau using a giant piston corer during the Warm Pool Subject Cruise in 1993. Holes 806A and 807A were retrieved on Leg 130 by the Ocean Drilling Program (ODP). The top 10 cm of sediment from CD107-A have been radiocarbon dated to be Holocene <3 ky (Thomson et al., 2000). Samples from multiple box cores from Indian Ocean sites were radiocarbon dated as Holocene <7.3 ky (Wilson et al., 2012). Samples from western equatorial Pacific Site 806B, close to site WP07-01, are dated to between 7.3-8.6 ky (Lea et al., 2000). Arabian Sea and Pacific core-top samples were not radiocarbon dated but are assumed to be Holocene.

3.2 Species

Around 50-100 foraminifera shells were picked from the 400-500 µm fraction size for *Globorotalia menardii* and *Globorotalia tumida*, >500 µm for *Orbulina universa*, from the 250-400 µm fraction size for *Trilobatus sacculifer* (w/o sacc, without sacc-like final chamber), *Trilobatus sacculifer* (sacc, sacc-like final chamber), *Globigerinoides ruber (*white, sensu stricto), *Neogloboquadrina dutertrei*, *Pulleniatina obliquiloculata*. The samples picked for analyses were visually well preserved.

3.3 Sample cleaning

Briefly, picked foraminifera were gently cracked open, clay removed and checked for coarse-grained silicates. The next stages of sample processing and chemical separation were performed in a class 1000 clean lab equipped with boron-free HEPA filters. Samples were then cleaned using full reductive and oxidative cleaning (Boyle and Keigwin, 19[illegible] Barker et al., 2003). A final leaching step with 0.001N HCl was done before dissolution in 1N HCl. Each sample was divided into two aliquots: an aliquot for boron purification and one aliquot for trace element analysis.

3.4 Reagents

Double-distilled HNO_3 and HCl acids (from Merck® grade) and a commercial bottle of HF Ultrapure grade were used at Brest. Double-distilled acids were used at Cambridge. All acids and further dilutions were

prepared using double-distilled 18.2 MΩ.cm-1 MQ water. Working standards for isotope ratio and trace element measurements were freshly diluted on a daily basis with the same acids used for sample preparation to avoid any matrix effect.

32.5 Boron isotopes

Boron purification for isotopic measurement was done utilizing microdistillation method developed by Gaillardet et al., (2001), for Ca-rich matrices by Wang et al., (2010) and adapted at Cambridge by Misra et al., (2014a). 70 µL of dissolved carbonate sample was loaded on a cap of a clean fin legged 5 mL conical beaker upside down. The tightly closed beaker was put on a hotplate at 95°C for 15 hours. The beakers were taken off the hotplate and were allowed to cool for 15 min. The cap where the residue formed was replaced by a clean one. Then, 100 µL of 0.5% HF were added to the distillate.

Boron isotopic measurements were carried out on a Thermo Scientific ®Neptune+ MC-ICP-MS at the University of Cambridge. Neptune+ was equipped with Jet interface and two 10^{13} Ω resistors. The instrumental setup included Savillex® 50µl/min C-flow self-aspirating nebulizer, single pass Teflon® Scott-type spray chamber constructed utilizing Savillex® column components, 2.0 mm Pt injector from ESI®, Thermo® Ni 'H' type sample cone and 'X' type skimmer cones. Both isotopes of boron were determined utilizing 10^{13} Ω resistors (Misra et al., 2014a; Lloyd et al., 2018).

The sample size for boron isotope analyses typically ranged from 10 ppb B (~5 ng B) to 20 ppb B samples (~10 ng B). Instrumental sensitivity for ^{11}B was 17 mV/ppb B (eg. 170 mV for 10ppb B) in wet plasma at 50µl/min sample aspiration rate. Intensity of ^{11}B for a sample at 10ppb B was typically 165mV ± 5mV closely matched the 170mV ± 5mV of the standard. Due to the low boron content of the samples extreme care was taken to avoid boron contamination during sample preparation and reduce memory effect during analysis. Procedural boron blanks ranged from 15pg B to 65 pg B (contributed to less than <1% of the sample signal). The acid blank during analyses was measured at ≤ 1mV on the ^{11}B, meaning a contribution < 1% of the sample intensity, no memory effect was observed within and across sessions.

Analyses of external standards were done to ensure data quality. For $\delta^{11}B$ measurements two carbonate standards were utilized: the JCP-1 (Geological Survey of Japan, Tsukuba, Japan) international standard (Gutjahr et al., 2014) and the NEP internal coral (Porites sp., $\delta^{11}B$ = 26.12 ± 0.92 ‰, 2SD, n=33 Holcomb et al., 2015 and Sutton et al., 2018, Table S2) from University of Western Australia/Australian National University. Certified boron isotopes liquid standard, the ERM© AE121 ($\delta^{11}B$ = 19.9 ± 0.6 ‰, SD, certified) was used to monitor reproducibility and drift during each session (Vogl and Rosner, 2011; Foster et al., 2013; Misra et al., 2014). Results for the isotopic composition of the NEP standard are shown in Table S2, average values are $\delta^{11}B_{NEP}$ = 25.70 ± 0.93 ‰ (2SD, n=22) over different 7 analytical sessions with each number representing an ab-initio processed sample - this study). Our results are within error of published values of 26.20 ± 0.88 ‰ (2SD, n = 27) and 25.80 ± 0.89 ‰ (2SD, n = 6) by Holcomb et al. (2015) and Sutton et al. (2018) respectively. Chemically cleaned JCP_1 samples were measured at 24.06 ± 0.20 (2SD, n=6) and is within error of published values of 24.37 ± 0.32 ‰ and 24.42 ± 0.28 ‰ by Holcomb et al. (2015) and Sutton et al. (2018) respectively.

3.6 Trace elements

The calcium concentration of each sample was measured on an ICP-AES ® Ultima 2 HORIBA at the Pôle spectrometrie Océan (PSO), UMR6538 (Plouzané, France). Samples were then diluted to fixed calcium concentrations (typically 10 ppm or 30 ppm Ca) using 0.1 M HNO3 & 0.3 M HF matching multi-element standards Ca concentration to avoid any matrix effect (Misra et al., 2014b). Trace elements (e.g. X/Ca ratios) were analyzed on a Thermo Scientific ® Element XR HR-ICP-MS at the PSO, Ifremer (Plouzané, France).

Trace element analyses were done at a Ca concentration of 10 or 30 ppm. The typical blanks for a 30 ppm Ca session were: ^{7}Li < 2%, ^{11}B < 7%, ^{25}Mg < 0.2% and ^{43}Ca < 0.02%. Additionally, blanks for a 10 ppm Ca session were: ^{7}Li < 2.5%, ^{11}B < 10%, ^{25}Mg < 0.4% and ^{43}Ca < 0.05%. Due to strong memory effect for boron and instrumental drift on the Element XR, long sessions of conditioning were done prior analyses. Boron blanks were driven below 5% of signal intensity usually after 4 to 5 days of continuous analyses of carbonate samples. External reproducibility was determined on the consistency standard Cam-Wuellestorfi (courtesy of the University of Cambridge) (Misra et al., 2014b), Table S3. Our X/Ca ratio measurements on the external standard Cam-Wuellestorfi were all the time within error of the published value (Table S3) validating the robustness of our trace elements data. Analytical uncertainty of a single measurement was calculated from the reproducibility of the Cam-Wuellestorfi, measured during a particular mass spectrometry session. The analytical uncertainties on the X/Ca ratios are: 0.4 µmol/mol for Li/Ca, 7 µmol/mol for B/Ca and 0.01 mmol/mol for Mg/Ca (2SD, n=31) respectively.

3.7 Oxygen isotopes

Carbonate $\delta^{13}C$ and $\delta^{18}O$ were measured on a Gas Bench II coupled to a Delta V mass spectrometer at the stable isotope facility of Pôle spectrometrie Océan (PSO), Plouzané. Around 20 shells were weighed, crushed and clay removed. The recovered foraminifera were weighed in tubes and flushed with He gas. Samples were then digested in phosphoric acid and analyzed. Results were calibrated to the VPDB scale by international standard NBS19 and analytical precision on the in-house standard Ca21 was better than 0.11‰ for $\delta^{18}O$ (1SD, n=5) and 0.03‰ for $\delta^{13}C$ (1SD, n=5).

3.8 Calcification depth determination

We utilized two different chemo-stratigraphic methods to estimate the calcification depth in this study (Table S6 and S7). The first method, commonly used in paleoceanography, utilizes $\delta^{18}O$ measurements of the carbonate ($\delta^{18}O_c$) to estimate calcification depths (referred to as $\delta^{18}O$-based calcification depths) (Schmidt et al., 2002; Mortyn et al., 2003; Sime et al., 2005; Farmer et al., 2007; Birsh et al., 2013). The second method utilizes Mg/Ca-based temperature estimates ($T_{Mg/Ca}$) to constrain calcification depths (Quintana Krupinski et al., 2017). In both cases, the postulate was that vertical profiles of seawater temperature are available for different seasons in ocean atlases and cruise reports, and that hydrographic data and geochemical proxy signatures can be compared to assess the depth in the water column that represents the species maximum abundance.

The two different methods to estimate calcification depth were then compared to published depth estimates for the basin, and where available, for the same site (Table S6). We chose literature values for calcification depths when available, or depths that were closest to what is known for the region or basin. As foraminifera can migrate in the water column along their ontogeny, we applied (based on uncertainties of our

measurements) an uncertainty of ±10m for calcification depths > 70 m and an uncertainty of ±20 m when calcification depths <70 m. The depth habitats utilized to derive *in situ* parameters are summarized in Table S7.

3.9 $\delta^{11}B_{borate}$

Two carbonate system parameters are needed to fully constrain the carbonate system. Following the approach of Foster et al., (2008) we used the GLODAP database (Key et al., 2004) corrected for anthropogenic inputs in order to estimate pre-industrial carbonate system parameters at each site. Temperature, salinity and pressure for each site are from the World ocean database 2013 (Boyer et al., 2013). We utilized the R© code in Henehan et al, (2016) (courtesy of Michael Henehan) to calculate the $\delta^{11}B_{borate}$ and derive our calibrations. Uncertainty for $\delta^{11}B_{borate}$ utilizing the code was similar to the one calculated by applying 2 standard deviations of the calculated $\delta^{11}B_{borate}$ within the limits imposed by the calcification depth.

The Matlab© template provided by Zeebe and Wolf-Gladow, (2001) was used to calculate pCO_2 from TA; temperature, salinity and pressure were included into the calculations. Total boron was calculated from Lee et al., (2010), K_1 and K_2 were calculated from Mehrbach et al. (1973) refitted by Dickson and Millero (1987).

Statistical tests were made utilizing GraphPad© software, linear regressions for calibration where derived utilizing R© code in Henehan et al, (2016) (courtesy of Michael Henehan) with a k=500.

4. Results

4.1 Depth habitat

The calcification depths utilized in this paper are summarized in Tables S6 and S7, including a comparison of calcification depth determination methods. The calculated calcification depths are consistent with the ecology of each species and the hydrography of the sites. Specimens of *G. ruber* and *T. sacculifer* appear to be living in the shallow mixed layer (0-100 m), with *T. sacculifer* living or migrating deeper than *G. ruber* (down to 125 m). Specimens of *O. universa* and *P. obliquiloculata* are living in the upper thermocline; *G. menardii* is found in the upper thermocline until the thermocline depth specific to the location; *N. dutertrei* is living around the thermocline depth and specimens of *G. tumida* are found in the lower thermocline.

Data from both approaches implies that some species inhabit deeper environments in the Western Equatorial Pacific (WEP) relative to the Arabian Sea, which in turn are deeper dwelling than in the Indian Ocean. In some cases, we find evidence for differences in habitat depth of up to ~100m between the WEP and the Arabian Sea. This trend is observed for *G. ruber* and *T. sacculifer*, but not for *O. universa*.

Some differences in calcification depth are observed between the two calcification depth determination methods. These differences might be due to the choice of calibrations. Alternatively, our uncertainties for $\delta^{18}O$ implies larger uncertainties on the calcification depth determination using this approach, compared to Mg/Ca measurements.

4.2 Empirical calibrations of foraminiferal $\delta^{11}B_{carbonate}$ to $\delta^{11}B_{borate}$

Results for the different species analyzed in this study are presented in Fig. 5, Fig. 6 and summarized in Table 2; additionally, published calibrations for comparison are summarized in Table 3.

4.2.1 *G. ruber*

Our results for *G. ruber* (Fig. 5) are in good agreement with published data from other core-tops, sediment traps, tows, and culture experiments for $\delta^{11}B_{borate}$>19 ‰ (Foster et al., 2008, Henehan et al., 2013, Raitzsch et al., 2018). However, for $\delta^{11}B_{borate}$<19 ‰ our results show lighter $\delta^{11}B_{carbonate}$ compared to published values. Whilst this species has been widely studied previously, the sites selected in this study allow us to extend the calibration. The positive offset from the 1:1 curve has been explained by the high photosynthetic activity (Hönisch et al., 2003; Zeebe et al., 2003). Two calibrations have been derived. Utilizing only our data, the sensitivity of $\delta^{11}B_{carbonate}$ to $\delta^{11}B_{borate}$ of our linear regression is not statistically different from 1, the uncertainty on this regression is important due to our small dataset and not inconsistent with the low sensitivity trend of the culture experiments from Sanyal et al., (2001) or Henehan et al., (2013). The second calibration made compiling all data from literature shows a sensitivity similar (e.g. 0.46 (±0.34) to the one recently published by Raitzsch et al., (2018) (e.g. 0.45 (±0.16), Table 3).

4.2.2 *T. sacculifer*

$\delta^{11}B_{carbonate}$ results for *T. sacculifer* (sacc and w/o sacc) (Fig. 5) are compared to published data (Foster et al., 2008; Martinez-Boti et al., 2015b, Raitzsch et al., 2018). Results for *T. sacculifer* are in good agreement with the literature and fall above the 1:1 line. Linear regression on our data yields a slope of 1.3 ± 0.2 but is not statistically different to the results from Martinez-Boti et al., (2015b) (Table 3), (p>0.05). However, when compiled with published data using the bootstrap method a slope of 0.83 ± 0.48 is calculated, with a large uncertainty given the variability in the data. It is also noticeable that *T. sacculifer* (w/o sacc) samples from the WEP have a $\delta^{11}B_{carbonate}$ close or below the 1:1 line and are significantly lower compared to the combined *T. sacculifer* of other sites (p=0.01, unpaired t-test).

4.2.3 *O. universa* and deeper dwelling species: *N. dutertrei, P. obliquiloculata, G. menardii* and *G. tumida*

Our results for *O. universa* (Fig. 5), *N. dutertrei, P. obliquiloculata, G. menardii* and *G. tumida* (Fig. 6) fall below the 1:1 line. These data for *O. universa* are not statistically different from the Henehan et al. (2016) calibration (p>0.05). Our results for *N. dutertrei* expand upon the initial measurements presented in Foster et al., (2008). The different environments experienced by *N. dutertrei* in our study permit us to extend the range and derive a calibration for this species; the slope is close to unity (0.93 ± 0.55), and is similar to the (0.95 ± 0.17) previously reported by Henehan et al., (2016) for *O. universa* and not statistically different (p>0.05). The data for *P. obliquiloculata* exhibits the largest offset from the theoretical line. The range of $\delta^{11}B_{borate}$ from the samples we have of *G. menardii* and *G. tumida* is not sufficient to derive calibrations, but the points are in good agreement with the *N. dutertrei* calibration and Henehan et al. (2016) calibration for *O. universa*.

For all species, the slopes are not statistically different from Henehan et al. (2016) (p>0.05) and are close to unity. If data for deep-dwelling foraminiferal species are pooled together with each other and with data from Henehan et al., (2016) and Raitzch et al., (2018), we calculate a slope of 0.95 (± 0.13) (R^2=0.7987, p<0.0001); if only our data are used, we calculate a slope that is not significantly different (0.82 ± 0.27; p<0.05). However, it may remain premature to assume that a unique calibration with a slope of ~0.9 can be used for all deeper-dwelling species; more data is needed for *P. obliquiloculata*, *G. menardii* and *G. tumida* to robustly test this assertion.

4.2.4 Comparison of core-top and culture data

The data for *G. ruber* and *T. sacculifer* from the core-tops we measured are broadly consistent with previous published results. The calibrations between these core-top derived estimates and culture experiments are not statistically different due to small datasets and uncertainties on the linear regressions (Henehan et al., 2013; Marinez-Boti et al., 2015; Raitzsch et al., 2018; Table 3). The sensitivities of the species analyzed are not statistically different and are close to unity.

4.3 B/Ca ratios

B/Ca ratios are presented in Table 2 and Fig. 7. Values are species-specific consistent with previous work (e.g., compiled in Henehan et al., 2016) with ratios higher for *G. ruber* > *T. sacculifer* > *T. sacculifer* (w/o sacc) > *P. obliquicloculata* > *O. universa* > > *G. menardii* > *N. dutertrei* > *G. tumida* > *G. inflata* > *N. pachyderma* > *G. bulloides* (Fig. 7). This study supports interspecific B/Ca ratios (Yu et al., 2007; Tripati et al., 2009, 2011; Allen and Hönisch, 2012; Henehan et al., 2016). Differences between surface- and deep-dwelling foraminifera are observed, with lower values and a smaller range for the deeper dwelling taxa (58-126 µmol/mol vs 83-190 µmol/mol for shallow dwellers), however, the trend for the surface-dwellers can also be driven by interspecies B/Ca variability. The B/Ca data for deep-dwelling taxa exhibits a significant correlation with $[B(OH)_4^-]/[HCO_3^-]$ ($p<0.05$), but no correlation with $\delta^{11}B_{carbonate}$ and temperature (Fig. S3). Surface-dwelling species have B/Ca ratios that exhibit significant correlations with $[B(OH)_4^-]/[HCO_3^-]$, $\delta^{11}B_{carbonate}$ and temperature. The sensitivity of B/Ca to $[B(OH)_4^-]/[HCO_3^-]$ is lower for deep-dwelling species compared to surface dwelling species. When all the B/Ca data are compiled, significant trends are observed with $[B(OH)_4^-]/[HCO_3^-]$, $\delta^{11}B_{carbonate}$ and temperature (Fig. S3). We also observe that if we compare data from all sites together, correlations exist between B/Ca and the water depths of the cores (not significant, Fig. S4) but these correlations may also be related to the different the depth habitats of different taxa in each region, a significant trend is observed when all the data are plotted ($R^2=0.11$, $p<0.05$, Fig. S4).

5. Discussion

5.1 Sources of uncertainty relating to depth habitat and seasonality at studied sites

5.1.1 Depth habitats and $\delta^{11}B_{borate}$

Because foraminifera will record ambient environmental conditions during calcification, the accurate characterization of *in-situ* data is needed not only for calibrations, but also to understand the reconstructed record of pH or pCO_2. The species we examined are ordered here from shallower to deeper depth habitats: *G. ruber* >*T. sacculifer* (sacc) > *T. sacculifer* (w/o sac) > *O. universa* > *P. obliquiloculata* > *G. menardii* > *N. dutertrei* > *G. tumida* (this study; Birch et al., 2013; Farmer et al., 2007), although the specific water depth will vary depending on the hydrology of the site (Kemle-von and Oberhänhsli, 1999). We note that calculation of absolute calcification depths can be challenging in some cases as many species migrate during their ontogeny (Steinhardt et al., 2015).

We find that assumptions about the specific depth habitat a species of foraminifera is calcifying over, in a given region, can lead to differences of a few per mil in calculated isotopic compositions of borate (Fig. 4). Hence this can cause a bias in calibrations if calcification depths are assumed instead of being calculated (i.e., with $\delta^{18}O$ and/or Mg/Ca). Factors including variations in thermocline depth can impact depth habitats for some taxa. At the sites we examined, most of the sampled species live in deeper depth habitats in the WEP relative to the Indian Ocean, which in turn is characterized by deeper depth habitats than in the Arabian Sea. In the tropical Pacific, *T. sacculifer* is usually found deeper than *G. ruber* except at sites characterized by a shallow thermocline, in which case they tend to overlap their habitat (e.g., ODP Site 806 in the WEP which has a deeper thermocline than at ODP Site 847 in the Eastern Equatorial Pacific; EEP) (Rickaby et al., 2005). The difference in depth habitats for *T. sacculifer* and *N. dutertrei* between the WEP and EEP can be as much as almost 100 m (Rickaby et al., 2005).

5.1.2 Seasonality and *in-situ* $\delta^{11}B_{borate}$

As discussed by Raitzsch et al., (2018), depending of the study area, foraminiferal fluxes can change throughout the year, so seasonality can have a major impact on hydrographic carbonate parameters calculations for any given water depth. We therefore recalculated the theoretical $\delta^{11}B_{borate}$ using seasonal data for temperature and salinity and annual values for TA and DIC for each depth at each site. The GLODAP (2013) database does not provide seasonal TA or DIC values.

The low sensitivity of $\delta^{11}B_{borate}$ to temperature and salinity means that calculated $\delta^{11}B_{borate}$ for each water depth at our sites were not strongly impacted (Fig. S1). Thus, these findings support Raitzsch et al. (2018), who concluded that calculated $\delta^{11}B_{borate}$ values corrected for seasonality was within error of non-corrected values for each water depth. As Raitzsch et al, (2018) highlight, seasonality might be more important at high latitude sites where seasonality is more marked, however, the seasonality of primary production will also be more tightly constrained due to the seasonal progression of winter light limitation and intense vertical mixing and summer nutrient limitation.

Data for our sites suggests that most $\delta^{11}B_{borate}$ variability we observe does not come from seasonality but from the assumed water depths for calcification. With the exception of a few specific areas such as the Red Sea (Henehan et al., 2016, Raitzsch et al., 2018), at most sites examined, seasonal $\delta^{11}B_{borate}$ at a fixed depth does not vary by more than ~0.2‰. We conclude that seasonality is not an important factor impacting carbonate system parameters at the sites we examined.

5.2 $\delta^{11}B$, microenvironment pH and depth habitats

In planktonic foraminifera, algal symbiosis is the more common symbiotic relationship. For most of planktonic foraminifera, the host presents only one species of symbionts (Gast and Caron, 2001). The family Globigerinidae, including *G. ruber*, *T. sacculifer* and *O. universa*, commonly have dinoflagellates or chrysophyte algal symbionts (Anderson and Be, 1976; Spero, 1987). The families Pulleniatinidae, Globorotaliidae, including *N. dutertrei*, *P. obliquiloculata*, *G. menardii* and *G. tumida*, have chrysophyte algal symbionts (Gastrich, 1988).

The relationship between the symbionts and the host is complex by nature. Nevertheless, this symbiotic relationship provides energy (Hallock, 1981b) and promotes calcification of the foraminifera (Duguay, 1983;

Erez et al., 1983) by providing the inorganic carbon to the host (Jorgensen et al., 1985). Also, for *T. sacculifer* and *O. universa* photosynthesis increases with higher insolation (Jorgensen et al., 1985; Rink et al., 1998).

Dinoflagellate-bearing foraminifera (*G. ruber*, *T. sacculifer* and *O. universa*) tend to have a higher symbiont density and photosynthesis activity while *P. obliquiloculata*, *G. menardii* and *N. dutertrei* have lowered symbiont density and *P. obliquiloculata*, *N. dutertrei* lower photosynthetic activity (Takagi et al., 2019). *P. obliquiloculata* showed the minimum symbiont density and photosynthetic activity (Takagi et al., 2019).

It is now accepted that the foraminifera $\delta^{11}B$ signature comes from the microenvironment pH (Jorgensen et al., 1985; Rink et al., 1998; Köhler-Rink and Kühl, 2000, Hönisch et al., 2003; Zeebe et el., 2003). Foraminifera with high photosynthetic activity and symbiont density like *G. ruber* and *T. sacculifer* present a pH of microenvironment higher than ambient seawater, $\delta^{11}B$ higher than 1:1 line (Foster et al., 2008, Henehan et al., 2013, Raitzsch et al., 2018). The opposite can also be true, from our study, species with lower photosynthetic activity and lower symbiont density present microenvironments lower than ambient seawater, $\delta^{11}B$ lower than 1:1 line (Martinez-Boti et al., 2015b; Henehan et al., 2016), this is the case in our data for *N. dutertrei*, *G. menardii* and *P. obliquiloculata* and likely *G. tumida*. Nevertheless, the low $\delta^{11}B$ of *O. universa* and *T. sacculifer (w/o sacc)* from the WEP are difficult to reconcile with a high photosynthetic activity compared to *T. sacculifer* et *G. ruber*.

The photosynthetic activity is also function of the light level they received which is, in the natural system, dependent of their depth in the water column, for the purpose of this study we will not consider turbidity which also influences the light penetration in the water column. In this case, the photosynthetically active foraminifera living close to the surface should see their microenvironment pH (thus $\delta^{11}B$) more sensitive to water depth changes. A deeper depth habitat will change the light intensity they received and as a consequence may lower their photosynthetic activity reducing their microenvironment pH. This thought is supported by the significant trend observed between our $\Delta^{11}B$ and the calcification depth for *G. ruber* and *T. sacculifer* of our sites (Fig. S2). This trend basically supports the fact that the microenvironment pH decrease with calcification depth. We observe a decrease of $\delta^{11}B$ in the WEP for *T. sacculifer (w/o sacc)*, significantly different from the other sites ($p<0.05$). The $\Delta^{11}B$ of *G. ruber*, *T. sacculifer* (w/o sacc and sacc) is also significantly lower in the WEP compared to the other sites ($p<0.05$). To test if the $\delta^{11}B$ signature was inferred to a light driven, we have been able to independently calculate the depth of the foraminifera based on various light insolation culture experiments (Jorgensen et al., 1985) and the Δmicroenvironment pH derived from our data (Fig. 8A and B). This exercise verified that this low $\delta^{11}B$ can be explained by the reduced light environment due to a deeper depth habitat in the WEP (Fig. 8B). Also, *T. sacculifer* has the potential to support more photosynthesis due to its higher symbiont density. Higher photosynthetic activity is observed compared to other species potentially supporting higher symbiont/host interactions. Those results could be in line with a greater sensitivity of *T. sacculifer* photosynthetic activity with changes in insolation/water depth. It can also be noted that this species presents the largest variations in symbiont density versus its test size. When applied to the other species *O. universa* data suggest a microenvironment pH 0.10 to 0.20 lower than ambient seawater pH which would be in line with species living deeper than 50m (light compensation point (Ec), Rink et al., 1998) also consistent with our calcification depth reconstructions. Δmicroenvironment pH is higher in *T. sacculifer* > *G. ruber* > *T. sacculifer* (w/o sacc - WEP) > *O. universa*, *N. dutertrei*, *G. menardii*, *G. tumida* > *P. obliquiloculata* in line with photosymbiosis findings from Tagazaki et al., (2019). Also, the higher $\delta^{11}B$ data from the African upwelling

published by Raitzsch et al., (2018) for *G. ruber* and *O. universa* might reflect the higher microenvironment pH due to a shallower depth habitat. This could highlight a potential issue with calibration when applied to sites with different oceanic regimes as the $\delta^{11}B$ specie-specific calibrations could be also location-specific for the mixed dweller species.

Microenvironment pH results for *N. dutertrei, G. menardii, G. tumida,* are similar to *O. universa* and suggest a threshold for respiration driven $\delta^{11}B$ signature. This threshold can be driven by a change of photosynthetic activity due to lower light intensity at deeper depth and/or a change in the symbiont assemblage with non-dinoflagellate symbionts at deeper depth. We can explain this threshold because deep dweller species do not experience important changes of insolation at those depths so their microenvironments should be respiration driven and relatively stable. We can also note that *P. obliquiloculata* which has the lowest symbiont density and photosynthetic activity has the lowest microenvironment pH compared to other deeper dweller species supporting this respiration driven microenvironment.

5.3 $\delta^{11}B$ sensitivity to $\delta^{11}B_{borate}$ and relationship with B/Ca signatures

$\delta^{11}B_{carbonate}$ and B/Ca data have shown to be sensitive to precipitation rate with at higher precipitation rate increasing $\delta^{11}B_{carbonate}$ (Farmer et al., 2019) and B/Ca (Farmer et al., 2019; Gabitov et al., 2014; Kaczmarek et al., 2016; Mavromatis et al., 2015; Ushikawa et al., 2015). A recent study from Farmer et al, (2019) has proposed that in foraminifera at higher precipitation rates, more borate ion is incorporated into the carbonate mineral, while at lower precipitation rates, more boric acid is incorporated. They also suggest this may explain low sensitivities of culture experiments.

When combining all literature data, *T. sacculifer* and *G. ruber* have sensitivities of $\delta^{11}B_{carbonate}$ to $\delta^{11}B_{borate}$ of 0.83 ± 0.48 and 0.46 ± 0.34 respectively in line with previous literature and paleo-CO_2 reconstructions. Also, if we only take into account our data, the observation that the sensitivity of $\delta^{11}B_{carbonate}$ to $\delta^{11}B_{borate}$ are not statistically different from unity for most of the species investigated we can speculate that for these taxa, changes in precipitation rate and contributions of boric acid are not likely to be important. If considering only the data from this study, *G. ruber* (1.12 ± 1.67) and *T. sacculifer* (1.38± 1.35) present higher sensitivities of $\delta^{11}B_{carbonate}$ to $\delta^{11}B_{borate}$. We can then again speculate that the observed high values for $\delta^{11}B_{carbonate}$ at high seawater pH can be due to higher precipitation rates. We note this could also be consistent with the higher sensitivity of B/Ca signatures in these two surface dwelling species to ambient $[B(OH)_4^-]/[HCO_3^-]$ relative to deeper dwelling species. Those interspecific differences still remain to be explained, however, part of this variability is likely due to changes in the carbonate chemistry of the microenvironment resulting in changing competition between borate and bicarbonate. A caveat is that we can not exclude specific biological processes, and that in taxa with a non respiration-driven microenvironment, changes in day/night calcification ratios also impacting observed values. As indicated by Farmer et al., (2019), studies of calcite precipitation rates in foraminifera may help to improve our understanding of the fundamental basis of boron-based proxies.

5.4 Evaluation of species for pH reconstructions and water depth pH reconstructions

This data set allows us to reassess the utility of boron-based proxies for the carbonate system. The main interest with utilizing boron-based proxies relates to the reconstruction of past oceanic conditions - specifically pH and pCO_2. Mixed-layer species (eg. *G. ruber* and *T. sacculifer)* are potential archives for atmospheric CO_2

reconstructions. Other species can shed light on other aspects of the carbon cycle including the physical and biological carbon pumps.

There are a few main inferences we can make. When compiled with data from the literature, sensitivities of $\delta^{11}B_{carbonate}$ to $\delta^{11}B_{borate}$ for *G. ruber* and *T. sacculifer* are similar to previous studies (Martinez-Boti et al., 2015b; Raitzsch et al., 2018) which is also supporting of previous paleo-reconstructions. Our data also support the observations of Henehan et al., (2016) for *O. universa*.

In order to derive accurate reconstructions of past ambient pH and pCO_2, accurate species-specific calibrations need to be used that are constrained by core-tops or samples from similar types of settings (Fig. 9, 10, S6). Lighter $\delta^{11}B$ signatures in *T. sacculifer* (w/o sacc) are observed in the WEP, which may be explained by the deeper depth habitat for these taxa, where lower light levels might reduce symbiont photosynthetic activity. Also, correction will be needed for *T. sacculifer* (w/o sacc) in the WEP. When applying the calibrations n°2 and 4 to *T. sacculifer* and *G. ruber* (compilation of all data, Table 3) our data show more variability, especially for *G. ruber* which lead to the larger mismatch compared to *in-situ* parameters. Henehan et al., (2013) reported a lighter $\delta^{11}B$ with smaller test size, our sample add a weight/shell of 11 ± 4 µg (n=4, SD) which, despite a narrow range, could still explain this variability. The higher divergence of reconstructed values from *in-situ* measurements are observed at site WPO7-01 for both *T. sacculifer* (w/o sacc) and *G. ruber*. More data would be needed to determine a proper correction for both species, coretop study will be determinant for future downcore reconstructions, especially in the WEP.

We also find that for two species, the boron proxy is a relatively straightforward recorder of ambient pH, with sensitivities close to unity for and *O. universa, and N. dutertrei*. There is also promise in using multiple species in a sample from different hydrographic regimes to reconstruct vertical profiles of pH and pCO_2. We are able to reproduce pH and pCO_2 profiles from multiple sites with different water column structures (Fig. 9) with those reconstructions within error of the *in-situ* values, for most sites. In order to avoid circularity, to validate these calibrations, we recalculated ambient pH and pCO_2 by first excluding site-specific data and then recalculating species-specific calibrations, followed by application to each specific site. The comparison of the two methods does not show significant differences and validates the robustness of the calibrations (Fig. S5). We utilized the calibrations derived from our data for *G. ruber* (calibration n°1 and 2, Table 3), *T. sacculifer* (calibration n°3 and 4, Table 3), *O. universa* (calibration n°8, Table 3), for *P. obliquiloculata* (calibration n°11, Table 3), and for *N. dutertrei*, *G. tumida* and *G. menardii* the calibration made on the compilation of the deep-dweller (calibration n°13, Table 3). Results are shown in Fig. 9 and evaluated in Fig. 10. For *G. menardii*, more data would be helpful to provide additional constraints. Results for *G. ruber* are the sparsest, potentially due to difference in test sizes (Henehan et al., 2013) or undocumented diagenetic effects. Results reaffirm the importance of working with narrow size fractions (Henehan et al., 2013) and the importance of core-top study to determine corrections.

6. Conclusions and future implications

Our study has extended the boron isotope proxy with data for new species and sites. The work supports previous work showing that depth habitats of foraminifera vary depending on the oceanic regime, and this impacts boron isotope signatures. Low $\delta^{11}B$ values in the WEP compared to other regions for *T. sacculifer* (w/o sacc) may be explained by a reduction in microenvironment pH due to a deeper depth habitat associated with

reduced irradiance and thus photosynthetic activity. Those results might also highlight a potential need for studying core-tops in order to establish what factors are important to accurately develop reconstructions in different areas.

The sensitivity of $\delta^{11}B$ to pH is in line with previously published data for *T. sacculifer*, *G. ruber*. The sensitivity of $\delta^{11}B$ to pH of *O. universa* (mixed-dweller), *N. dutertrei*. *G. menardii* and *G. tumida* (deep-dwellers) are similar but more data are needed to fully determine those sensitivities. The similarity of boron isotope calibrations for deep-dwelling taxa might be related to respiration-driven microenvironments.

Reconstruction of seawater pH and carbonate system parameters is achievable using foraminiferal $\delta^{11}B$ but additional core-top and down-core studies reconstructing depth profiles will be needed in order to further verify those calibrations. Past pH and pCO_2 water depth profiles can potentially be created by utilizing multiple foraminiferal species in concert with taxa-specific calibrations for similar settings. This approach has much potential for enhancing our understanding of the past workings of the oceanic carbon cycle, and the biological pump.

Author contribution

R.E and A.T. wrote the proposals that funded the work. A.T. and F.C. provided the samples. M.G., S.M. and A.T. contributed to the experimental design. A.V. helped for sample preparation. M.G. and S.M contributed to developing the method of boron isotope analysis. M.G. performed the measurements with assistance from S.M. M.G conducted the data analysis. M.G. drafted the paper, which was edited by all authors. Interpretation was led by M.G., A.T., S.M. with input from R.E., A.V. and F.C.

Competing interests

The authors declare that they have no conflict of interest.

Acknowledgments:

The authors wish to thank Jesse Farmer for his valuable and detailed comments on the actual and a previous version of the manuscript. We wish to thank Michael Henehan for helpful discussion, comments on the manuscript and help with the code. We also want to thank the anonymous reviewer for helpful comments. Lea Bonnin for assistance with picking samples, the IODP repository for provision of samples, the Tripati Laboratory (UCLA) for their technical support, Mervyn Greaves, Madeleine Bohlin (University of Cambridge) for technical support and use of laboratory space, Yoan Germain, Emmanuel Ponzevera and Oanez Lebeau for technical support and use of laboratory space in Brest, Jill Sutton for helpful conversation on the manuscript. Research is supported by DOE BES grant DE-FG02-13ER16402, by the International Research Chair Program that is funded by the French government (LabexMer ANR-10-LABX-19-01), and IAGC student research grant 2017.

References

Allen, K. A. and Hönisch, B.: The planktic foraminiferal B/Ca proxy for seawater carbonate chemistry: A critical evaluation, Earth Planet. Sci. Lett, 345–348, 203–211, 2012.

Anand, P., Elderfield, H. and Conte, M. H.: Calibration of Mg/Ca thermometry in planktonic foraminifera from a sediment trap time series. Paleoceanography 18, 2003.

Anderson, O. R. and Bé, A.W. H.: The ultrastructure of a planktonic foraminifer, Globigerinoides sacculifer (Brady), and its symbiotic dinoflagellates, J. Foramin. Res., 6, 1–21, 1976.

Arbuszewski, J., DeMenocal, P., Kaplan, A. and Farmer, E. C.: On the fidelity of shell-derived δ18Oseawater estimates, Earth Planet. Sci. Lett., 300, 185–196, 2010.

Axelsson, M. D., Rodushkin, I., Ingri, J. and Öhlander, B.: Multielemental analysis of Mn–Fe nodules by ICP-MS: optimisation of analytical method, Analyst, 127, 76–82, 2002.

Babila, T.L., Rosenthal, Y., Conte, M.H.: Evaluation of the biogeochemical controls on B/Ca of Globigerinoides ruber white from the Oceanic Flux Pro-gram, Bermuda. Earth Planet. Sci. Lett.404, 67–76, 2014.

Barker S., Greaves M. and Elderfield H.: A study of cleaning procedures used for foraminiferal Mg/Ca paleothermometry. Geochemistry, Geophys. Geosystems 4, 1–20, 2003.

Bartoli, G., Hönisch, B. and Zeebe, R. E.: Atmospheric CO2 decline during the Pliocene intensification of Northern Hemisphere glaciations. Paleoceanography 26, 1–14, 2011.

Bemis, B. E., Spero, H. J., Bijma, J. and Lea, D. W.: Reevaluation of the oxygen isotopic composition of planktonic foraminifera: Experimental results and revised paleotemperature equations. Paleoceanography 13, 150–160, 1998.

Bemis, B. E., Spero, H. J. and Thunell, R. C.: Using species-specific paleotemperature equations with foraminifera: a case study in the Southern California Bight, Mar. Micropaleontol, 46, 405–430, 2002.

Bijma, J., Faber Jr., W.W., Hemleben, C.: Temperature and salinity limits for growth and survival of some planktonic foraminifers in laboratory cultures, J. Foraminiferal Res. 20 (2), 95–116, 1990.

Bijma, J., Hönisch, B. and Zeebe, R. E.: Impact of the ocean carbonate chemistry on living foraminiferal shell weight: Comment on "Carbonate ion concentration in glacial-age deep waters of the Caribbean Sea" by W. S. Broecker and E. Clark, Geochemistry, Geophys. Geosystems, 3, 1–7, 2002.

Birch, H., Coxall, H. K., Pearson, P. N., Kroon, D. and O'Regan, M.: Planktonic foraminifera stable isotopes and water column structure: Disentangling ecological signals, Mar. Micropaleontol., 101, 127–145, 2013.

Boyer, T.P., Antonov, J. I., Baranova, O. K., Coleman, C., Garcia, H. E., Grodsky, A., Johnson, D. R., Locarnini, R. A., Mishonov, A. V., O'Brien, T.D., Paver, C.R., Reagan, J.R., Seidov, D., Smolyar, I. V., and Zweng, M. M.: World Ocean Database, NOAA Atlas NESDIS 72, S. Levitus, Ed., A. Mishonov, Technical Ed., Silver Spring, MD, 209, 2013.

Boyle, E. A.: Manganese carbonate overgrowths on foraminifera tests, Geochim. Cosmochim. Acta., 47, 1815–1819, 1983.

Branson, O., Kaczmarek, K., Redfern, S. A. T., Misra, S., Langer, G., Tyliszczak, T., Bijma, J. and Elderfield, H.: The coordination and distribution of B in foraminiferal calcite, Earth Planet. Sci. Lett., 416, 67–72, 2015.

691 Catanzaro, E.J., Champion, C.E., Garner, A.L., Marinenko, G., Sappenfield, K.M. and Shields, W.R.: Boric
692 Acid; Isotopic and Assay Standard Reference Materials. U.S. Natl. Bur. Stand. Spec., Publ. 260-17, 70p,
693 1970.

694 Chalk, T. B., Hain, M. P., Foster, G. L., Rohling, E. J., Sexton, P. F., Badger, M. P. S., Cherry, S. G., Hasenfratz,
695 A. P., Haug, G. H., Jaccard, S. L., Martínez-García, A., Pälike, H., Pancost, R. D. and Wilson, P. A.:
696 Causes of ice age intensification across the Mid-Pleistocene Transition, Proc. Natl. Acad. Sci., 114,
697 13114–13119, 2017.

698 Coadic, R., Bassinot, F., Dissard, D., Douville, E., Greaves, M. and Michel, E.: A core-top study of dissolution
699 effect on B/Ca in Globigerinoides sacculifer from the tropical Atlantic: Potential bias for paleo-
700 reconstruction of seawater carbonate chemistry, Geochemistry, Geophys. Geosystems 14, 1053–1068,
701 2013.

702 de Nooijer, L. J., Spero, H. J., Erez, J., Bijma, J. and Reichart, G. J.: Biomineralization in perforate foraminifera.
703 Earth-Science Rev., 135, 48–58, 2014.

704 Dekens, P. S., Lea, D. W., Pak, D. K. and Spero, H. J.: Core top calibration of Mg/Ca in tropical foraminifera:
705 Refining paleotemperature estimation, Geochemistry, Geophys. Geosystems 3, 1–29, 2002.

706 Deuser, W.G., Ross, E.H., Hemleben, Ch., Spindler, M.: Seasonal changes in species composition, numbers,
707 mass, size, and isotopic composition of planktonic foraminifera settling into the deep Sargasso Sea,
708 Palaeogeogr., Palaeoclimat., Palaeoecol., 33:103-127, 1981.

709 Deuser, W. G. and Ross, E. H.: Seasonally abundant planktonic foraminifera of the Sargasso Sea; succession,
710 deep-water fluxes, isotopic compositions, and paleoceanographic implications, J. Foraminifer. Res. 19,
711 268–293, 1989.

712 Dickson, A. G.: Thermodynamics of the dissociation of boric acid in synthetic seawater from 273.15 to 318.15
713 K., Deep Sea Res., Part A, Oceanogr. Res. Pap. 37, 755–766, 1990.

714 Dickson, A.G., Millero, F.J.: A comparison of the equilibrium constants for the dissociation of carbonic acid in
715 seawater media, Deep-Sea Res., 34, 1733–1743, 1987.

716 Douville, E., Paterne, M., Cabioch, G., Louvat, P., Gaillardet, J., Juillet-Leclerc, A. and Ayliffe, L.: Abrupt sea
717 surface pH change at the end of the Younger Dryas in the central sub-equatorial Pacific inferred from
718 boron isotope abundance in corals (Porites), Biogeosciences 7, 2445–2459, 2010.

719 Duguay, L.E.: Comparative laboratory and field studies on calcification and carbon fixation in foraminiferal-
720 algal associations, Journal of Foraminiferal Research 13, 252-261, 1983.

721 Duplessy, J., Labeyrie, L., Juilletleclerc, A., Maitre, F., Duprat, J. and Sarnthein, M.: Surface salinity
722 reconstruction of the north-atlantic ocean during the last glacial maximum, Oceanol. Acta, 14, 311–324,
723 1991.

724 Elderfield, H., Yu, J., Anand, P., Kiefer, T. and Nyland, B.: Calibrations for benthic foraminiferal Mg/Ca
725 paleothermometry and the carbonate ion hypothesis, Earth Planet. Sci. Lett., 250, 633–649., 2006.

726 Elderfield, H. and Granssen, G.: Past temperatures and O18 of surface ocean waters inferred from foraminiferal
727 Mg/Ca ratios, Nature 405, 442–445, 2000.

728 Erez J.: Calcification Rates, Photosynthesis and Light in Planktonic Foraminifera. In: Westbroek P., de Jong
729 E.W. (eds) Biomineralization and Biological Metal Accumulation. Springer, Dordrecht, 1983.

730 Erez, J.: The Source of Ions for Biomineralization in Foraminifera and Their Implications for Paleoceanographic
731 Proxies, Rev. Mineral. Geochemistry, 54, 115–149, 2003.

Fairbanks, R. G. and Wiebe, P. H.: Foraminifera and Chlorophyll Maximum: Vertical Distribution, Seasonal Succession, and Paleoceanographic Significance, Science, 209, 1524–1526, 1980.

Fairbanks, R. G., Sverdlove, M., Free, R., Wiebe, P. H. and Bé, A. W. H.: Vertical distribution and isotopic fractionation of living planktonic foraminifera from the Panama Basin, Nature, 298, 841–844, 1982.

Farmer, E. C., Kaplan, A., de Menocal, P. B. and Lynch-Stieglitz, J.: Corroborating ecological depth preferences of planktonic foraminifera in the tropical Atlantic with the stable oxygen isotope ratios of core top specimens, Paleoceanography, 22, 1–14, 2007.

Feely, R.: Impact of Anthropogenic CO2 on the CaCO3 System in the Oceans, Science, 305, 362–366, 2004.

Ferguson, J. E., Henderson, G. M., Kucera, M. and Rickaby, R. E. M.: Systematic change of foraminiferal Mg/Ca ratios across a strong salinity gradient, Earth Planet. Sci. Lett., 265, 153–166, 2008.

Foster, G. L.: Seawater pH, pCO2 and [CO32−] variations in the Caribbean Sea over the last 130 kyr: A boron isotope and B/Ca study of planktic foraminifera, Earth Planet. Sci. Lett., 271, 254–266, 2008.

Foster, G. L. and Sexton, P. F.: Enhanced carbon dioxide outgassing from the eastern equatorial Atlantic during the last glacial, Geology, 42, 1003–1006, 2014.

Foster, G. L., Lear, C. H. and Rae, J. W. B.: The evolution of pCO2, ice volume and climate during the middle Miocene, Earth Planet. Sci. Lett., 341–344, 243–254, 2012.

Foster, G. L. and Rae, J. W. B.: Reconstructing Ocean pH with Boron Isotopes in Foraminifera, Annu. Rev. Earth Planet. Sci., 44, 207–237, 2016.

Gabitov, R. I., Rollion-bard, C., Tripati, A. and Sadekov, A.: In situ study of boron partitioning between calcite and fluid at different crystal growth rates, Geochim. Cosmochim. Acta, 137, 81–92, 2014.

Gaillardet, J., Lemarchand, D., Göpel, C. and Manhès, G.: Evaporation and Sublimation of Boric Acid : Application for Boron Purification from Organic Rich Solutions, Geostand. Newsl., 25, 67–75, 2001.

Gast R. J. and Caron D. A.: Photosymbiotic associations in planktonic foraminifera and radiolaria, 1–7, 2001.

Gastrich, M.D.: Ultrastructure of a new intracellular symbiotic alga found within planktonic foraminifera, Journal of Phycology 23, 623-632, 1988.

Gattuso, J.P. and Hansson, L.: Ocean acidification, Oxford University Press, 2011.

Hallock P.: Algal Symbiosis : A Mathematical Analysis Marine Biology 62, 249-255, 1981b.

Hemming, N. G. and Hanson, G. N. Boron isotopic composition and concentration in modern marine carbonates, Geochim. Cosmochim. Acta, 56, 537–543, 1992.

Hendry, K.R., Rickaby, R.E.M., Meredith, M.P., Elderfield, H.: Controls on sta-ble isotope and trace metal uptake in Neogloboquadrina pachyderma (sinis-tral) from an Antarctic sea-ice environment. Earth Planet. Sci. Lett.278, 67–77, 2009.

Henehan, M. J., Foster, G. L., Bostock, H. C., Greenop, R., Marshall, B. J. and Wilson, P. A.: A new boron isotope-pH calibration for Orbulina universa, with implications for understanding and accounting for 'vital effects', Earth Planet. Sci. Lett., 454, 282–292, 2016.

Henehan, M. J., Foster, G. L., Rae, J. W. B., Prentice, K. C., Erez, J., Bostock, H. C., Marshall, B. J. and Wilson, P. A.: Evaluating the utility of B/Ca ratios in planktic foraminifera as a proxy for the carbonate system: A case study of Globigerinoides ruber, Geochemistry, Geophys. Geosystems 16, 1052–1069, 2015.

Henehan, M. J., Rae, J. W. B., Foster, G. L., Erez, J., Prentice, K. C., Kucera, M., Bostock, H. C., Martínez-Botí, M. A., Milton, J. A., Wilson, P. A., Marshall, B. J. and Elliott, T.: Calibration of the boron isotope proxy in the planktonic foraminifera Globigerinoides ruber for use in palaeo-CO2reconstruction, Earth Planet. Sci. Lett. 364, 111–122, 2013.

Holcomb, M., Decarlo, T. M., Schoepf, V., Dissard, D., Tanaka, K. and McCulloch, M.: Cleaning and pre-treatment procedures for biogenic and synthetic calcium carbonate powders for determination of elemental and boron isotopic compositions, Chem. Geol., 398, 11–21, 2015.

Hönisch, B., Hemming, N. G., Archer, D., Siddall, M. and McManus, J. F.: Atmospheric Carbon Dioxide Concentration Across the Mid-Pleistocene Transition, Science, 324, 1551–1554, 2009.

Hönisch, B., Bijma, J., Russell, A. D., Spero, H. J., Palmer, M. R., Zeebe, R. E. and Eisenhauer, A.: The influence of symbiont photosynthesis on the boron isotopic composition of foraminifera shells, Mar. Micropaleontol., 49, 87–96, 2003.

Hönisch, B. and Hemming, N. G.: Ground-truthing the boron isotope-paleo-pH proxy in planktonic foraminifera shells: Partial dissolution and shell size effects, Paleoceanography 19, 1–13, 2004.

Hönisch, B., Bickert, T. and Hemming, N. G.: Modern and Pleistocene boron isotope composition of the benthic foraminifer Cibicidoides wuellerstorfi, Earth Planet. Sci. Lett., 272, 309–318, 2008.

Howes, E. L., Kaczmarek, K., Raitzsch, M., Mewes, A., Bijma, N., Horn, I., Misra, S., Gattuso, J. P. and Bijma, J.: Decoupled carbonate chemistry controls on the incorporation of boron into Orbulina universa, Biogeosciences, 14, 415–430, 2017.

IPCC: Climate Change 2014 - The Physical Science Basis, edited by Intergovernmental Panel on Climate Change, Cambridge University Press, Cambridge., 2014.

Jørgensen, B. B., Erez, J., Revsbech, P. and Cohen, Y.: Symbiotic photosynthesis in a planktonic foraminifera, Globigerinoides sacculifer (Brady), studied with microelectrodes, Limnol. Oceanogr., 30, 1253–1267 1985.

Kaczmarek, K., Nehrke, G., Misra, S., Bijma, J. and Elderfield, H.: Investigating the effects of growth rate and temperature on the B/Ca ratio and δ11B during inorganic calcite formation, Chem. Geol., 421, 81–92, 2016.

Kemle-von Mücke S. and Oberhänsli H.: The Distribution of Living Planktic Foraminifera in Relation to Southeast Atlantic Oceanography, Use Proxies Paleoceanogr., 91–115, 1999.

Key, R.M.: A global ocean carbon climatology: Results from Global Data Analysis Project (GLODAP), Global Biogeochem. Cycles, 18, GB4031, 2004.

Kim, S.-T. and O'Neil, J. R.: Equilibrium and nonequilibrium oxygen isotope effects in synthetic carbonates, Geochim. Cosmochim. Acta, 61, 3461–3475, 1997.

Klochko, K., Cody, G. D., Tossell, J. A., Dera, P. and Kaufman, A. J.: Re-evaluating boron speciation in biogenic calcite and aragonite using 11B MAS NMR, Geochim. Cosmochim. Acta, 73, 1890–1900, 2009.

Klochko, K., Kaufman, A. J., Yao, W., Byrne, R. H. and Tossell, J. A.: Experimental measurement of boron isotope fractionation in seawater, Earth Planet. Sci. Lett., 248, 276–285, 2006.

Köhler-Rink, S. and Kühl, M.: Microsensor studies of photosynthesis and respiration in larger symbiotic foraminifera. I. The physico-chemical microenvironment of Marginopora vertebralis, Amphistegina lobifera and Amphisorus hemrichii, Mar. Biol., 137, 473–486, 2000.

Köhler-Rink, S. and Kühl, M., Microsensor studies of photosynthesis and respiration in the larger symbiont bearing foraminifera Amphistegina lobifera, and Amphisorus hemprichii, Ophelia, 55, 111–122, 2001.

Lea, D. W., Pak, D. K. and Spero, H. J.: Climate impact of late quaternary equatorial Pacific sea surface temperature variations, Science, 289, 1719–1724, 2000.

Lemarchand, D., Gaillardet, J., Lewin, A. and Allègre, C. J.: Boron isotope systematics in large rivers: Implications for the marine boron budget and paleo-pH reconstruction over the Cenozoic, Chem. Geol., 190, 123–14, 2002.

Liu, Y., Liu, W., Peng, Z., Xiao, Y., Wei, G., Sun, W., He, J., Liu, G. and Chou, C.-L.: Instability of seawater pH in the South China Sea during the mid-late Holocene: Evidence from boron isotopic composition of corals, Geochim. Cosmochim. Acta, 73, 1264–1272, 2009.

Lloyd, N. S., Sadekov, A. Y. and Misra, S.: Application of 1013ohm Faraday cup current amplifiers for boron isotopic analyses by solution mode and laser ablation multicollector inductively coupled plasma mass spectrometry, Rapid Commun. Mass Spectrom., 32, 9–18, 2018.

Martínez-Botí, M. A., Foster, G. L., Chalk, T. B., Rohling, E. J., Sexton, P. F., Lunt, D. J., Pancost, R. D., Badger, M. P. S. and Schmidt, D. N.: Plio-Pleistocene climate sensitivity evaluated using high-resolution CO2 records, Nature, 518, 49–54, 2015a.

Martínez-Botí M. A., Marino G., Foster G. L., Ziveri P., Henehan M. J., Rae J. W. B., Mortyn P. G. and Vance D.: Boron isotope evidence for oceanic carbon dioxide leakage during the last deglaciation. Nature, 518, 219–222, 2015b.

Martínez-Botí, M. A., Mortyn, P. G., Schmidt, D. N., Vance, D. and Field, D. B.: Mg/Ca in foraminifera from plankton tows: Evaluation of proxy controls and comparison with core tops, Earth Planet. Sci. Lett., 307, 113–125, 2011.

Mavromatis, V., Montouillout, V., Noireaux, J., Gaillardet, J. and Schott, J.: Characterization of boron incorporation and speciation in calcite and aragonite from co-precipitation experiments under controlled pH, temperature and precipitation rate, Geochim. Cosmochim. Acta, 150, 299–313, 2015.

McCulloch, M. T., D'Olivo, J. P., Falter, J. L., Georgiou, L., Holcomb, M., Montagna, P. and Trotter, J. A. Boron Isotopic Systematics in Scleractinian Corals and the Role of pH Up-regulation, Boron Isot. Adv. Isot. Geochemistry, 2018.

Millero, F.: Speciation of metals in natural waters, Geochem. Trans., 2, 57, 2001.

Millero, F., Woosley, R., DiTrolio, B. and Waters, J.: Effect of Ocean Acidification on the Speciation of Metals in Seawater, Oceanography 22, 72–85, 2009.

Misra, S., Greaves, M., Owen, R., Kerr, J., Elmore, A. C. and Elderfield, H.: Determination of B/Ca of natural carbonates by HR-ICP-MS, Geochemistry, Geophys. Geosystems, 15, 1617–1628, 2014a.

Misra, S., Owen, R., Kerr, J., Greaves, M. and Elderfield, H.: Determination of δ11B by HR-ICP-MS from mass limited samples: Application to natural carbonates and water samples, Geochim. Cosmochim. Acta, 140, 531–552, 2014b.

Mortyn, P. G. and Charles, C. D.: Planktonic foraminiferal depth habitat and δ 18 O calibrations: Plankton tow results from the Atlantic sector of the Southern Ocean, Paleoceanography, 18, 2003.

Mulitza, S., Boltovskoy, D., Donner, B., Meggers, H., Paul, A. and Wefer, G.: Temperature:δ18O relationships of planktonic foraminifera collected from surface waters, Palaeogeogr. Palaeoclimatol. Palaeoecol., 202, 143–152, 2003.

Ni, Y., Foster, G. L., Bailey, T., Elliott, T., Schmidt, D. N., Pearson, P., Haley, B. and Coath, C.: A core top assessment of proxies for the ocean carbonate system in surface-dwelling foraminifers, Paleoceanography 22, 2007.

Nir, O., Vengosh, A., Harkness, J. S., Dwyer, G. S. and Lahav, O.: Direct measurement of the boron isotope fractionation factor: Reducing the uncertainty in reconstructing ocean paleo-pH, Earth Planet. Sci. Lett., 414, 1–5, 2015.

Noireaux, J., Mavromatis, V., Gaillardet, J., Schott, J., Montouillout, V., Louvat, P., Rollion-Bard, C. and Neuville, D. R.: Crystallographic control on the boron isotope paleo-pH proxy, Earth Planet. Sci. Lett., 430, 398–407, 2015.

Orr, J. C., Fabry, V. J., Aumont, O., Bopp, L., Doney, S. C., Feely, R. A., Gnanadesikan, A., Gruber, N., Ishida, A., Joos, F., Key, R. M., Lindsay, K., Maier-Reimer, E., Matear, R., Monfray, P., Mouchet, A., Najjar, R. G., Plattner, G. K., Rodgers, K. B., Sabine, C. L., Sarmiento, J. L., Schlitzer, R., Slater, R. D., Totterdell, I. J., Weirig, M. F., Yamanaka, Y. and Yool, A.: Anthropogenic ocean acidification over the twenty-first century and its impact on calcifying organisms, Nature, 437, 681–686, 2005.

Pagani. M.: Marked Decline in Atmospheric Carbon Dioxide Concentrations During the Paleogene, Science, 309, 600–603, 2005.

Palmer, M. R., Pearson, P. N. and Cobb, S. J., Reconstructing Past Ocean pH-Depth Profiles, Science, 282, 1468–1471, 1998.

Pearson, P. N. and Palmer, M. R.: Middle Eocene seawater pH and atmospheric carbon dioxide concentrations, Science, 284, 1824–1826, 1999.

Peeters, F. J. C. and Brummer, G.-J. a.: The seasonal and vertical distribution of living planktic foraminifera in the NW Arabian Sea, Geol. Soc. London, Spec. Publ., 195, 463–497, 2002.

Quintana Krupinski, N. B., Russell, A. D., Pak, D. K. and Paytan, A.: Core-top calibration of B/Ca in Pacific Ocean Neogloboquadrina incompta and Globigerina bulloides as a surface water carbonate system proxy, Earth Planet. Sci. Lett., 466, 139–151, 2017.

Rae, J.W.B.: Boron Isotopes in Foraminifera: Systematics, Biomineralisation, and CO_2 Reconstruction. In: Marschall, H., Foster, G. (eds), Boron Isotopes. Advances in Isotope Geochemistry. Springer, Cham, 2018.

Rae, J. W. B., Foster, G. L., Schmidt, D. N. and Elliott, T.: Boron isotopes and B/Ca in benthic foraminifera: Proxies for the deep ocean carbonate system, Earth Planet. Sci. Lett., 302, 403–413, 2011.

Raitzsch, M., Bijma, J., Benthien, A., Richter, K.-U., Steinhoefel, G. and Kučera, M.: Boron isotope-based seasonal paleo-pH reconstruction for the Southeast Atlantic – A multispecies approach using habitat preference of planktonic foraminifera, Earth Planet. Sci. Lett., 487, 138–150, 2018.

Ravelo, A. C. and Fairbanks, R. G.: Oxygen isotopic composition of multiple species of planktonic foraminifera: recorder of the modern photic zone temperature gradient, Palaeogeogr. Palaeoclimatol. Palaeoecol., 7, 815–831, 1992.

Regenberg, M., Nürnberg, D., Steph, S., Groeneveld, J., Garbe-Schönberg, D., Tiedemann, R. and Dullo, W.-C.: Assessing the effect of dissolution on planktonic foraminiferal Mg/Ca ratios: Evidence from Caribbean core tops, Geochemistry, Geophys. Geosystems, 7, 2006.

Regenberg, M., Steph, S., Nürnberg, D., Tiedemann, R. and Garbe-Schönberg, D.: Calibrating Mg/Ca ratios of multiple planktonic foraminiferal species with δ18O-calcification temperatures: Paleothermometry for the upper water column, Earth Planet. Sci. Lett., 278, 324–336, 2009.

892 Rickaby, R. E. M. and Halloran, P.: Cool La Nina During the Warmth of the Pliocene?, Science, 307, 1948–
893 1952, 2005.

894 Ries, J. B., Cohen, A. L. and McCorkle, D. C.: Marine calcifiers exhibit mixed responses to CO2-induced ocean
895 acidification, Geology, 37, 1131–1134, 2009.

896 Rink, S., Kühl, M., Bijma, J. and Spero, H. J.: Microsensor studies of photosynthesis and respiration in the
897 symbiotic foraminifer Orbulina universa, Mar. Biol., 131, 583–595, 1998.

898 Rollion-Bard, C. and Erez, J.: Intra-shell boron isotope ratios in the symbiont-bearing benthic foraminiferan
899 Amphistegina lobifera: Implications for δ11B vital effects and paleo-pH reconstructions, Geochim.
900 Cosmochim. Acta, 74, 1530–1536, 2010.

901 Rostek, F., Ruhland, G., Bassinot, F. C., Muller, P. J., Labeyrie, L. D., Lancelot, Y. and Bard, E.: Reconstructing
902 Sea-Surface Temperature and Salinity Using δ18O and Alkenone Records, Nature, 364, 319–321, 1993.

903 Russell, A. D., Hönisch, B., Spero, H. J. and Lea, D. W.: Effects of seawater carbonate ion concentration and
904 temperature on shell U, Mg, and Sr in cultured planktonic foraminifera, Geochim. Cosmochim. Acta, 68,
905 4347–4361, 2004.

906 Sanyal, A., Bijma, J., Spero, H. J. and Lea, D. W.: Empirical relationship between pH and the boron isotopic
907 composition of Globigerinoides sacculifer: Implications for the boron isotopes paleo-pH proxy,
908 Paleoceanography, 16, 515–519, 2001.

909 Sanyal, A., Hemming, N. G., Broecker, W. S., Lea, D. W., Spero, H. J., & Hanson, G. N. Oceanic pH control on
910 the boron isotopic composition of foraminifera: evidence from culture experiments, Paleoceanography,
911 11(5), 513-517, 1996.

912 Schmidt, G. A. and Mulitza, S.: Global calibration of ecological models for planktic foraminifera from core-top
913 carbonate oxygen-18, Mar. Micropaleontol., 44, 125–140, 2002.

914 Seki, O., Foster, G. L., Schmidt, D. N., Mackensen, A., Kawamura, K. and Pancost, R. D.: Alkenone and boron-
915 based Pliocene pCO2records, Earth Planet. Sci. Lett., 292, 201–211, 2010.

916 Shirayama, Y.: Effect of increased atmospheric CO2 on shallow water marine benthos, J. Geophys. Res., 110,
917 C09S08, 2005.

918 Sime, N. G., De La Rocha, C. L. and Galy, A.: Negligible temperature dependence of calcium isotope
919 fractionation in 12 species of planktonic foraminifera, Earth Planet. Sci. Lett., 232, 51–66, 2005.

920 Spero H. J.: Symbiosis in the planktonic foraminifer, orbulina universa, and the isolation of its symbiotic
921 dinoflagellate, gymnodinium beii sp.nov, J. Phycol 23, 307-317, 1987.

922 Sutton, J. N., Liu, Y. W., Ries, J. B., Guillermic, M., Ponzevera, E. and Eagle, R. A.: δ11B as monitor of
923 calcification site pH in divergent marine calcifying organisms, Biogeosciences, 15, 1447–1467, 2018.

924 Takagi H., Kimoto K., Fujiki T., Saito H., Schmidt C. and Kucera M.: Characterizing photosymbiosis in modern
925 planktonic foraminifera, biogeosciences, 3377–3396, 2019.

926 Thomson, J., Brown, L., Nixon, S., Cook, G. T. and MacKenzie, A. B.: Bioturbation and Holocene sediment
927 accumulation fluxes in the north-east Atlantic Ocean (Benthic Boundary Layer experiment sites), Mar.
928 Geol., 169, 21–39, 2000.

929 Tripati, A.: Deep-Sea Temperature and Circulation Changes at the Paleocene-Eocene Thermal Maximum.
930 Science, 308, 1894–1898, 2005.

931 Tripati, A. K., Roberts, C. D. and Eagle, R. A.: Coupling of CO2 and Ice Sheet Stability Over Major Climate
932 Transitions of the Last 20 Million Years, Science, 326, 1394–1397, 2009.

933 Tripati, A. K., Roberts, C. D., Eagle, R. A. and Li, G.: A 20 million year record of planktic foraminiferal B/Ca
934 ratios: Systematics and uncertainties in pCO2reconstructions, Geochim. Cosmochim. Acta, 75, 2582–
935 2610, 2011.

936 Uchikawa, J., Penman, D. E., Zachos, J. C. and Zeebe, R. E.: Experimental evidence for kinetic effects on B/Ca
937 in synthetic calcite: Implications for potential B(OH)4− and B(OH)3 incorporation, Geochim. Cosmochim.
938 Acta, 150, 171–191, 2015.

939 Urey, H.C., Lowenstam, H.A., Epstein, S. & McKinney, C.R.: Measurement of paleo-temperature and
940 temperatures of the upper cretaceous of England, Denmark, and the southeastern United-States. Geol. Soc.
941 Am. Bull., 62, 399-416, 1951.

942 Wang, B.-S., You, C.-F., Huang, K.-F., Wu, S.-F., Aggarwal, S. K., Chung, C.-H. and Lin, P.-Y.: Direct
943 separation of boron from Na- and Ca-rich matrices by sublimation for stable isotope measurement by MC-
944 ICP-MS, Talanta, 82, 1378–1384, 2010.

945 Wang, G., Cao, W., Yang, D. and Xu, D.: Variation in downwelling diffuse attenuation coefficient in the
946 northern South China Sea, Chinese J. Oceanol. Limnol., 26, 323–333, 2008.

947 Weare, B. C., Strub, P. T. and Samuel, M. D. Annual Mean Surface Heat Fluxes in the Tropical Pacific Ocean, J.
948 Phys. Oceanogr., 11, 705–717, 1981.

949 Wei, G., McCulloch, M. T., Mortimer, G., Deng, W. and Xie, L.: Evidence for ocean acidification in the Great
950 Barrier Reef of Australia, Geochim. Cosmochim. Acta, 73, 2332–2346, 2009.

951 Wilson, D. J., Piotrowski, A. M., Galy, A. and McCave, I. N.: A boundary exchange influence on deglacial
952 neodymium isotope records from the deep western Indian Ocean, Earth Planet. Sci. Lett., 341–344, 35–47,
953 2012.

954 Wolf-Gladrow, D. A., Riebesell, U., Burkhardt, S. and Buma, J.: Direct effects of CO2 concentration on growth
955 and isotopic composition of marine plankton, Tellus B Chem. Phys. Meteorol., 51, 461–476, 1999.

956 Yu, J., Menviel, L., Jin, Z. D., Thornalley, D. J. R., Barker, S., Marino, G., Rohling, E. J., Cai, Y., Zhang, F.,
957 Wang, X., Dai, Y., Chen, P. and Broecker, W. S.: Sequestration of carbon in the deep Atlantic during the
958 last glaciation, Nat. Geosci., 9, 319–324, 2016.

959 Yu, J., Thornalley, D. J. R., Rae, J. W. B. and McCave, N. I.: Calibration and application of B/Ca, Cd/Ca, and δ
960 11 B in Neogloboquadrina pachyderma (sinistral) to constrain CO 2 uptake in the subpolar North Atlantic
961 during the last deglaciation, Paleoceanography, 28, 237–252, 2013.

962 Yu, J., Foster, G. L., Elderfield, H., Broecker, W. S. and Clark, E.: An evaluation of benthic foraminiferal B/Ca
963 and δ11B for deep ocean carbonate ion and pH reconstructions, Earth Planet. Sci. Lett., 293, 114–120, 20,
964 2010.

965 Yu, J., Elderfield, H., Hönisch, B.: B/Ca in planktonic foraminifera as a proxy for surface seawater pH.
966 Paleoceanography22, PA2202, 2007.

967 Yu, J., Day, J., Greaves, M. and Elderfield, H., Determination of multiple element/calcium ratios in foraminiferal
968 calcite by quadrupole ICP-MS, Geochemistry, Geophys. Geosystems 6, 2005.

969 Zeebe, R. E. and Wolf-Gladrow, D., CO2 in Seawater: Equilibrium, Kinetics, Isotopes Elsevier Oceanography
970 Series 65, Amsterdam, 2001.

971 Zeebe, R. E., Wolf-Gladrow, D. A., Bijma, J. and Hönisch, B.,Vital effects in foraminifera do not compromise
972 the use of δ 11 B as a paleo- pH indicator: Evidence from modeling, Paleoceanography, 18, 2003.

Figure caption

Figure 1: Reactions governing dissolved inorganic carbon equilibria**.**

Figure 2: (A) Speciation of H_3BO_3 and $H_4BO_4^-$ as function of seawater pH (total scale), (B) $\delta^{11}B$ of dissolved inorganic boron species as a function of seawater pH, (C) sensitivity of $\delta^{11}B$ of $H_4BO_4^-$ for a pH ranging from 7.6 to 8.4. T=25°C, S=35, $\delta^{11}B$=39.61 ‰ (Foster et al., 2010), dissociation constant α = 1.0272 (Klochko et al., 2006).

Figure 3: Map showing locations of the core-tops used in this study (white diamonds). Red open circles represent the sites used for *in-situ* carbonate parameters from GLODAP database (Key et al., 2004).

Figure 4: Pre-industrial data versus depth of the sites used in this study. The figure shows seasonal temperatures (extracted from World Ocean Database 2013), density anomaly (kg/m^3), pre-industrial pH and pre-industrial $\delta^{11}B$ of $H_4BO_4^-$ (calculated from the GLODAP database and corrected for anthropogenic inputs).

Figure 5: Boron isotopic measurements of mixed-layer foraminifera plotted against the $\delta^{11}B_{borate}$. $\delta^{11}B_{borate}$ were characterized by determination of the calcification depth of the foraminifera, A) *G. ruber*, B) *T. sacculifer*, C) *O. universa*. Mono-specific calibrations are summarized in Table 3.

Figure 6: Boron isotopic measurements of deep-dwelling foraminifera ($\delta^{11}B_{carbonate}$) plot against $\delta^{11}B_{borate}$. $\delta^{11}B_{borate}$ were characterized by determining the calcification depth of foraminifera, A) *P. obliquiloculata*, B) *G. menardii*, C) *N. dutertrei*, D) *G. tumida* and E) Compilation of deep dweller species. Mono-specific calibrations are summarized in Table 3.

Figure 7: Boxplots of B/Ca ratios for multiple species, *T. sacculifer* (this study; Foster et al., 2008; Ni et al; 2007; Seki et al., 2010), *G. ruber* (this study; Babila et al., 2014; Foster et al., 2008; Ni et al., 2007), *G. inflata*, *G. bulloides* (Yu et al., 2007), *N. pachyderma* (Hendry et al., 2009; Yu et al., 2013), *N. dutertrei* (this study; Foster et al., 2008), *O. universa*, *P.obliquiloculata*, *G. menardii*, *G. tumida* (this study).

Figure 8: A) Boxplot showing the calculated microenvironment pH difference (Δmicroenvironment pH) between microenvironment and external pH based on the $\delta^{11}B$ data. B) This figure shows that a decrease in insolation can explain the low $\delta^{11}B$ from the WEP. Light penetration profile in the Western Pacific, with E_0 in the WEP of 220 J.s-1.m-2 (Weare et al., 1981) and a light attenuation coefficient of 0.028 (Wang et al., 2008). Theoretical depths were calculated for a decrease in microenvironment pH of ΔpH_1= -0.02 (e.g. WP07-a); ΔpH_1= -0.04 (e.g. A14), ΔpH_2= -0.06 (e.g. 806A). Light penetration corresponding to Ec is ~12%, ΔpH_0~7%, ΔpH_1 ~5%, ΔpH_2 ~1% respective depth are 75m, 90m, 110m and 150m. Grey band is the calcification depth of *T. sacculifer* (w/o sacc) utilized in this study.

Figure 9: Water depth pH profiles reconstructed at every site applying the mono-specific calibrations derived from our results (Table 3). Figure is showing measured $\delta^{11}B_{calcite}$, $\delta^{11}B_{borate}$ calculated according to different calibrations (see Table 3 and text), calculated pH based on $\delta^{11}B$ ($pH_{\delta 11B}$) and pCO_2 calculated from $pH_{\delta 11B}$ and alkalinity.

Figure 10: Evaluation of the reconstructed parameters, $\delta^{11}B_{borate}$, pH and pCO_2 versus *in-situ* parameter. The recalculated parameters are consistent with *in-situ* data, except for *G. ruber*. This variability might be explained by the different test sizes.

Table caption

Table 1: Box-core information

Table 2: Analytical results of $\delta^{13}C$, $\delta^{18}O$, $\delta^{11}B$ and elemental ratios Li/Ca, B/Ca and Mg/Ca

Table 3: Species-specific $\delta^{11}B_{carbonate}$ to $\delta^{11}B_{borate}$ calibrations from literature and from our data

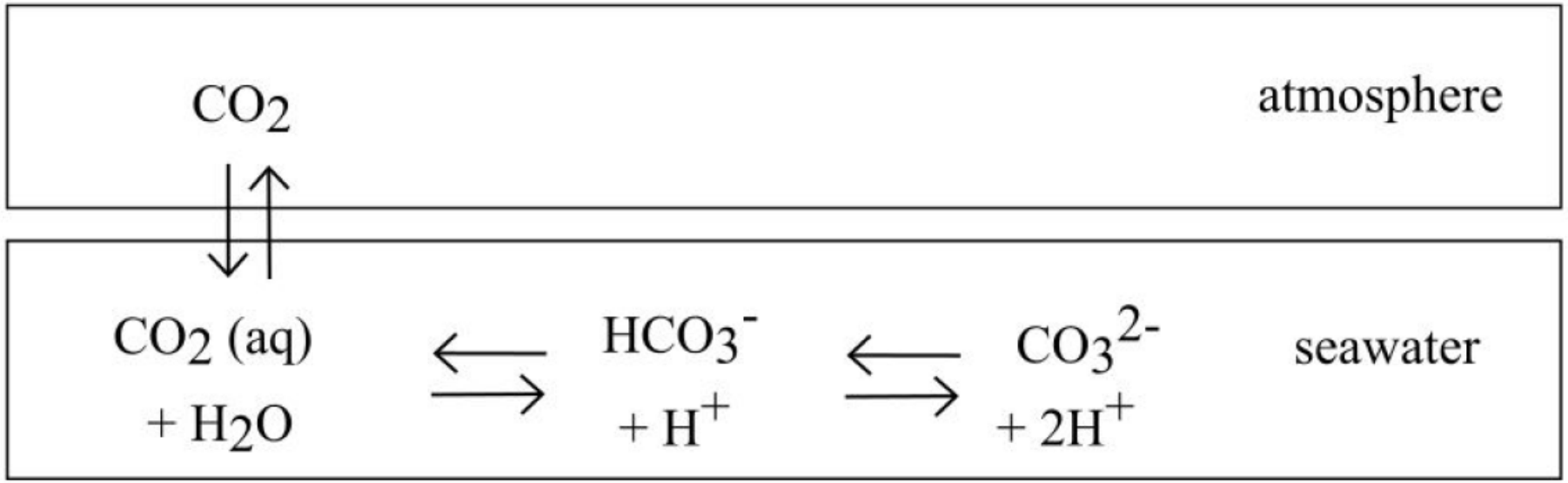

Figure 1

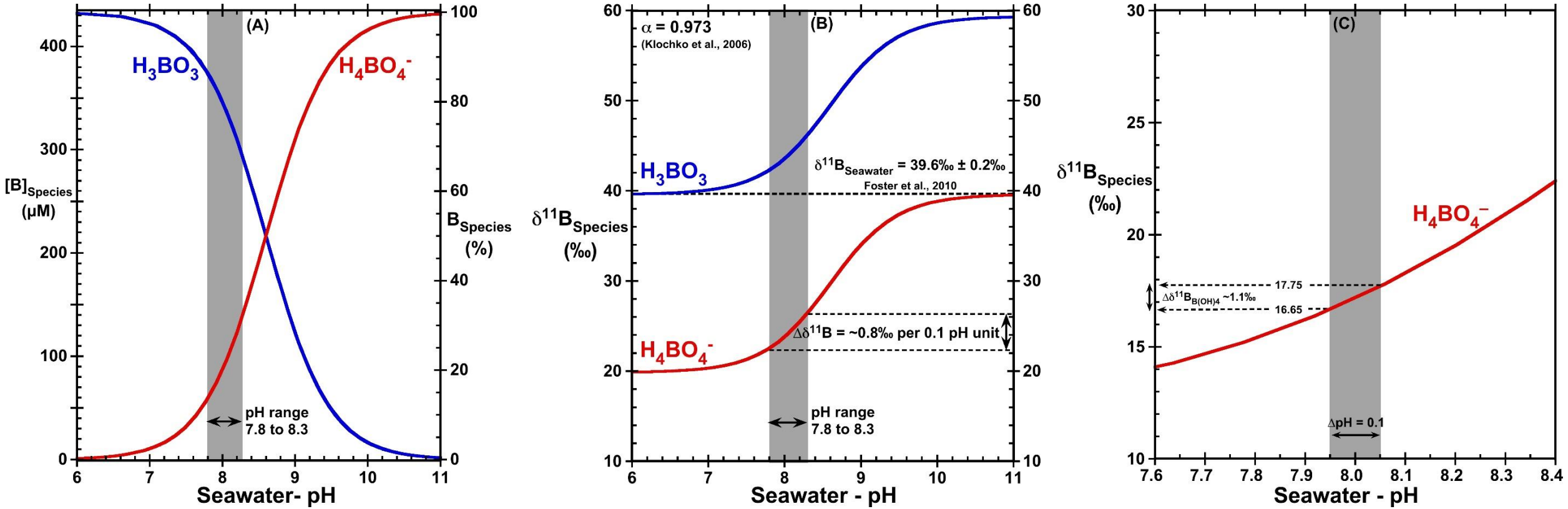
(A)
H_3BO_3
$H_4BO_4^-$
$[B]_{Species}$ (μM)
$B_{Species}$ (%)
pH range
7.8 to 8.3
Seawater- pH
(B)
α = 0.973
(Klochko et al., 2006)
$\delta^{11}B_{Seawater}$ = 39.6‰ ± 0.2‰
Foster et al., 2010
$\delta^{11}B_{Species}$ (‰)
Δδ^{11}B = ~0.8‰ per 0.1 pH unit
pH range
7.8 to 8.3
Seawater - pH
(C)
$H_4BO_4^-$
17.75
$\Delta\delta^{11}B_{B(OH)4}$ ~1.1‰
16.65
ΔpH = 0.1
Seawater - pH

Figure 2

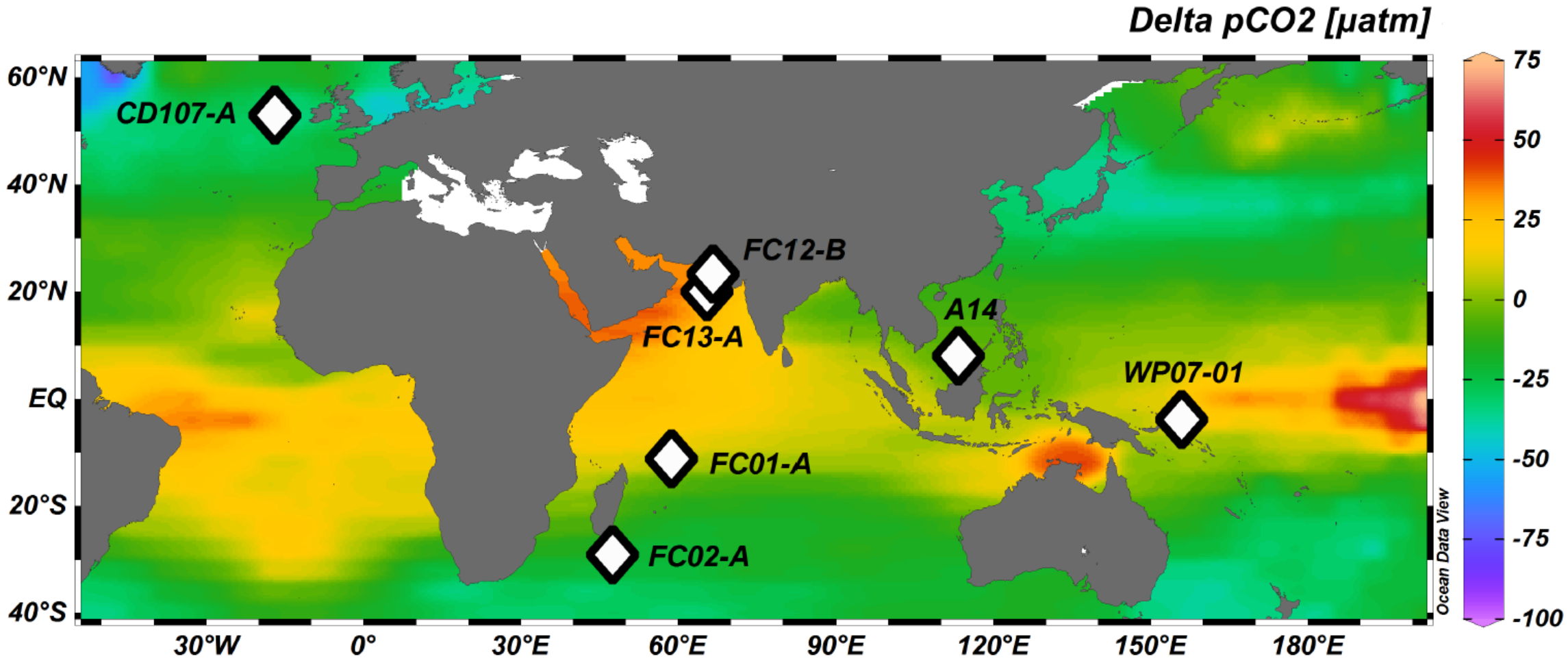
Delta pCO2 [µatm]
CD107-A
FC12-B
FC13-A
A14
WP07-01
FC01-A
FC02-A
60°N
40°N
20°N
EQ
20°S
40°S
30°W
0°
30°E
60°E
90°E
120°E
150°E
180°E
75
50
25
0
-25
-50
-75
-100
Ocean Data View

Figure 3

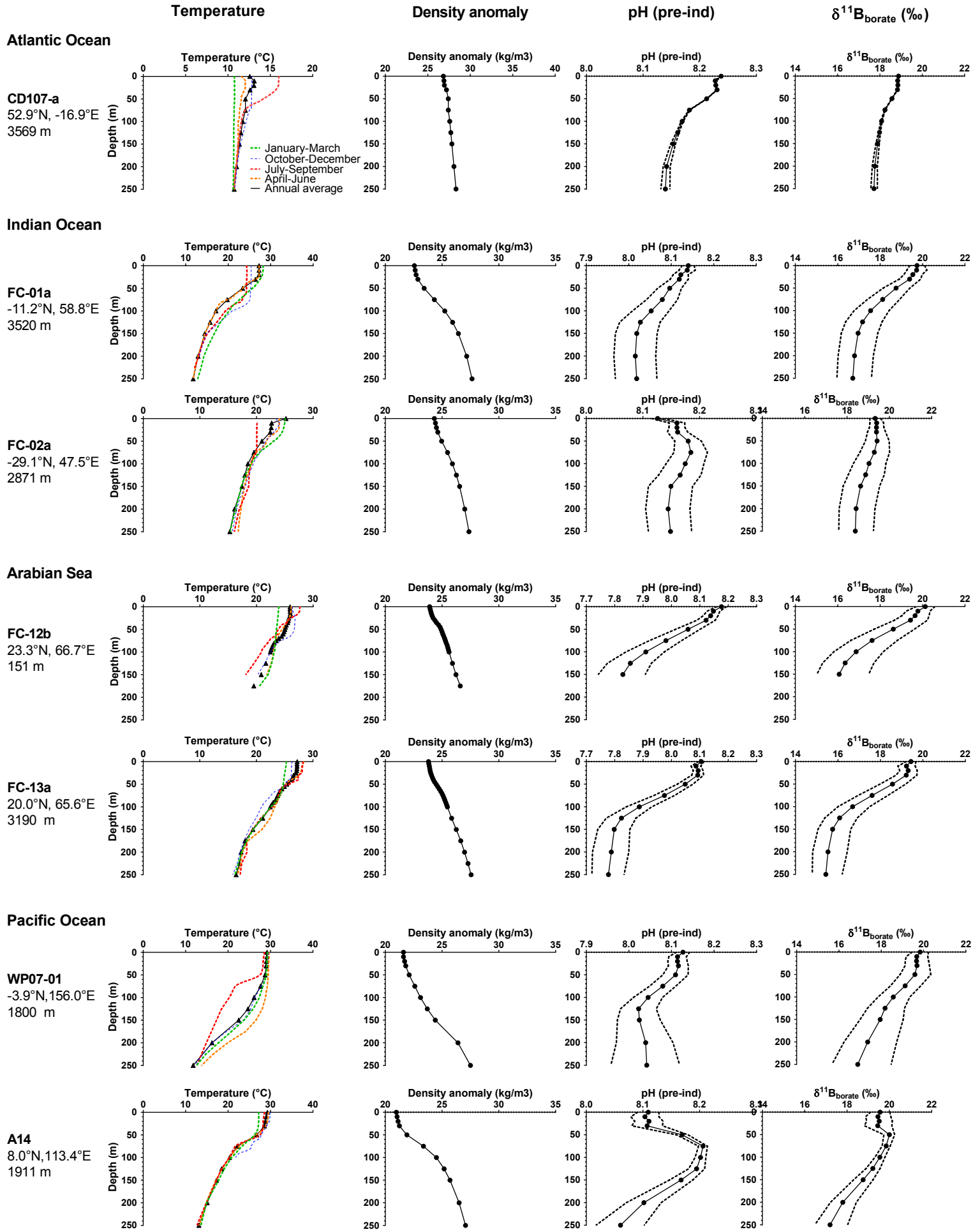
Temperature
Density anomaly
pH (pre-ind)
δ11Bborate (‰)
Atlantic Ocean
CD107-a
52.9°N, -16.9°E
3569 m
Indian Ocean
FC-01a
-11.2°N, 58.8°E
3520 m
FC-02a
-29.1°N, 47.5°E
2871 m
Arabian Sea
FC-12b
23.3°N, 66.7°E
151 m
FC-13a
20.0°N, 65.6°E
3190 m
Pacific Ocean
WP07-01
-3.9°N,156.0°E
1800 m
A14
8.0°N,113.4°E
1911 m
Temperature (°C)
Density anomaly (kg/m3)
pH (pre-ind)
δ11Bborate (‰)
Depth (m)
January-March
October-December
July-September
April-June
Annual average

Figure 4

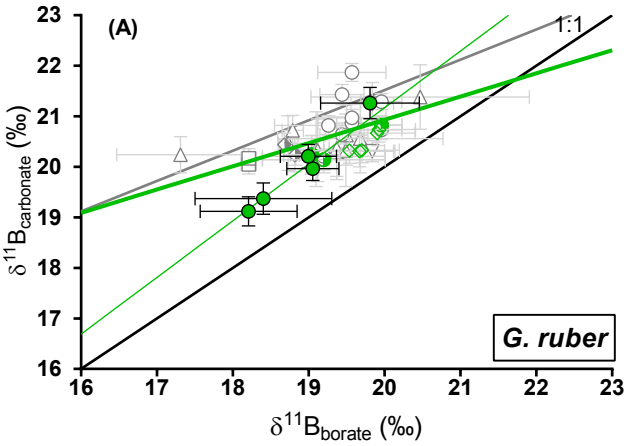

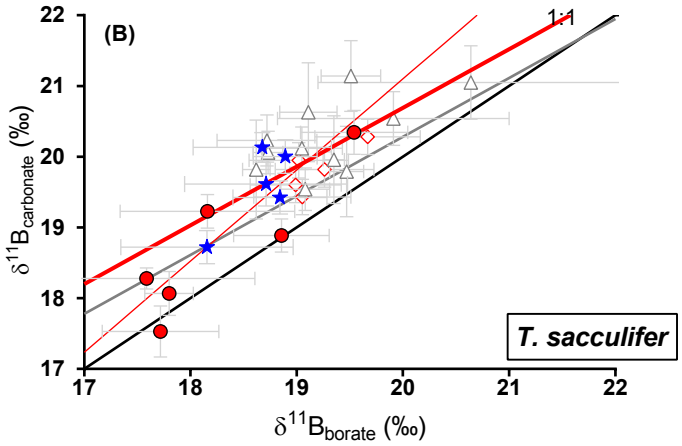

- $\delta^{11}B_{G.\ ruber}$ (core-top, this study)
- $\delta^{11}B_{G.\ ruber}$ (core-top, Foster et al., 2008)
- $\delta^{11}B_{G.\ ruber}$ (core-top, 250-300µm, Henehan et al., 2013)
- $\delta^{11}B_{G.\ ruber}$ (core-top, Henehan et al., 2013)
- $\delta^{11}B_{G.\ ruber}$ (sediment trap, Henehan et al., 2013)
- $\delta^{11}B_{G.\ ruber}$ (tow, Henehan et al., 2013)
- $\delta^{11}B_{G.\ ruber}$ (grab sample, Henehan et al., 2013)
- $\delta^{11}B_{G.\ ruber}$ (Raizsch et al., 2018)
- *G. ruber* calibration line (All data, this study)
- *G. ruber* calibration line (Core-top, this study)
- *G. ruber* calibration line (Culture, Henehan et al., 2013)

- $\delta^{11}B_{T.sacculifer\ (w/o\ sacc)}$ (core-top, this study)
- $\delta^{11}B_{T.\ sacculifer\ (w/o\ sacc)}$ (core-top, Raitzsch et al., 2018)
- $\delta^{11}B_{T.sacculifer\ (sacc)}$ (core-top, this study)
- $\delta^{11}B_{T.\ sacculifer\ (sacc)}$ (core-top, Foster et al., 2008)
- *T. sacculifer (w/o sacc and sacc)* calibration line (All data, this study)
- *T. sacculifer (w/o sacc and sacc)* calibration line (Core-top, this study)
- *T. sacculifer (s)* calibration line (Martinez-Boti et al., 2015)

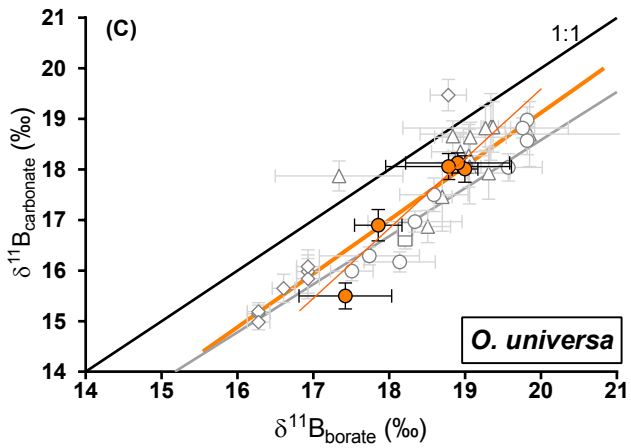

- $\delta^{11}B_{O.\ universa}$ (core-top, this study)
- $\delta^{11}B_{O.\ universa}$ (core-top, Henehan et al., 2016)
- $\delta^{11}B_{O.\ universa}$ (sediment trap, Henehan et al., 2016)
- $\delta^{11}B_{O.\ universa}$ (tow, Henehan et al., 2016)
- $\delta^{11}B_{O.\ universa}$ (core-top, Raitzsch et al., 2018)
- *O. universa* calibration line (core-top, this study)
- *O. universa* calibration line (this study,Henehan et al., 2016, Raitzsch et al., 2018)
- *O. universa* calibration line (wild, Henehan et al., 2016)

Figure 5

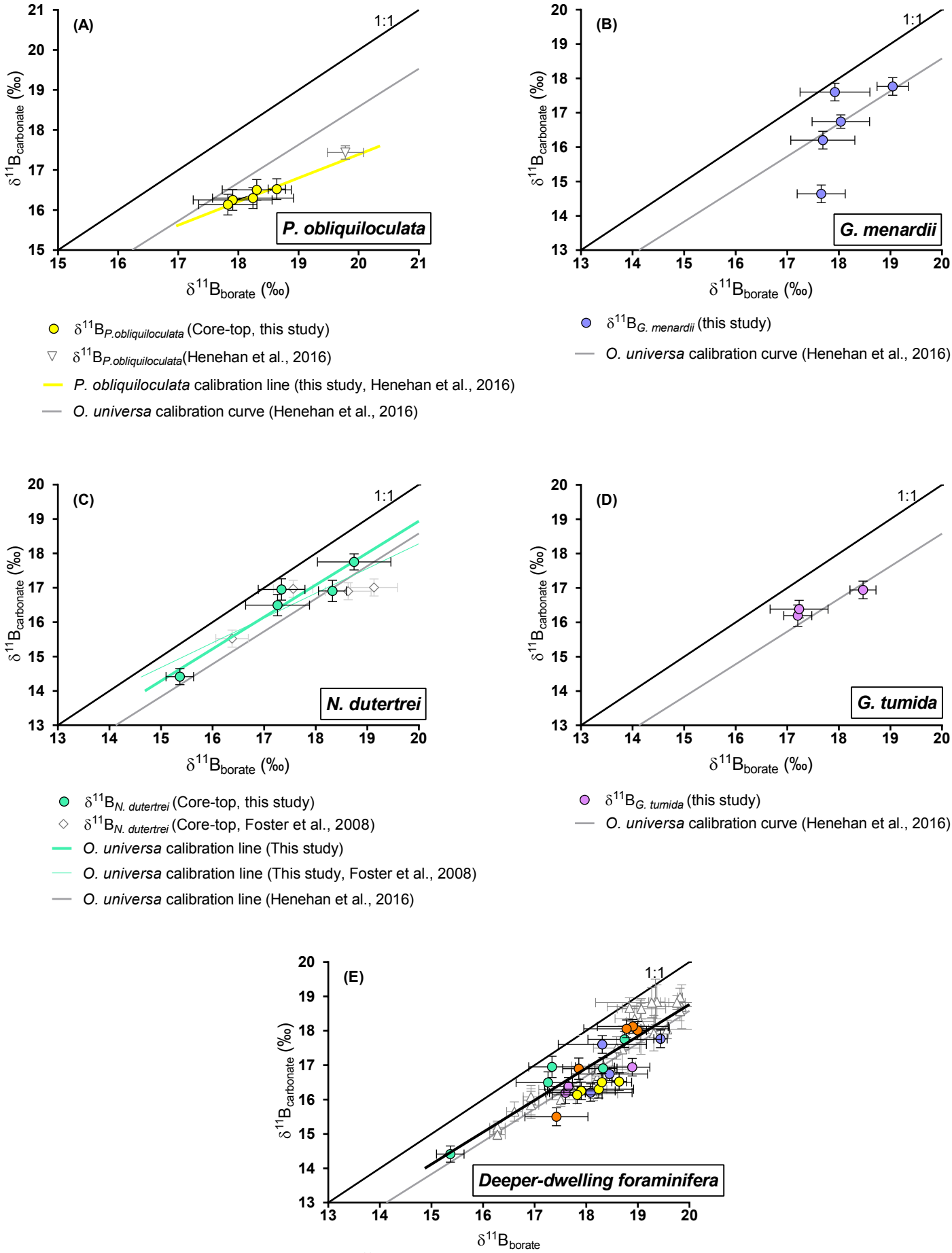
(A)
1:1
P. obliquiloculata
δ11Bcarbonate (‰)
δ11Bborate (‰)
δ11BP.obliquiloculata (Core-top, this study)
δ11BP.obliquiloculata (Henehan et al., 2016)
P. obliquiloculata calibration line (this study, Henehan et al., 2016)
O. universa calibration curve (Henehan et al., 2016)
(B)
1:1
G. menardii
δ11Bcarbonate (‰)
δ11Bborate (‰)
δ11BG. menardii (this study)
O. universa calibration curve (Henehan et al., 2016)
(C)
1:1
N. dutertrei
δ11Bcarbonate (‰)
δ11Bborate (‰)
δ11BN. dutertrei (Core-top, this study)
δ11BN. dutertrei (Core-top, Foster et al., 2008)
O. universa calibration line (This study)
O. universa calibration line (This study, Foster et al., 2008)
O. universa calibration line (Henehan et al., 2016)
(D)
1:1
G. tumida
δ11Bcarbonate (‰)
δ11Bborate (‰)
δ11BG. tumida (this study)
O. universa calibration curve (Henehan et al., 2016)
(E)
1:1
Deeper-dwelling foraminifera
δ11Bcarbonate (‰)
δ11Bborate
δ11BO.universa
δ11BP.obliquiloculata
δ11BN. dutertrei
δ11BG. menardii
δ11BG. tumida
δ11Bdeep-dweller from literature
Deep-dweller calibration line
O. universa calibration line (Henehan et al., 2016)

Figure 6

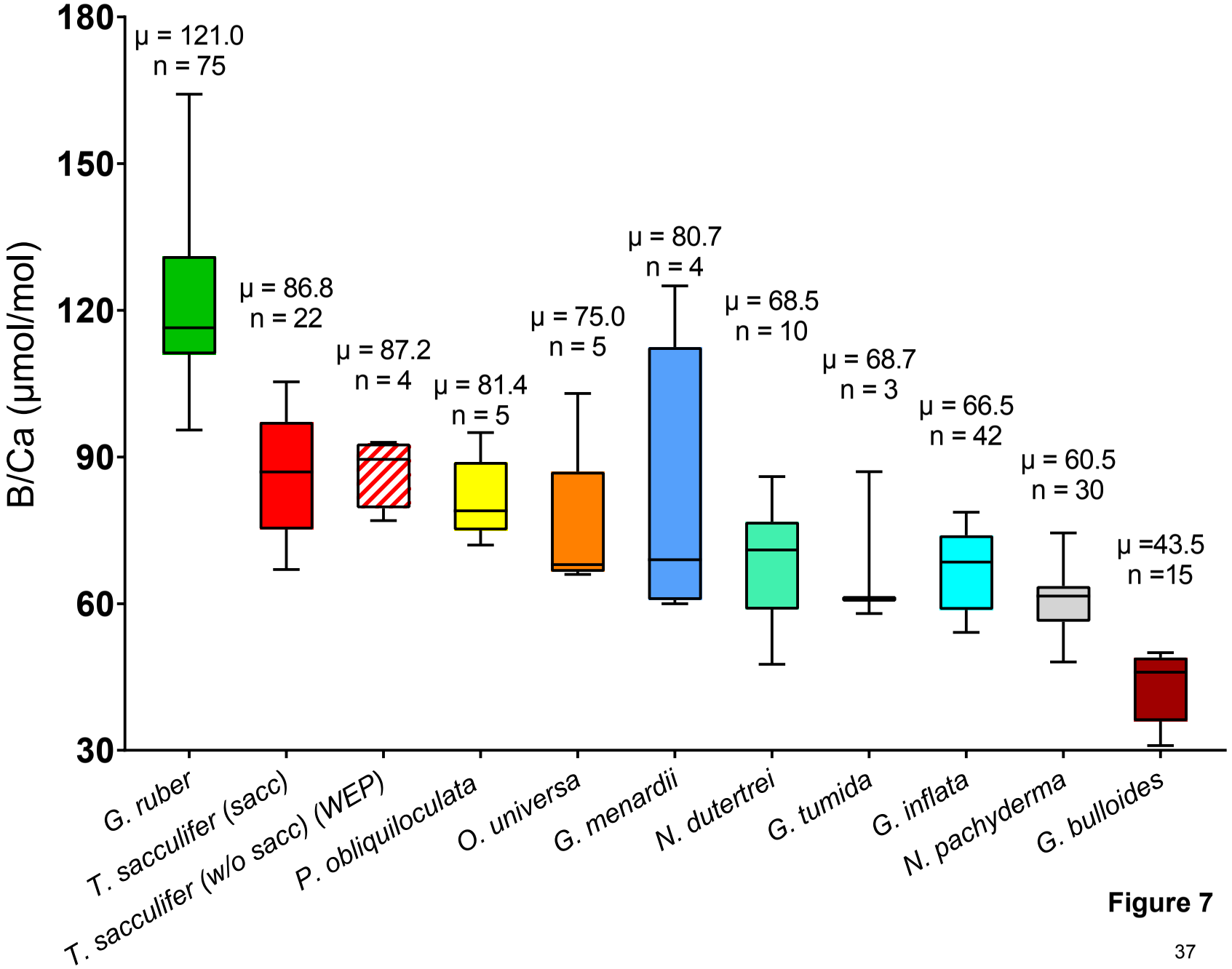
B/Ca (µmol/mol)
180
150
120
90
60
30
µ = 121.0
n = 75
µ = 86.8
n = 22
µ = 87.2
n = 4
µ = 81.4
n = 5
µ = 75.0
n = 5
µ = 80.7
n = 4
µ = 68.5
n = 10
µ = 68.7
n = 3
µ = 66.5
n = 42
µ = 60.5
n = 30
µ =43.5
n =15
G. ruber
T. sacculifer (sacc)
T. sacculifer (w/o sacc) (WEP)
P. obliquiloculata
O. universa
G. menardii
N. dutertrei
G. tumida
G. inflata
N. pachyderma
G. bulloides

Figure 7

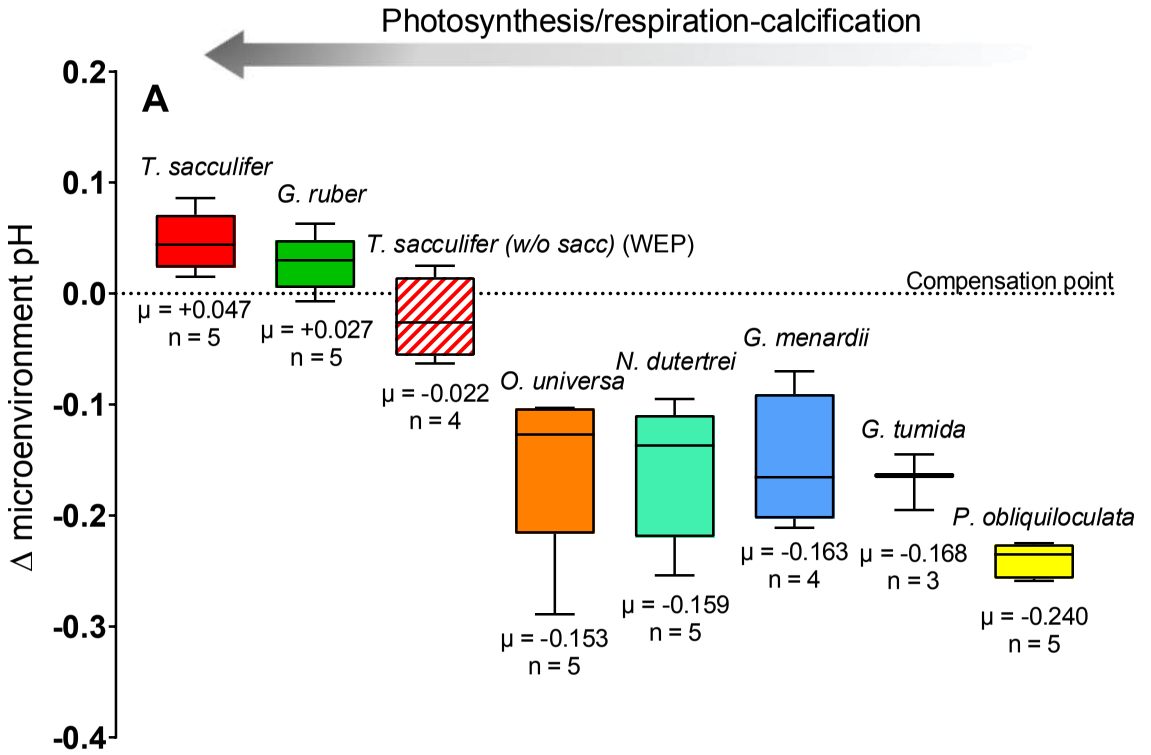
Photosynthesis/respiration-calcification
A
Δ microenvironment pH
0.2
0.1
0.0
-0.1
-0.2
-0.3
-0.4
T. sacculifer
μ = +0.047
n = 5
G. ruber
μ = +0.027
n = 5
T. sacculifer (w/o sacc) (WEP)
μ = -0.022
n = 4
Compensation point
O. universa
μ = -0.153
n = 5
N. dutertrei
μ = -0.159
n = 5
G. menardii
μ = -0.163
n = 4
G. tumida
μ = -0.168
n = 3
P. obliquiloculata
μ = -0.240
n = 5

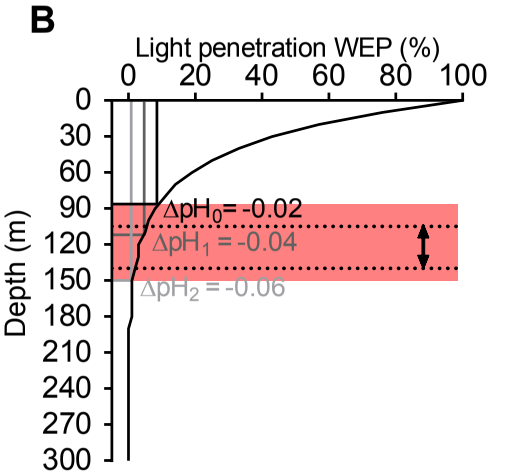
B
Light penetration WEP (%)
0
20
40
60
80
100
Depth (m)
0
30
60
90
120
150
180
210
240
270
300
ΔpH0 = -0.02
ΔpH1 = -0.04
ΔpH2 = -0.06

Figure 8

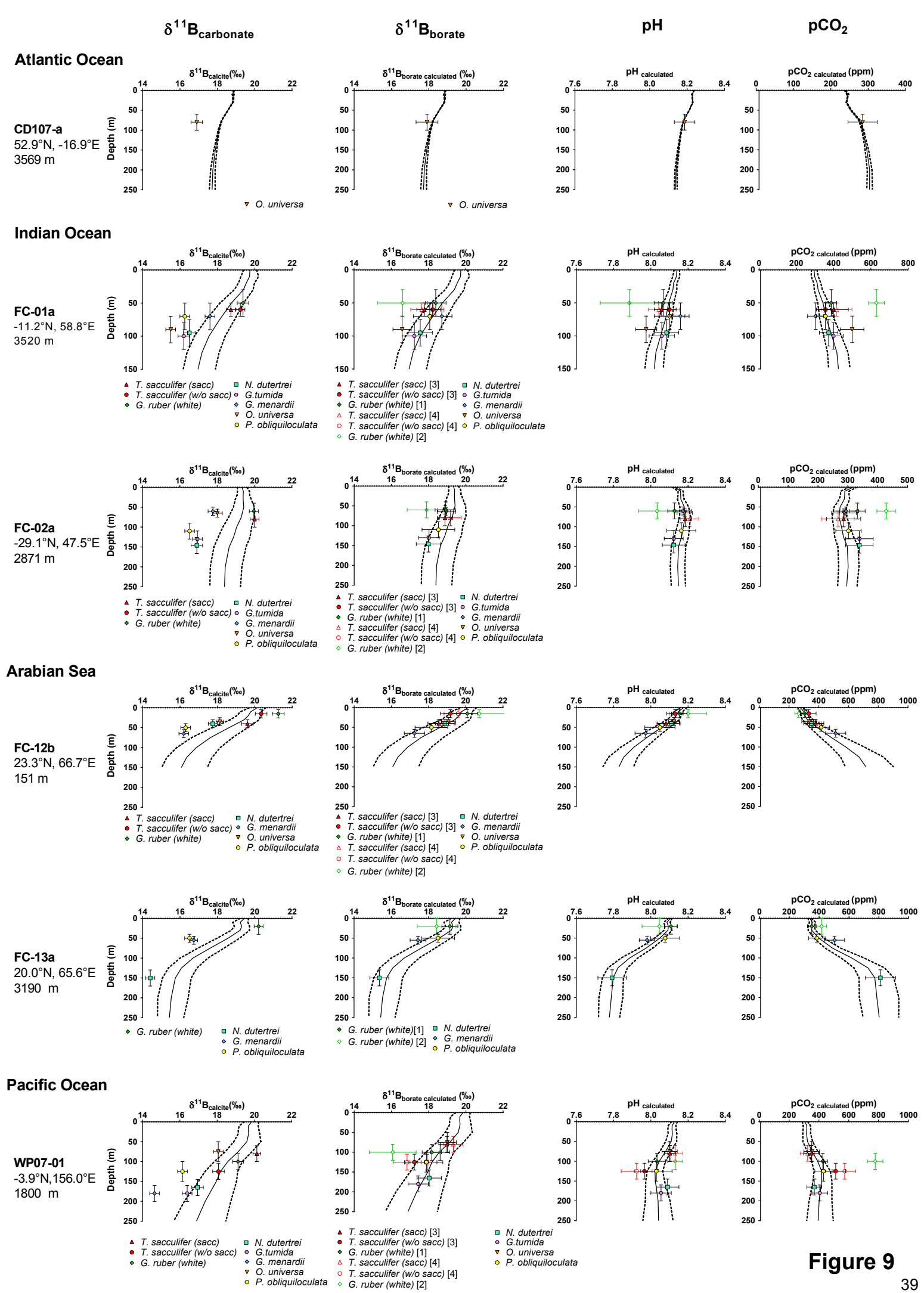
δ11Bcarbonate
δ11Bborate
pH
pCO2
Atlantic Ocean
CD107-a
52.9°N, -16.9°E
3569 m
Indian Ocean
FC-01a
-11.2°N, 58.8°E
3520 m
FC-02a
-29.1°N, 47.5°E
2871 m
Arabian Sea
FC-12b
23.3°N, 66.7°E
151 m
FC-13a
20.0°N, 65.6°E
3190 m
Pacific Ocean
WP07-01
-3.9°N,156.0°E
1800 m
Depth (m)
δ11Bcalcite(‰)
δ11Bborate calculated (‰)
pH calculated
pCO2 calculated (ppm)
T. sacculifer (sacc)
T. sacculifer (w/o sacc)
G. ruber (white)
N. dutertrei
G.tumida
G. menardii
O. universa
P. obliquiloculata
T. sacculifer (sacc) [3]
T. sacculifer (w/o sacc) [3]
G. ruber (white) [1]
T. sacculifer (sacc) [4]
T. sacculifer (w/o sacc) [4]
G. ruber (white) [2]

Figure 9

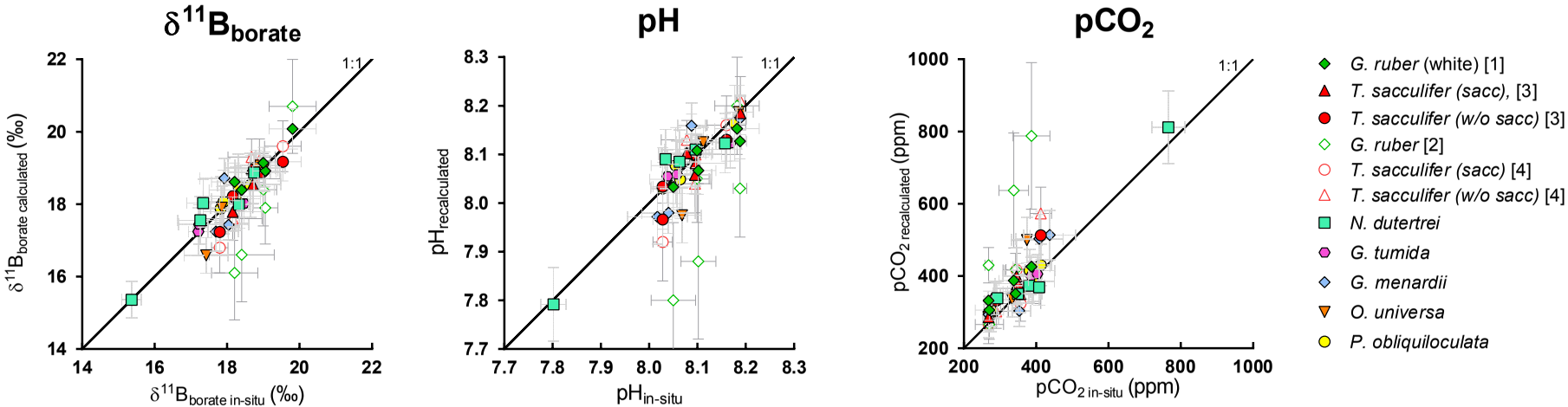
δ11Bborate
1:1
δ11Bborate calculated (‰)
δ11Bborate in-situ (‰)
22
20
18
16
14
pH
1:1
pHrecalculated
pHin-situ
8.3
8.2
8.1
8.0
7.9
7.8
7.7
pCO2
1:1
pCO2 recalculated (ppm)
pCO2 in-situ (ppm)
1000
800
600
400
200
G. ruber (white) [1]
T. sacculifer (sacc), [3]
T. sacculifer (w/o sacc) [3]
G. ruber [2]
T. sacculifer (sacc) [4]
T. sacculifer (w/o sacc) [4]
N. dutertrei
G. tumida
G. menardii
O. universa
P. obliquiloculata

Figure 10

Table 1

Label	Box-Core	Site	Latitude (N)	Longitude (E)	Depth (mbsl)	Oceanic Regime	Δ^{14}C age (year)
Atlantic Ocean							
CD107-a	CD107	A	52.92	-16.92	3569	non-upwelling	<3000[a]
Indian Ocean							
FC-01a	WIND-33B	I	-11.21	58.77	3520	non-upwelling	
FC-02a	WIND-10B	K	-29.12	47.55	2871	non-upwelling	7252 ± 27[b]
Arabian Sea							
FC-12b	CD145	A150	23.30	66.70	151	seasonal upwelling	
FC-13a	CD145	A3200	20.00	65.58	3190	seasonal upwelling	
Pacific Ocean							
WP07-01			-3.93	156.00	1800	non-upwelling	7.3-8.6[c]
A14			8.02	113.39	1911	non-upwelling	7.3-8.6[c]
806		A	0.32	159.36	2521	equatorial divergence	7.3-8.6[c]
807		A	3.61	156.62	2804	equatorial divergence	7.3-8.6[c]

[a] Thomson et al., 2000

[b] Wilson et al., 2012

[c] Age for core-top of site 806B from Lea et al., 2000

Table 2

Core	Species	Fraction size (µm)	Cleaning	$\delta^{13}C$* (‰)	$\delta^{18}O$* (‰)	$\delta^{11}Bc_1$ (‰)	$\delta^{11}Bc_2$ (‰)	$\delta^{11}B_{average}$** (‰)	Li/Ca*** (µmol/mol)	B/Ca*** (µmol/mol)	Mg/Ca*** (mmol/mol)	Mn/Ca*** (µmol/mol)	Fe/Ca*** (mmol/mol)
Atlantic Ocean													
CD107a	*O. universa*	>500	Ox-Red	1.99 ± 0.03	1.25 ± 0.11	16.85 ± 0.31 (2SD, nAE121=11)	16.95 ± 0.31 (2SD, nAE121=11)	16.90 ± 0.22	13.9 ± 0.4	68 ± 7	3.60 ± 0.01	13 ± 7	0.16 ± 0.01
Indian Ocean													
FC-01a	*G. ruber (white ss)*	250-300	Ox-Red	1.37 ± 0.03	-1.32 ± 0.11	19.33 ± 0.31 (2SD, nAE121=11)	19.41 ± 0.31 (2SD, nAE121=11)	19.37 ± 0.22	15.4 ± 0.4	109 ± 7	3.98 ± 0.01	10 ± 7	0.07 ± 0.01
FC-01a	*T. sacculifer (sacc)*	300-400	Ox-Red	1.88 ± 0.03	-2.20 ± 0.11	18.71 ± 0.24 (2SD, nAE121=10)	18.73 ± 0.24 (2SD, nAE121=10)	18.72 ± 0.17	12.1 ± 0.4	87 ± 7	3.45 ± 0.01	9 ± 7	0.03 ± 0.01
FC-01a	*T. sacculifer (w/o sacc)*	300-400	Ox-Red	2.02 ± 0.03	-1.05 ± 0.11	19.13 ± 0.24 (2SD, nAE121=10)	19.32 ± 0.24 (2SD, nAE121=10)	19.23 ± 0.17	12.1 ± 0.4	82 ± 7	3.42 ± 0.01	14 ± 7	0.03 ± 0.01
FC-01a	*O. universa*	>500	Ox-Red			15.50 ± 0.26 (2SD, nAE121=14)		15.50 ± 0.26					
FC-01a	*P. obliquiloculata*	300-400	Ox-Red	1 .00± 0.03	-0.55 ± 0.11	16.40 ± 0.26 (2SD, nAE121=14)	16.10 ± 0.26 (2SD, nAE121=14)	16.25 ± 0.18	15.4 ± 0.4	78 ± 7	2.06 ± 0.01	14 ± 7	0.05 ± 0.01
FC-01a	*G. menardii*	300-400	Ox-Red	1.64 ± 0.03	0.43 ± 0.11	17.52 ± 0.26 (2SD, nAE121=14)	17.69 ± 0.26 (2SD, nAE121=14)	17.60 ± 0.18	12.7 ± 0.4	63 ± 7	2.26 ± 0.01	8 ± 7	0.07 ± 0.01
FC-01a	*N. dutertrei*	300-400	Ox-Red	1.28 ± 0.03	-0.43 ± 0.11	16.40 ± 0.31 (2SD, nAE121=11)	16.59 ± 0.31 (2SD, nAE121=11)	16.50 ± 0.22	18.6 ± 0.4	73 ± 7	1.81 ± 0.01	11 ± 7	0.03 ± 0.01
FC-01a	*G. tumida*	300-400	Ox-Red	1.29 ± 0.03	-0.53 ± 0.11	16.21 ± 0.31 (2SD, nAE121=11)	16.18 ± 0.31 (2SD, nAE121=11)	16.20 ± 0.22	10.0 ± 0.4	61 ± 7	1.79 ± 0.01	11 ± 7	0.02 ± 0.01
FC-02a	*G. ruber (white ss)*	250-300	Ox-Red	0.30 ± 0.03	-1.40 ± 0.11	20.02 ± 0.24 (2SD, nAE121=10)	19.90 ± 0.24 (2SD, nAE121=10)	19.96 ± 0.17	18.2 ± 0.4	125 ± 7	3.47 ± 0.01	10 ± 7	0.07 ± 0.01
FC-02a	*T. sacculifer (sacc)*	300-400	Ox-Red	1.43 ± 0.03	-1.60 ± 0.11	20.07 ± 0.24 (2SD, nAE121=10)	19.93 ± 0.24 (2SD, nAE121=10)	20.00 ± 0.17	14.2 ± 0.4	106 ± 7	3.30 ± 0.01	10 ± 7	0.03 ± 0.01
FC-02a	*T. sacculifer (w/o sacc)*	300-400	Ox-Red	1.52 ± 0.03	-1.40 ± 0.11	23.23 ± 0.24 (2SD, nAE121=10)	23.22 ± 0.24 (2SD, nAE121=10)	23.22 ± 0.17	13.7 ± 0.4	106 ± 7	3.34 ± 0.01	10 ± 7	0.04 ± 0.01
FC-02a	*O. universa*	>500	Ox-Red	1.79 ± 0.03	0.02 ± 0.11	18.05 ± 0.26 (2SD, nAE121=14)	17.97 ± 0.26 (2SD, nAE121=14)	18.01 ± 0.18	14.8 ± 0.4	67 ± 7	4.40 ± 0.01	11 ± 7	0.05 ± 0.01
FC-02a	*P. obliquiloculata*	300-400	Ox-Red	0.34 ± 0.03	0.56 ± 0.11	16.35 ± 0.26 (2SD, nAE121=14)	16.69 ± 0.26 (2SD, nAE121=14)	16.52 ± 0.18	16.6 ± 0.4	83 ± 7	2.33 ± 0.01	7 ± 7	0.03 ± 0.01
FC-02a	*G. menardii*	300-400	Ox-Red	1.73 ± 0.03	-0.51 ± 0.11	17.77 ± 0.26 (2SD, nAE121=14)		17.77 ± 0.26	15.8 ± 0.4	125 ± 7	2.21 ± 0.01	17 ± 7	0.03 ± 0.01
FC-02a	*N. dutertrei*	300-400	Ox-Red	1.03 ± 0.03	-0.55 ± 0.11	16.78 ± 0.31 (2SD, nAE121=11)	17.03 ± 0.31 (2SD, nAE121=11)	16.91 ± 0.22	18.6 ± 0.4	82 ± 7	2.13 ± 0.01	13 ± 7	0.07 ± 0.01
FC-02a	*G. tumida*	300-400	Ox-Red	1.64 ± 0.03	-0.28 ± 0.11	16.93 ± 0.26 (2SD, nAE121=14)	16.95 ± 0.26 (2SD, nAE121=14)	16.94 ± 0.18	15.6 ± 0.4	87 ± 7	1.90 ± 0.01	17 ± 7	0.04 ± 0.01
Arabian Sea													
FC-12b	*G. ruber (white ss)*	250-300	Ox-Red	0.58 ± 0.03	-2.82 ± 0.11	21.30 ± 0.31 (2SD, nAE121=11)	21.23 ± 0.31 (2SD, nAE121=11)	21.26 ± 0.22	19.5 ± 0.4	164 ± 7	5.76 ± 0.01	14 ± 7	0.16 ± 0.01
FC-12b	*G. sacculifer (s)*	300-400	Ox-Red	1.76 ± 0.03	-2.15 ± 0.11	19.65 ± 0.31 (2SD, nAE121=11)	19.57 ± 0.31 (2SD, nAE121=11)	19.61 ± 0.22	14.6 ± 0.4	101 ± 7	4.28 ± 0.01	17 ± 7	0.14 ± 0.01
FC-12b	*T. sacculifer (w/o sacc)*	300-400	Ox-Red	1.97 ± 0.03	-2.19 ± 0.11	20.32 ± 0.31 (2SD, nAE121=11)	20.37 ± 0.31 (2SD, nAE121=11)	20.34 ± 0.22	16.7 ± 0.4	116 ± 7	4.90 ± 0.01	20 ± 7	0.26 ± 0.01
FC-12b	*O. universa*	>500	Ox-Red	1.89 ± 0.03	-1.59 ± 0.11	18.13 ± 0.20 (2SD, nAE121=6)		18.13 ± 0.20	13.6 ± 0.4	103 ± 7	6.91 ± 0.01	10 ± 7	0.06 ± 0.01
FC-12b	*P. obliquiloculata*	300-400	Ox-Red	0.5 ± 0.03	-1.58 ± 0.11	16.45 ± 0.26 (2SD, nAE121=14)	16.15 ± 0.26 (2SD, nAE121=14)	16.30 ± 0.18	16.7 ± 0.4	95 ± 7	3.61 ± 0.01	69 ± 7	0.38 ± 0.01
FC-12b	*G. menardii*	300-400	Ox-Red	1.05 ± 0.03	-0.97 ± 0.11	16.2 ± 0.26 (2SD, nAE121=14)		16.20 ± 0.26	14.8 ± 0.4	75 ± 7	3.44 ± 0.01	52 ± 7	0.17 ± 0.01
FC-12b	*N. dutertrei*	300-400	Ox-Red	1.35 ± 0.03	-1.57 ± 0.11	17.77 ± 0.24 (2SD, nAE121=10)	17.73 ± 0.24 (2SD, nAE121=10)	17.75 ± 0.17	17.1 ± 0.4	75 ± 7	3.25 ± 0.01	46 ± 7	0.25 ± 0.01
FC-13a	*G. ruber (white ss)*	250-300	Ox-Red	0.08 ± 0.03	-3.71 ± 0.11	20.27 ± 0.24 (2SD, nAE121=10)	20.15 ± 0.24 (2SD, nAE121=10)	20.21 ± 0.17	16.4 ± 0.4	147 ± 7	4.52 ± 0.01	13 ± 7	0.08 ± 0.01
FC-13a	*T. sacculifer (w/o sacc)*	300-400	Ox-Red	1.59 ± 0.03	-2.46 ± 0.11	17.85 ± 0.29 (2SD, nAE121=12)		17.85 ± 0.29	15.7 ± 0.4	121 ± 7	5.49 ± 0.01	21 ± 7	0.49 ± 0.01
FC-13a	*P. obliquiloculata*	300-400	Ox-Red	0.00 ± 0.03	-0.97 ± 0.11	16.51 ± 0.26 (2SD, nAE121=14)	16.50 ± 0.26 (2SD, nAE121=14)	16.51 ± 0.18	18.7 ± 0.4	79 ± 7	4.43 ± 0.01	30 ± 7	0.43 ± 0.01
FC-13a	*G. menardii*	300-400	Ox-Red	0.75 ± 0.03	-1.07 ± 0.11	16.74 ± 0.20 (2SD, nAE121=6)		16.74 ± 0.20	9.2 ± 0.4	60 ± 7	1.99 ± 0.01	19 ± 7	0.07 ± 0.01
FC-13a	*N. dutertrei*	300-400	Ox-Red	0.71 ± 0.03	-1.41 ± 0.11	14.43 ± 0.24 (2SD, nAE121=10)	14.40 ± 0.24 (2SD, nAE121=10)	14.41 ± 0.17	15.7 ± 0.4	69 ± 7	1.98 ± 0.01	15 ± 7	0.06 ± 0.01
Pacific Ocean													
WP07-a	*G. ruber (white ss)*	250-400	Ox-Red			19.12 ± 0.29 (2SD, nAE121=12)		19.12 ± 0.29	14.5 ± 0.4	144 ± 7	4.32 ± 0.01	15 ± 7	0.16 ± 0.01
WP07-a	*T. sacculifer (sacc)*	250-400	Ox-Red			20.13 ± 0.21 (2SD, nAE121=11)		20.13 ± 0.21	12.7 ± 0.4	92 ± 7	4.44 ± 0.01	22 ± 7	0.05 ± 0.01
WP07-a	*T. sacculifer (w/o sacc)*	250-400	Ox-Red			18.10 ± 0.31 (2SD, nAE121=11)	18.04 ± 0.31 (2SD, nAE121=11)	18.07 ± 0.22	12.3 ± 0.4	192 ± 7	4.51 ± 0.01	21 ± 7	0.08 ± 0.01
WP07-a	*O.universa*	500-630	Ox-Red			18.13 ± 0.26 (2SD, nAE121=14)	17.99 ± 0.26 (2SD, nAE121=14)	18.06 ± 0.18	11.9 ± 0.4	71 ± 7	7.52 ± 0.01	11 ± 7	0.02 ± 0.01
WP07-a	*P. obliquiloculata*	250-400	Ox-Red			16.08 ± 0.26 (2SD, nAE121=14)	16.19 ± 0.26 (2SD, nAE121=14)	16.14 ± 0.18	13.4 ± 0.4	72 ± 7	3.02 ± 0.01	7 ± 7	0.03 ± 0.01
WP07-a	*G. menardii*	250-400	Ox-Red			14.74 ± 0.26 (2SD, nAE121=14)	14.53 ± 0.26 (2SD, nAE121=14)	14.64 ± 0.18	13.5 ± 0.4	85 ± 7	2.68 ± 0.01	26 ± 7	0.08 ± 0.01
WP07-a	*N. dutertrei*	250-400	Ox-Red			16.91 ± 0.31 (2SD, nAE121=11)	16.99 ± 0.31 (2SD, nAE121=11)	16.95 ± 0.22	21.7 ± 0.4	86 ± 7	3.66 ± 0.01	42 ± 7	0.63 ± 0.01
WP07-a	*G. tumida*	250-400	Ox-Red			16.45 ± 0.26 (2SD, nAE121=14)	16.32 ± 0.26 (2SD, nAE121=14)	16.39 ± 0.18	10.6 ± 0.4	58 ± 7	2.55 ± 0.01	16 ± 7	0.10 ± 0.01
806A	*T. sacculifer (w/o sacc)*	250-400	Ox-Red			17.53 ± 0.36 (2SD, nAE121=11)		17.53 ± 0.36	14.40 ± 0.4	77 ± 7	3.89 ± 0.01	7 ± 7	0.15 ± 0.01
807A	*T. sacculifer (w/o sacc)*	250-400	Ox-Red			18.38 ± 0.21 (2SD, nAE121=11)	18.17 ± 0.21 (2SD, nAE121=11)	18.28 ± 0.15	12.54 ± 0.4	87 ± 7	4.24 ± 0.01	17 ± 7	0.09 ± 0.01
A14	*G. ruber (white ss)*	250-400	Ox-Red			18.91 ± 0.24 (2SD, nAE121=10)	19.17 ± 0.24 (2SD, nAE121=10)	19.04 ± 0.17					
A14	*T. sacculifer (sacc)*	250-400	Ox-Red			19.53 ± 0.24 (2SD, nAE121=10)	19.32 ± 0.24 (2SD, nAE121=10)	19.42 ± 0.17	12.0 ± 0.4	102 ± 7	3.91 ± 0.01	22 ± 7	0.02 ± 0.01
A14	*T. sacculifer (w/o sacc)*	250-400	Ox-Red			18.93 ± 0.24 (2SD, nAE121=10)	18.84 ± 0.24 (2SD, nAE121=10)	18.88 ± 0.17	12.3 ± 0.4	93 ± 7	3.76 ± 0.01	25 ± 7	0.06 ± 0.01
A14	*O. universa*	500-560	Ox-Red			17.33 ± 0.26 (2SD, nAE121=14)	17.08 ± 0.26 (2SD, nAE121=14)	17.20 ± 0.18	11.3 ± 0.4	66 ± 7	6.59 ± 0.01	10 ± 7	0.02 ± 0.01
A14	*N. dutertrei*	250-400	Ox-Red			14.39 ± 0.31 (2SD, nAE121=11)		14.39 ± 0.31	16.9 ± 0.4	75 ± 7	1.99 ± 0.01	35 ± 7	0.04 ± 0.01

* uncertainties given in 1SD (see text)

** When two measurements were carried out uncertaity was calculated with $\Delta a = \sqrt{(1/\sum_i(1/\Delta_{ai})^2)}$; with only one measurement the error was determined on reproducibility of the AE121 standard

***Uncertainty given in 2SD , calculated on the reproducibility of CamWuellestorfi (see text and table S3, ref in Misra et al., 2014)

Table 3

Species	Size fraction (µm)	Material	Instrument (original)	Regression method	$\delta^{11}B_{borate}= f(\delta^{11}B_{calcite})$	n	Calibration number	Reference
G. ruber	~380	Culture/core tops/plankton tows	MC-ICP-MS		$\delta^{11}B_{borate}=[\delta^{11}B_{calcite} - 9.52 (\pm2.02)]/0.6 (\pm0.11)$			Henehan et al., 2013
G. ruber	315-355	Core-tops	MC-ICP-MS		$\delta^{11}B_{borate}=[\delta^{11}B_{calcite} - 11.78 (\pm3.20)]/0.45 (\pm0.16)$			Raitzsch et al., 2018
T. sacculifer	n.d.	Culture/artificial seawater enriched in B	N-TIMS		$\delta^{11}B_{borate}=[\delta^{11}B_{calcite} - 3.94 (\pm4.02)]/0.82 (\pm0.22)$			Sanyal et al., 2001 refitted Martinez-Boti et al., 2015
T. sacculifer	315-355	Core-tops	MC-ICP-MS		$\delta^{11}B_{borate}=[\delta^{11}B_{calcite} - 8.86 (\pm5.27)]/0.59 (\pm0.21)$			Raitzsch et al., 2018
O. universa	no effect	Core-tops/plankton tows/sediment traps	MC-ICP-MS		$\delta^{11}B_{borate}=[\delta^{11}B_{calcite} + 0.42 (\pm2.85)]/0.95 (\pm0.17)$			Henehan et al., 2016
O. universa	>425	Core-tops	MC-ICP-MS		$\delta^{11}B_{borate}=[\delta^{11}B_{calcite} + 5.69 (\pm7.51)]/1.26 (\pm0.39)$			Raitzsch et al., 2018
G. bulloides	300-355	Core-top/sediment trap	MC-ICP-MS		$\delta^{11}B_{borate}=[\delta^{11}B_{calcite} + 3.440 (\pm4.584)]/1.074 (\pm0.252)$			Martinez-Boti et al., 2015
G. bulloides	315-355	Core-tops	MC-ICP-MS		$\delta^{11}B_{borate}=[\delta^{11}B_{calcite} + 3.81 (\pm13.17)]/1.13 (\pm0.72)$			Raitzsch et al., 2018
N. pachyderma	150-200	Core-tops	MC-ICP-MS		$\delta^{11}B_{borate}= \delta^{11}B_{calcite} + 3.38$			Yu et al., 2013
G. ruber	250-400	Core-tops	MC-ICP-MS	Bootstrap	$\delta^{11}B_{borate}=[\delta^{11}B_{calcite} + 1.23 (\pm0.59)]/1.12 (\pm1.67)$	5	**1**	This study
G. ruber	250-400	Core-tops	MC-ICP-MS	Bootstrap	$\delta^{11}B_{borate}=[\delta^{11}B_{calcite} - 11.73 (\pm0.83)]/0.46 (\pm0.34)$	40	**2**	This study; Foster et al., 2008; Henehan et al., 2016; Raitzsch et al., 2018
T. sacculifer (sacc and w/o sacc)	250-400	Core-tops	MC-ICP-MS	Bootstrap	$\delta^{11}B_{borate}=[\delta^{11}B_{calcite} + 6.06 (\pm 0.25)/1.38 (\pm 1.33)$	11	**3**	This study
T. sacculifer (sacc and w/o sacc)	250-400	Core-tops	MC-ICP-MS	Bootstrap	$\delta^{11}B_{borate}=[\delta^{11}B_{calcite} - 4.09 (\pm0.86)]/0.83 (\pm0.48)$	27	**4**	This study; Foster et al., 2008; Raitzsch et al., 2018
N. dutertrei	300-400	Core-tops	MC-ICP-MS	Bootstrap	$\delta^{11}B_{borate}=[\delta^{11}B_{calcite} - 0.34 (\pm1.83)]/0.93 (\pm0.55)$	5	**5**	This study
N. dutertrei	300-400	Core-tops	MC-ICP-MS	Bootstrap	$\delta^{11}B_{borate}=[\delta^{11}B_{calcite} - 3.88 (\pm0.65)]/0.72 (\pm0.74)$	9	**6**	This study; Foster et al., 2008
O. universa	400-600	Core-tops	MC-ICP-MS	Bootstrap	$\delta^{11}B_{borate}=[\delta^{11}B_{calcite} + 8.01 (\pm23)]/1.38 (\pm2.67)$	5	**7**	This study
O. universa	400-600	Core-tops	MC-ICP-MS	Bootstrap	$\delta^{11}B_{borate}=[\delta^{11}B_{calcite} + 2.08 (\pm0.59)]/1.06 (\pm0.13)$	36	**8**	This study; Henehan et al., 2016; Raitzsch et al., 2018
G. menardii	400-600	Core-tops	MC-ICP-MS	Bootstrap	$\delta^{11}B_{borate}=[\delta^{11}B_{calcite} - 5.36 (\pm1.36)]/0.65 (\pm0.76)$	5	**9**	This study
G. tumida	400-600	Core-tops	MC-ICP-MS	Bootstrap	$\delta^{11}B_{borate}=[\delta^{11}B_{calcite} - 6.33 (\pm2.52)]/0.57 (\pm1.2)$	3	**10**	This study
P. obliquiloculata	300-400	Core-tops	MC-ICP-MS	Bootstrap	$\delta^{11}B_{borate}=[\delta^{11}B_{calcite} - 5.59 (\pm4.16)]/0.59(\pm0.65)$	6	**11**	This study; Henehan et al., 2016
Deep-dweller	300-600	Core-tops	MC-ICP-MS	Bootstrap	$\delta^{11}B_{borate}=[\delta^{11}B_{calcite} -1.99 (\pm0.13)]/0.82 (\pm0.27)$	22	**12**	This study
Deep-dweller	300-600	Core-tops	MC-ICP-MS	Bootstrap	$\delta^{11}B_{borate}=[\delta^{11}B_{calcite} - 0.18 (\pm0.6)]/0.95 (\pm0.13)$	54	**13**	This study; Foster et al., 2008; Henehan et al., 2016; Raitzsch et al., 2018

Supplemental information

Seawater pH reconstruction using boron isotopes in multiple planktonic foraminifera species with different depth habitats and their potential to constrain pH and pCO_2 gradients

Maxence Guillermic[1,2], Sambuddha Misra[3,4], Robert Eagle[1,2], Alexandra Villa[2,5], Fengming Chang[6], Aradhna Tripati [1,2]

[1] Department of Earth, Planetary, and Space Sciences, Department of Atmospheric and Oceanic Sciences, Institute of the Environment and Sustainability, UCLA, University of California – Los Angeles, Los Angeles, CA 90095 USA
[2] Laboratoire Géosciences Océan UMR6538, UBO, Institut Universitaire Européen de la Mer, Rue Dumont d'Urville, 29280, Plouzané, France
[3] Indian Institute of Science, Centre for Earth Sciences, Bengaluru, Karnataka 560012, India
[4] The Godwin Laboratory for Palaeoclimate Research, Department of Earth Sciences, University of Cambridge, UK
[5] Department of Geology, University of Wisconsin-Madison, Madison, WI 53706 USA
[6] Key Laboratory of Marine Geology and Environment, Institute of Oceanology, Chinese Academy of Sciences, Qingdao 266071, China

Submitted to Biogeosciences

*Corresponding author:
E-mail address: maxence.guillermic@gmail.com

Supplemental Figures

Figure S1: An example of the impact of seasonality on results. Based on data from GLODAP used for site FC13-a. Seasonality has less of an impact that a change in the depth habitats.

Figure S2: Figure showing the offset $\Delta^{11}B=\delta^{11}B_{carbonate}-\delta^{11}B_{borate}$ versus calcification depth, red symbols are from Arabian Sea, green from Indian Ocean and Blue from the WEP, blue with black line symbols are data from site A14. This figure highlights a decrease of $\delta^{11}B_{carbonate}$ for *T. sacculifer* and *G. ruber* with a deeper depth habitat.

Figure S3: Multi-panels figure showing the correlation between B/Ca and boron geochemistry and different variables. A to C show comparison of B/Ca and A) $[B(OH)_4^-]/[HCO_3^-]$, B) $\delta^{11}B_{carbonate}$ and C) temperature. Panel D) shows the correlation between $\delta^{11}B_{carbonate}$ and temperature. Symbol in brackets is high B/Ca; this point is included in the linear regressions. Linea regression (LR - black line) is when compiling *G. ruber* and *T. sacculifer*, LR of *G. ruber* (dotted line green), *T. sacculifer* (red line – $p<0.05$), *T. sacculifer* (w/o sacc – red dotted line).

Figure S4: Boron geochemistry against water depth. A) $\delta^{11}B_{carbonate}$ versus water depth, B) B/Ca against water depth and C) $\delta^{11}B_{carbonate}$ versus calcification depth and linear regressions for *G. ruber*, *T. sacculifer* (w/o sacc), *T. sacculifer* (sacc) and *O. universa*.

Figure S5: Figure evaluating the circularity of our reconstructions. It is showing in the y-axis the difference between reconstruction utilizing calibrations derive from the entire dataset and compare to *in-situ* values and in the x-axis the difference between the reconstruction utilizing the species-specific calibrations derived excluding the site of interest (no circularity) compared to *in-situ* values. Results show that difference is not significant between the two reconstruction methods (e.g. following the 1:1 line), validating the method and the calibrations.

Supplemental Tables

Table S1: Elemental ratios of multi-elemental standards utilized in this study.

Table S2: Reproducibility of boron isotope standards.

Table S3: Reproducibility of elemental ratios for CamWuellestorfi standard.

Table S4: Seasonality of foraminifera utilized in this study.

Table S5: Mg/Ca-T calibrations used for reconstructions and $\delta^{18}O_w$-T calibrations used for calcification depth reconstructions.

Table S6: Calcification depth (CD) calculations from $\delta^{18}O$ (CD1), Mg/Ca (CD2) and literature (CD3).

Table S7: Pre-industrial in-situ parameters estimated using calcification depths for each species and calculated parameters based on analytical results.

Trace element standards

A series of multi-element standards (Table S1) with fixed Ca concentration and variable B, Mg, Sr, Mn, Ba, Zn, Cd, U, Li, Al and Fe concentrations were prepared for elemental ratios analysis in Brest following the method developed by Yu et al., (2005). Multi-element stock standard mixtures were prepared gravimetrically by spiking a 10,000 ppm Ca standard with appropriate amounts of Li, B, Al, Mn, Zn, Sr, Cd and U mono-elemental 1,000 ppm (SCP Science). They were diluted with OPTIMA grade HNO_3 acid and 18.2 MΩ.cm-1water to reach a 0.28M HNO_3 final solution. The stock standards (1500 ppm Ca) were prepared in 500mL cleaned PFA bottles. Working standards were made by diluting the stock solutions to a final concentration of 100 ppm Ca. The multi-element standards were calibrated at the University of Cambridge, elemental ratios are presented in Table S1. An external standard CamWuellestorfi (Misra et al., 2014a) was used in Brest for cross-calibration and reproducibility (Table S3).

Potential contaminations

Possible contamination of samples due to presence of silicate minerals was monitored with the Fe/Mg ratio. Samples with Fe/Mg > 0.1 mol/mol would be rejected due to potential contamination by silicate minerals (Barker et al., 2003). Samples (site E035 excluded) have an average Fe/Mg of 0.03 ± 0.05 mol/mol (2SD, n=42), meaning that silicate minerals have been efficiently removed during our cleaning.

Contribution of Mn-Fe-oxide coatings to Mg/Ca ratio has been calculated to be 0.5 µmol/mol Mg/Ca (change for 5 µmol/mol Mn/Ca ratio Barker et al., 2003). The maximum Mn/Ca ratio in our samples is 89 µmol/mol which can lead to a potential contribution of ~9 µmol/mol Mg/Ca or in other words a decrease of 0.1°C in our reconstructed temperatures. However, the calibration error is much larger and is estimated to be ~1.4°C (Dekens et al., 2002). The range in Mn/Ca values in our samples is 0.021 ± 0.033 mmol/mol (2SD, n=42) which allows us to not be ignore *Mn-Fe-oxide* coating related complications. Additionally, no correlations were found between Mg/Ca and Fe/Ca (R^2=0.006) or with Mn/Ca (R^2=0.008), and between B/Ca ratio and Mn/Ca (R^2=0.003) or Fe/Ca (R^2=0.062) ratios.

Contamination by clays was monitored with Ti/Ca calculated from blank corrected intensities. Al/Ca ratios were not reliable as we are using an alumina injector for HF matrix in our lab. A minor correlation was found between Ti/Ca and Mg/Ca (R^2=0.1388) but none with B/Ca (R^2=0.0887).

Calcification depth determination

The first approach involves comparing measured $\delta^{18}O_c$ with theoretical predictions of $\delta^{18}O_c$ based on vertical profiles of temperature and the $\delta^{18}O$ of seawater ($\delta^{18}O_w$). We assume $\delta^{18}O_c$ is in equilibrium with seawater. First, $\delta^{18}O_w$ was calculated using location-specific $\delta^{18}O_w$-salinity relationships and salinity profiles. We used salinity values from the World Ocean Atlas database (Boyer et al., 2013). Oxygen isotopes may be affected by both temperature and salinity. As our sites present different hydrographic settings and freshwater inputs, location-specific $\delta^{18}O_w$-salinity relationship relationships are utilized for accurate $\delta^{18}O_w$ reconstructions. For Site CD107-a, we used a $\delta^{18}O_w$-salinity relationship of 0.56*S-19.3 (Duplessy et al., 1991). For FC01-a and FC02-a, we used a $\delta^{18}O_w$-salinity relationship of 0.24*S-7.8 (Sime et al., 2005), and for FC13-a and FC12-b, we used a $\delta^{18}O_w$-salinity relationship of 0.28*S-9.24-0.27 (Rosteket al., 1993). Then, we used the calculated ambient $\delta^{18}O_w$ in concert with: (1) temperature profiles from the World Ocean Atlas database (Boyer et al., 2013), and (2) published calcite-water oxygen isotope fractionation factors, to calculate theoretical values for $\delta^{18}O_c$. Species-

specific relationships were used when available, including for *T. sacculifer* (Mulitza et al., 2003), *G. ruber* (Mulitza et al., 2003), and *O. universa* (Bemis et al., 2002, medium light). For all other, species we used the calcite equation from Kim and O'Niel (1997), adapted to a quadratic form by Bemis et al., (1998) following the approach of Sime et al., (2005). To take into account the ecology of each species, theoretical $\delta^{18}O_c$ profiles were made for the season of maximum abundance (Table S4). Therefore spring and summer profiles were used for *T. sacculifer*, summer profiles used for *G. ruber*, and winter and annual average profiles was used for *N. dutertrei.* Annual average profiles were used for the other species.

For the two sites WP07-1 and A14, a different approach was necessary because $\delta^{18}O_c$ data is sparse. At these sites, and for our other sites, we utilized Mg/Ca-derived temperatures to estimate calcification depths (Table S6). $T_{Mg/Ca}$ was derived using species-specific Mg/Ca-temperature calibrations (Table S6) along with the Mg/Ca ratios determined in this study. Calcification depth was estimated by comparing $T_{Mg/Ca}$ to modern temperature profiles from the World Ocean atlas database 2013 (Boyer et al., 2013) in light of the ecology (seasonality of growth) of the species of interest. A caveat is that in certain cases $T_{Mg/Ca}$ may be partially biased by a carbonate ion effect or salinity effect (Russell et al., 2004; Elderfield et al., 2006; Ferguson et al., 2008; Arbuszewski et al., 2010; Martinez-Boti et al., 2011). These artifacts on $T_{Mg/Ca}$ may be significant at high-latitude sites such as CD107-a which is located in the North Atlantic Ocean.

Depth habitat

Planktonic foraminifera live in the upper 500 m of the water column. Their preferred depth habitat depends on their ecology, which in turn relies on the hydrographic conditions. For example, *G. ruber is* commonly found in the mixed layer (Fairbanks and Wiebe, 1980; Dekens et al., 2002; Farmer et al., 2007) during summer (Deuser et al., 1981) whereas *T. sacculifer* (n or ns) is present in the mixed layer until the mid-thermocline depth (Farmer et al., 2007) during spring and summer (Deuser et al., 1981, 1989). Specimens of *P. obliquiloculata* and *N. dutertrei* are found during winter (Deuser et al., 1989), in the mixed layer (~60m) for *P. obliquiloculata*, and at mid-thermocline depth for *N. dutertrei* (Farmer et al., 2007). Whereas, *O. universa* tends to record annual average conditions and is living within the mixed layer. Specimens of *G .menardii* calcify within the seasonal thermocline (Fairbanks et al., 1982, Farmer et al., 2007, Regenberg et al., 2009) even upper thermocline (Farmer et al., 2007) and records annual temperatures. And specimens of *G. tumida* are found at the lower thermocline or below the thermocline and record annual average conditions (Fairbanks and Wiebe, 1980; Farmer et al., 2007, Birch et al., 2013). Our calcification depth reconstructions are summarized in Table 3, also see Table S6 for comparison.

Atlantic Ocean

Farmer et al., (2007) determined the depth habitat for *O. universa* to be ranging from 0 to 60m (LL, Bemis et al., 1998). Our calculation, through $\delta^{18}O$ measurement, suggests a deeper habitat of around 70m (LL, Bemis et al., 1998), 80m (ML, Bemis et al., 2002). Whereas, the Mg/Ca method derived depth habitat calculation yields a depth habitat of 50 m. The lower habitat depth can also come from the different size fractions, as our size fraction is lower than Farmer's. *O.universa* is thought to migrate to shallower depth along its ontogeny (Emiliani et al., 1954) younger individuals are thus living deeper but smaller individuals might also have a

deeper habitat as already suggested by Hönisch and Heming, (2004). Since most of the published studies have used the $\delta^{18}O$-based depth calcification, we will preferentially adopt this method.

Indian Ocean

Calcification depths for the Indian Ocean cores have already been determined for majority of the species by Sime et al., (2005). Additionally, Birch et al., (2013) have reconstructed the depth habitat of multiple species from a core collected in the offshore region of Tanzania (Glow 3). In Indian Ocean specimens of *G. ruber* is found in the top 50m (Birch et al., 2013) and until 60 m (Sime et al., 2005), *T. sacculifer* is found in the surface mixed layer (SML) but also in the upper thermocline between 50-70 m for Birch et al., (2013) and between 60 to 80 m for Sime et al., (2005). Our results are consistent with these reported depth habitats. We calculate that specimens of *G. ruber*, *T. sacculifer* with and without sac are living in the top 80m; *O. universa* lives between 50 to 90 m (Sime et al., 2005, Birch et al., 2013). For *N. dutertrei* we calculate a depth habitat of 90m at site FC01a, calcification depths derived from both $\delta^{18}O$ and Mg/Ca methods agree with the 93 m estimate by Sime et al., (2005). At site FC02a the calculated calcification depth based on $\delta^{18}O$ method is 65 m, and, the Mg/Ca derived depth is 100m; however, Sime et al., (2005) proposed a calcification depth of 146 m. A deeper depth habitat than site FC01a seems to be in line with the weaker stratification of the water column at site FCO2a. The depth habitat for *P. obliquiloculata*'s was determined to be 106–120m by Sime et al., (2005); however, our calculations predict a lower and narrower depth habitat of 60 – 70m. Calcification depth for *G.menardii* has been calculated to be 60 – 70m, which is consistent with an upper thermocline depth habitat. Specimens of *G.tumida* is commonly found at the bottom of the thermocline which is around 200-250m at our Indian Ocean sites, Birch et al., (2013) found this species ranging from 100 to 200 m but our $\delta^{18}O$ based habitat reconstruction suggests a shallower depth of 70m at both sites. It seems that the calcification derived Mg/Ca for *G. tumida* is more realistic than with our $\delta^{18}O_c$ reconstructions, the Mg/Ca based calculation predicts a depth habitat of 100 – 130 m.

Arabian Sea

In the Arabian Sea foraminifera are affected by changes in local hydrology caused by the Indian summer and winter monsoons. The specimens of different species collectively record a shallower habitat during SW monsoon (e.g., upwelling) and a deeper habitat during NE monsoon (Peeters and Brummer, 2002). Except for *N. dutertrei,* our two methods of calcification depth reconstruction closely agree with each other within their respective uncertainties. The depth habitat reconstructions for *G. ruber* and for *T. sacculifer* are consistent with species living in the shallow mixed layer (SML) at a depth of 30m for *G. ruber* and 40 m for *T. sacculifer*. Specimens of *O. universa* are calculated to live at 30m depth; *N. dutertrei* at site FC12-b (water depth 151m) is living around 40m and at 150m at site FC13-b (water depth 3200m), which is consistent with the hydrography at this site (Fig. 4). The depth habitat of *P. obliquiloculata* is calculated to be 50m at both sites. Specimens of *G. menardii* is found at depths of 60m, consistent with Peeters and Brummer, (2002) estimate of 50 – 130m.

Pacific Ocean

For Pacific Ocean samples the Mg/Ca derived calcification depths were used in absence of $\delta^{18}Oc$ values. The Sites WP07-01 and A14 are located in the Western Equatorial Pacific with Site WP07-01

characterized by a deep thermocline. At these sites *G. ruber* and *T. sacculifer* have deep depth habitat of around 100m for *G. ruber* (Elderfield and Ganssen, 2000) and around 125m for *T. sacculifer* (Rickaby et al., 2005). The depth habitat for specimens of *O. universa* was determined to be 75m depth at site WP07-01 and at 55m depth at site A14. We calculate that *P. obliquiloculata* is living at 125m deep. Rickaby et al., (2005) estimated the living depth of *N. dutertrei* at 165m in agreement with our calculated depths (~125m). Specimens of *G. menardii* were determined to live at 180m like *G. tumida* (Rickaby et al., 2005).

The data are not consistent with a dissolution effect to explain the low $\delta^{11}B$ *T. sacculifer* in the WEP

Documented dissolution effects have been attributed to the preferential dissolution of ontogenic calcite relative to the light $\delta^{11}B$ of gametogenic calcite (Ni et al., 2007; Seki et al., 2010; Henehan et al., 2016). *T. sacculifer* (w/o sacc) should be less impacted compared to the *T. sacculifer* (sacc). Hönisch and Hemming, (2004) and Ni et al., (2007) reported a dissolution effect at site 806 (close to our WP07-01 site) for *T. sacculifer* (sacc), however, in our data the $\delta^{11}B_{carbonate}$ for *T. sacculifer* (sacc) is not decreasing with water depth when *T. sacculifer* (w/o sacc) is which suggests that at these sites and at the same size-fraction no dissolution is observed (eg. different water depth). $\Delta^{11}B$ for *T. sacculifer* (w/o sacc) and for *G. ruber* shift to lighter with higher calcification depth, a trend that does not support a dissolution effect. The lethal temperature for *T. sacculifer* is 14°C, which at site WP07-01 corresponds to a $\delta^{11}B_{borate}$ of 17.5 ‰ which makes our low $\delta^{11}B_{carbonate}$ realistic. If no dissolution is observed, a deep depth habitat inducing a respiration-driven microenvironment might explain the low $\delta^{11}B$ of the measured carbonate.

Microenvironment calculations

We observe a trend between $\Delta^{11}B$ (eg. $\Delta^{11}B=\delta^{11}B_{carbonate}-\delta^{11}B_{borate}$) with derived calcification depth (Fig. S2). In order to verify why the WEP $\delta^{11}B_{carbonate}$ of *T. sacculifer* (w/o sacc) is low and to test the hypothesis of the depth habitat we try to recalculate independently the theoretical water depth habitat based on culture results from Jorgensen et al., (1985) and our microenvironment pH results. A change of microenvironment pH for *T. sacculifer* will change the theoretical light intensity needed to reach this microenvironment pH. The compensation light intensity (E_c) for *T. sacculifer* has been calculated by Jorgensen et al., (1985) to be ~30 $\mu Eistn.m^{-2}.s^{-1}$, E_c corresponds to the energy where photosynthesis compensates respiration or where $\delta^{11}B_{carbonate}$ reaches the 1:1 theoretical line. We tested two microenvironment pH, ΔpH_1 = -0.04 and ΔpH_2 = -0.06 (Fig S3). We've recalculated the light energy needed to decrease the pH of ΔpH_1 and ΔpH_2 and apply these changes to the light penetration profile determined with an insolation E_0 in the WEP of 220 $J.s^{-1}.m^{-2}$ (Weare et al., 1981) and a light attenuation coefficient of 0.028 (Wang et al., 2008). A decrease of ΔpH_1 would lead to a decrease of 15 $\mu Eistn.m^{-2}.s^{-1}$ and a decrease of ΔpH_2 would lead to a decrease of 24 $\mu Eistn.m^{-2}.s^{-1}$ (Jorgensen et al., 1985). These results correspond in our case of a light penetration of 12% to reach Ec, 5% for a decrease of ΔpH_1 and 1% for a decrease of ΔpH_2. This means that in the WEP if *T. sacculifer* calcifies below 75m where E_c is reached the $\delta^{11}B_{carbonate}$ is below the theoretical 1:1 line. *T. sacculifer* (w/o sacc) in the WEP is decreasing its pH of ~ΔpH_1 which would imply a calcification depth of 110m consistent with the reconstruction of Rickaby et al., (2005).

$$\Delta\text{microenvironment pH} = -\log\left(\frac{(\delta 11\text{Bseawater} - \delta 11\text{Bcarbonate}) \times \text{Kb}*}{\varepsilon - \delta 11\text{Bseawater} + \delta 11\text{Bcarbonate}}\right) - \text{pHseawater}$$

References

Arbuszewski, J., DeMenocal, P., Kaplan, A. and Farmer, E. C.: On the fidelity of shell-derived δ18Oseawater estimates, Earth Planet. Sci. Lett., 300, 185–196, 2010.

Barker, S., Greaves, M. and Elderfield, H: A study of cleaning procedures used for foraminiferal Mg/Ca paleothermometry, Geochemistry, Geophys. Geosystems 4, 1–20, 2003.

Bemis, B. E., Spero, H. J. and Thunell, R. C.: Using species-specific paleotemperature equations with foraminifera: a case study in the Southern California Bight, Mar. Micropaleontol., 46, 405–430, 2002.

Bemis, B. E., Spero, H. J., Bijma, J. and Lea, D. W.: Reevaluation of the oxygen isotopic composition of planktonic foraminifera: Experimental results and revised paleotemperature equations, Paleoceanography, 13, 150–160, 1998.

Birch, H., Coxall, H. K., Pearson, P. N., Kroon, D. and O'Regan, M.: Planktonic foraminifera stable isotopes and water column structure: Disentangling ecological signals, Mar. Micropaleontol., 101, 127–145, 2013.

Boyer, T.P., J. I. Antonov, O. K. Baranova, C. Coleman, H. E. Garcia, A. Grodsky, D. R. Johnson, R. A. Locarnini, A. V. Mishonov, T.D. O'Brien, C.R. Paver, J.R. Reagan, D. Seidov, I. V. Smolyar, and M. M. Zweng: World Ocean Database 2013, NOAA Atlas NESDIS 72, S. Levitus, Ed., A. Mishonov, Technical Ed.; Silver Spring, 2013

Dekens, P. S., Lea, D. W., Pak, D. K. and Spero, H. J.: Core top calibration of Mg/Ca in tropical foraminifera: Refining paleotemperature estimation, Geochemistry, Geophys. Geosystems, 3, 1–29, 2002.

Deuser, W.G., Ross, E.H., Hemleben, Ch., Spindler, M.: Seasonal changes in species composition, numbers, mass, size, and isotopic composition of planktonic foraminifera settling into the deep Sargasso Sea, Palaeogeogr., Palaeoclimat., Palaeoecol., 33:103-127, 1981.

Deuser, W. G. and Ross, E. H., Seasonally abundant planktonic foraminifera of the Sargasso Sea; succession, deep-water fluxes, isotopic compositions, and paleoceanographic implications, J. Foraminifer. Res., 19, 268–293, 1989.

Duplessy, J., Labeyrie, L., Juilletleclerc, A., Maitre, F., Duprat, J. and Sarnthein, M., Surface salinity reconstruction of the north-atlantic ocean during the last glacial maximum, Oceanol. Acta, 14, 311–324, 1991.

Elderfield, H., Yu, J., Anand, P., Kiefer, T. and Nyland, B.: Calibrations for benthic foraminiferal Mg/Ca paleothermometry and the carbonate ion hypothesis, Earth Planet. Sci. Lett., 250, 633–649, 2006.

Farmer, E. C., Kaplan, A., de Menocal, P. B. and Lynch-Stieglitz, J.: Corroborating ecological depth preferences of planktonic foraminifera in the tropical Atlantic with the stable oxygen isotope ratios of core top specimens, Paleoceanography, 22, 1–14, 2007.

Fairbanks, R. G., Sverdlove, M., Free, R., Wiebe, P. H. and Bé, A. W. H.: Vertical distribution and isotopic fractionation of living planktonic foraminifera from the Panama Basin, Nature, 298, 841–844, 1982.

Fairbanks, R. G. and Wiebe, P. H., Foraminifera and Chlorophyll Maximum: Vertical Distribution, Seasonal Succession, and Paleoceanographic Significance, Science, 209, 1524–1526, 1980.

Ferguson, J. E., Henderson, G. M., Kucera, M. and Rickaby, R. E. M.: Systematic change of foraminiferal Mg/Ca ratios across a strong salinity gradient, Earth Planet. Sci. Lett., 265, 153–166, 2008.

Henehan, M. J., Foster, G. L., Bostock, H. C., Greenop, R., Marshall, B. J. and Wilson, P. A.: A new boron isotope-pH calibration for Orbulina universa, with implications for understanding and accounting for 'vital effects.', Earth Planet. Sci. Lett., 454, 282–292, 2016.

Hönisch, B. and Hemming, N. G.: Ground-truthing the boron isotope-paleo-pH proxy in planktonic foraminifera shells: Partial dissolution and shell size effects, Paleoceanography, 19, 1–13, 2004.

Jørgensen, B. B., Erez, J., Revsbech, P. and Cohen, Y.: Symbiotic photosynthesis in a planktonic foraminiferan, Globigerinoides sacculifer (Brady), studied with microelectrodes, Limnol. Oceanogr. 30, 1253–1267, 1985.

Kim, S.-T. and O'Neil, J. R.: Equilibrium and nonequilibrium oxygen isotope effects in synthetic carbonates, Geochim. Cosmochim. Acta, 61, 3461–3475, 1997.

Martínez-Botí, M. A., Mortyn, P. G., Schmidt, D. N., Vance, D. and Field, D. B.: Mg/Ca in foraminifera from plankton tows: Evaluation of proxy controls and comparison with core tops, Earth Planet. Sci. Lett., 307, 113–125, 2011.

Misra, S., Greaves, M., Owen, R., Kerr, J., Elmore, A. C. and Elderfield, H.: Determination of B/Ca of natural carbonates by HR-ICP-MS, Geochemistry, Geophys. Geosystems, 15, 1617–1628 ,2014.

Mulitza, S., Boltovskoy, D., Donner, B., Meggers, H., Paul, A. and Wefer, G.: Temperature:δ18O relationships of planktonic foraminifera collected from surface waters, Palaeogeogr. Palaeoclimatol. Palaeoecol, 202, 143–152, 2003.

Ni, Y., Foster, G. L., Bailey, T., Elliott, T., Schmidt, D. N., Pearson, P., Haley, B. and Coath, C.: A core top assessment of proxies for the ocean carbonate system in surface-dwelling foraminifers, Paleoceanography, 22, 2007.

Peeters, F. J. C. and Brummer, G.-J. a.: The seasonal and vertical distribution of living planktic foraminifera in the NW Arabian Sea, Geol. Soc. London, Spec. Publ., 195, 463–497, 2002.

Rostek, F., Ruhland, G., Bassinot, F. C., Muller, P. J., Labeyrie, L. D., Lancelot, Y. and Bard, E.: Reconstructing Sea-Surface Temperature and Salinity Using δ18O and Alkenone Records, Nature, 364, 319–321, 1993.

Russell, A. D., Hönisch, B., Spero, H. J. and Lea, D. W.: Effects of seawater carbonate ion concentration and temperature on shell U, Mg, and Sr in cultured planktonic foraminifera, Geochim. Cosmochim. Acta, 68, 4347–4361, 2004.

Seki, O., Foster, G. L., Schmidt, D. N., Mackensen, A., Kawamura, K. and Pancost, R. D.: Alkenone and boron-based Pliocene pCO2records, Earth Planet. Sci. Lett., 292, 201–211, 2010.

Sime, N. G., De La Rocha, C. L. and Galy, A.: Negligible temperature dependence of calcium isotope fractionation in 12 species of planktonic foraminifera, Earth Planet. Sci. Lett., 232, 51–66, 2005.

Yu, J., Day, J., Greaves, M. and Elderfield, H.: Determination of multiple element/calcium ratios in foraminiferal calcite by quadrupole ICP-MS, Geochemistry, Geophys. Geosystems 6, 2005

Rickaby, R. E. M. and Halloran, P.: Cool La Nina During the Warmth of the Pliocene?, Science, 307, 1948–1952, 2005.

Wang, G., Cao, W., Yang, D. and Xu, D. Variation in downwelling diffuse attenuation coefficient in the northern South China Sea, Chinese J. Oceanol. Limnol., 26, 323–333, 2008.

Weare, B. C., Strub, P. T. and Samuel, M. D.: Annual Mean Surface Heat Fluxes in the Tropical Pacific Ocean, J. Phys. Oceanogr., 11, 705–717, 1981.

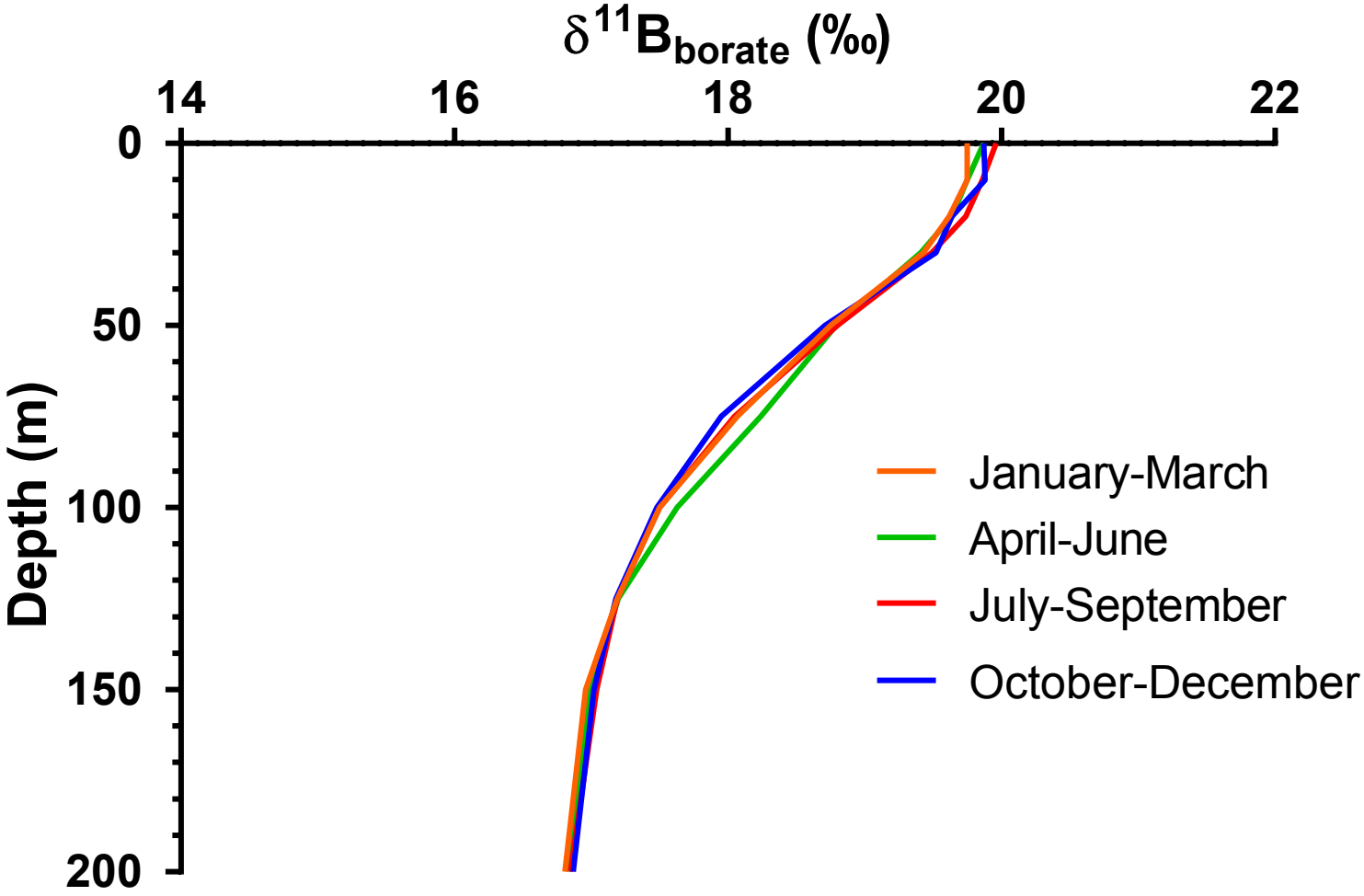
δ11Bborate (‰)
14
16
18
20
22
0
50
100
150
200
Depth (m)
January-March
April-June
July-September
October-December

Figure S1

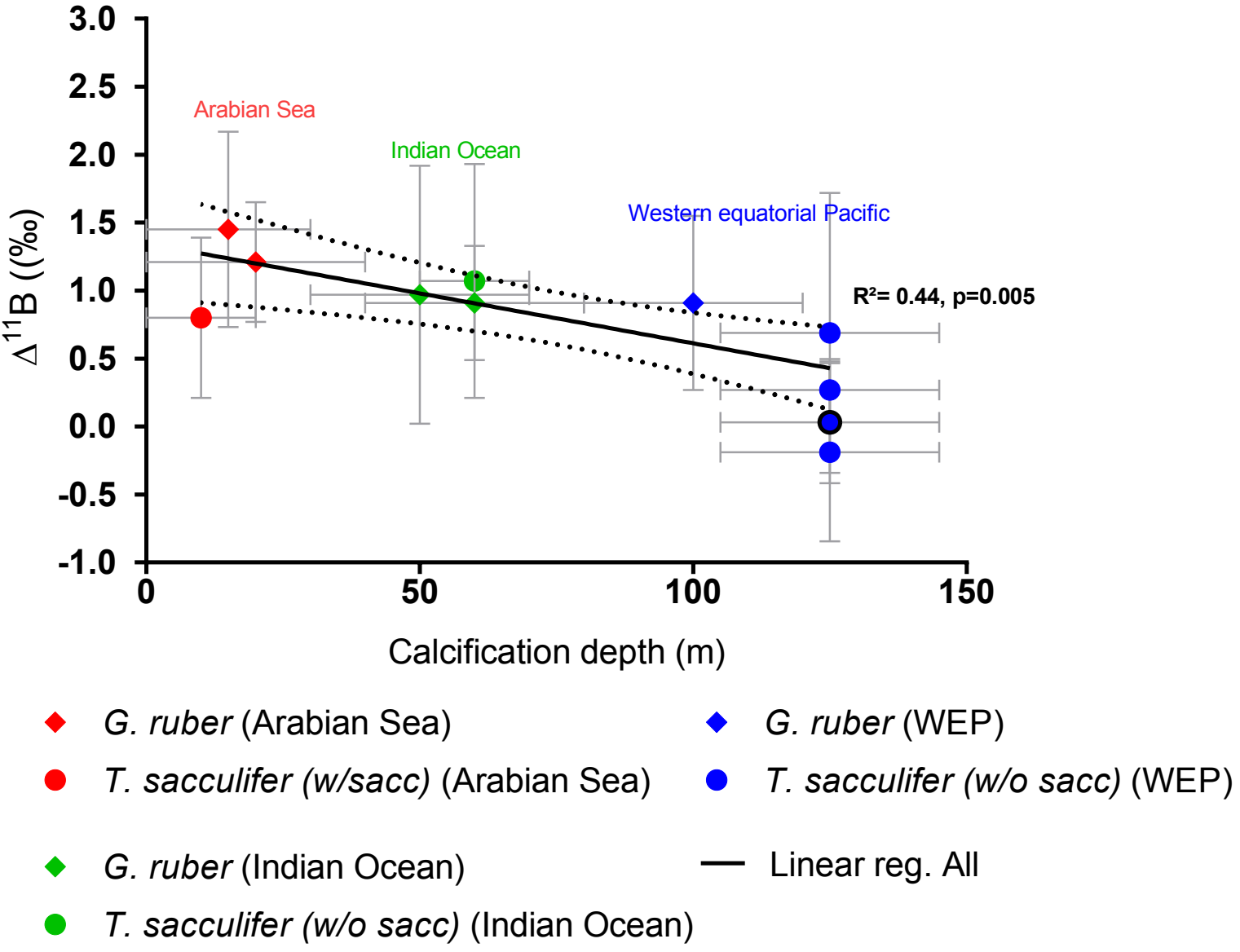
3.0
2.5
2.0
1.5
1.0
0.5
0.0
-0.5
-1.0
0
50
100
150
Δ11B ((‰)
Calcification depth (m)
Arabian Sea
Indian Ocean
Western equatorial Pacific
R²= 0.44, p=0.005
G. ruber (Arabian Sea)
T. sacculifer (w/sacc) (Arabian Sea)
G. ruber (Indian Ocean)
T. sacculifer (w/o sacc) (Indian Ocean)
G. ruber (WEP)
T. sacculifer (w/o sacc) (WEP)
Linear reg. All

Figure S2

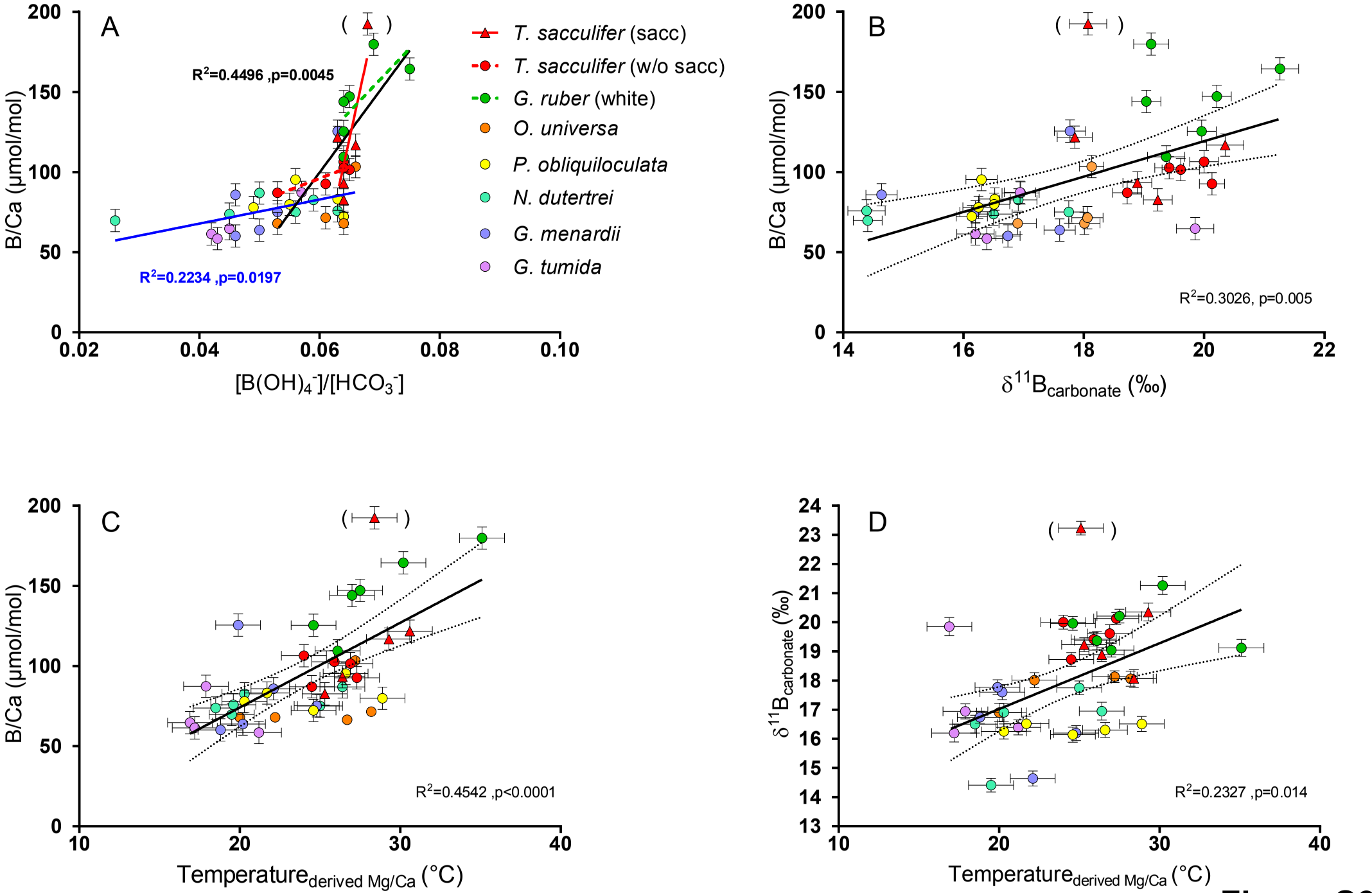
A
B
C
D
B/Ca (µmol/mol)
[B(OH)4-]/[HCO3-]
R2=0.4496 ,p=0.0045
R2=0.2234 ,p=0.0197
T. sacculifer (sacc)
T. sacculifer (w/o sacc)
G. ruber (white)
O. universa
P. obliquiloculata
N. dutertrei
G. menardii
G. tumida
δ11Bcarbonate (‰)
R2=0.3026, p=0.005
Temperaturederived Mg/Ca (°C)
R2=0.4542 ,p<0.0001
R2=0.2327 ,p=0.014

Figure S3

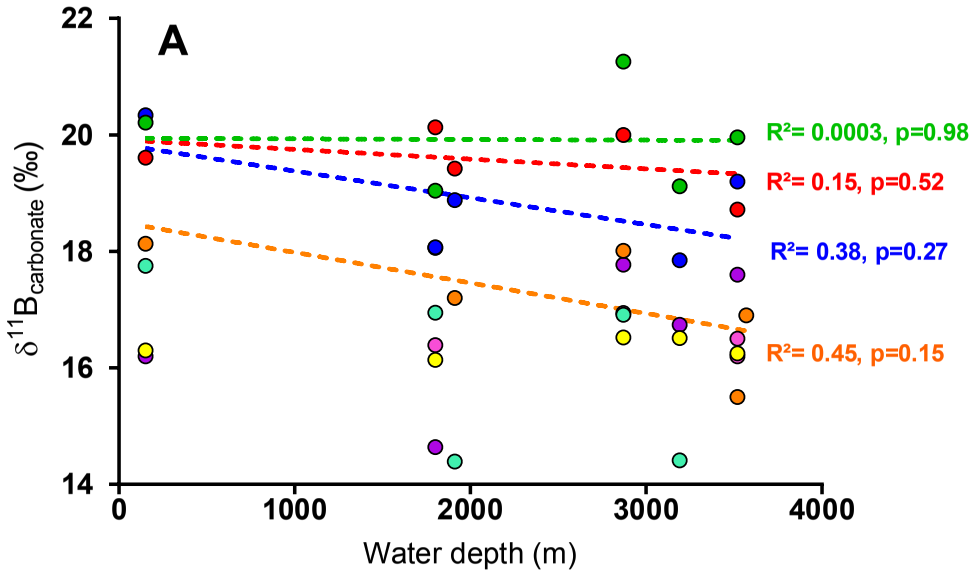
A
δ11Bcarbonate (‰)
Water depth (m)
R²= 0.0003, p=0.98
R²= 0.15, p=0.52
R²= 0.38, p=0.27
R²= 0.45, p=0.15

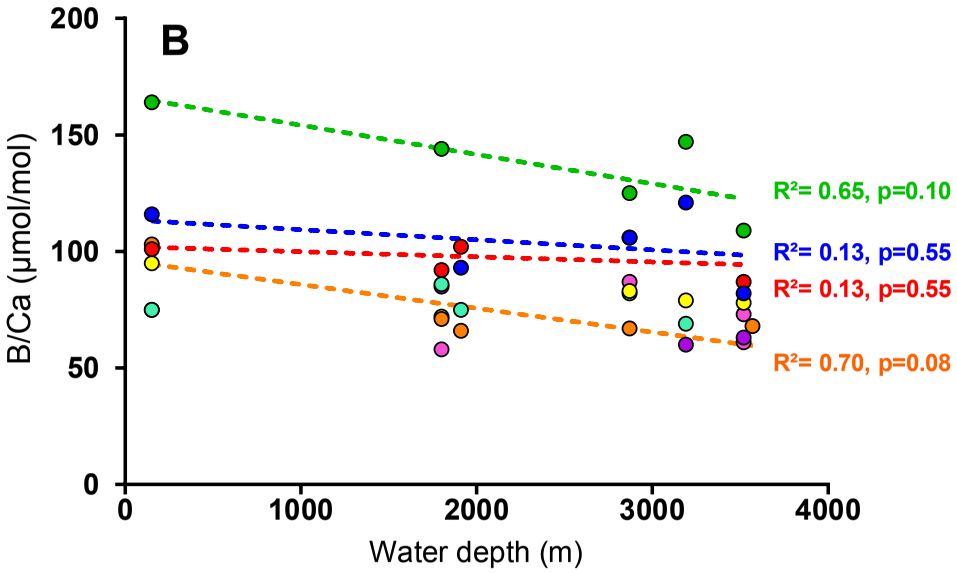
B
B/Ca (µmol/mol)
Water depth (m)
R²= 0.65, p=0.10
R²= 0.13, p=0.55
R²= 0.13, p=0.55
R²= 0.70, p=0.08

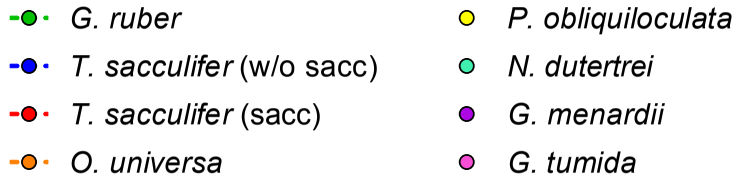
G. ruber
T. sacculifer (w/o sacc)
T. sacculifer (sacc)
O. universa
P. obliquiloculata
N. dutertrei
G. menardii
G. tumida

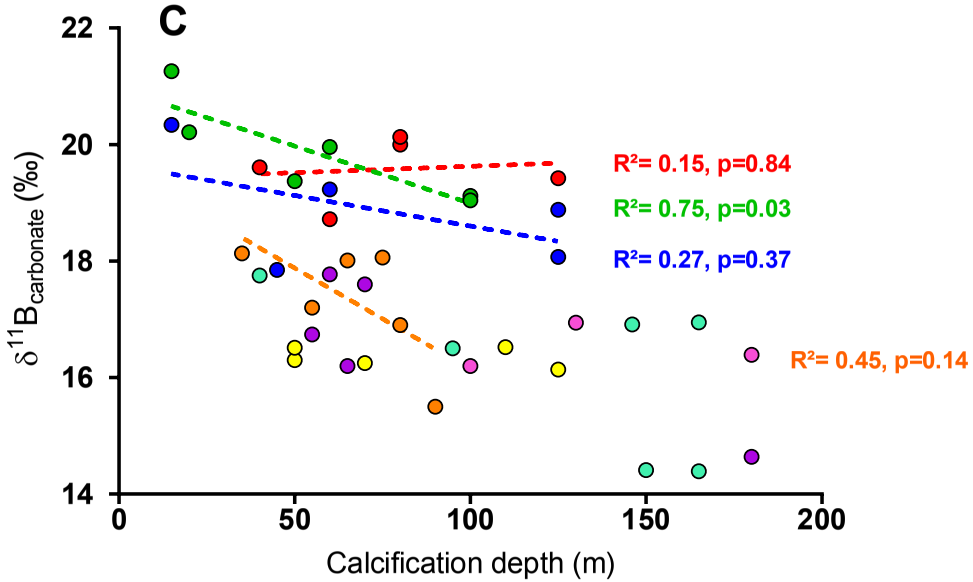
C
δ11Bcarbonate (‰)
Calcification depth (m)
R²= 0.15, p=0.84
R²= 0.75, p=0.03
R²= 0.27, p=0.37
R²= 0.45, p=0.14

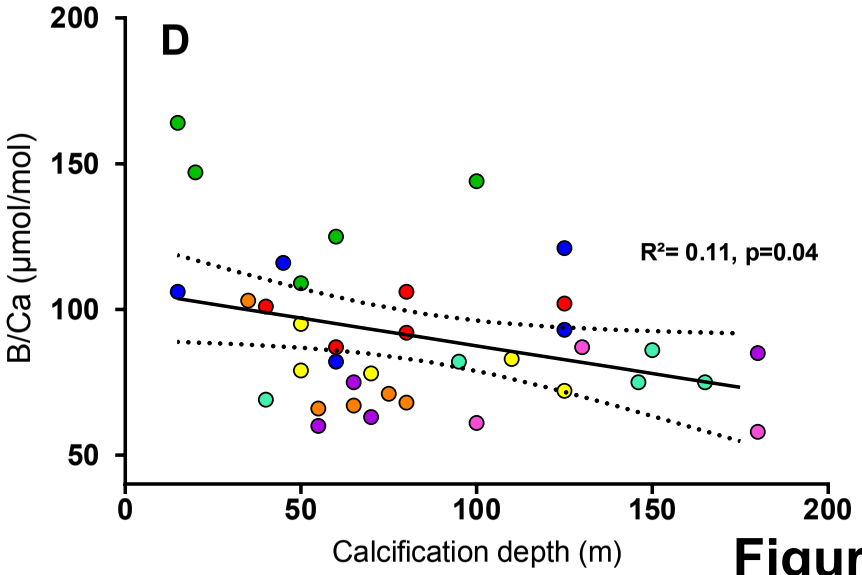
D
B/Ca (µmol/mol)
Calcification depth (m)
R²= 0.11, p=0.04

Figure S4

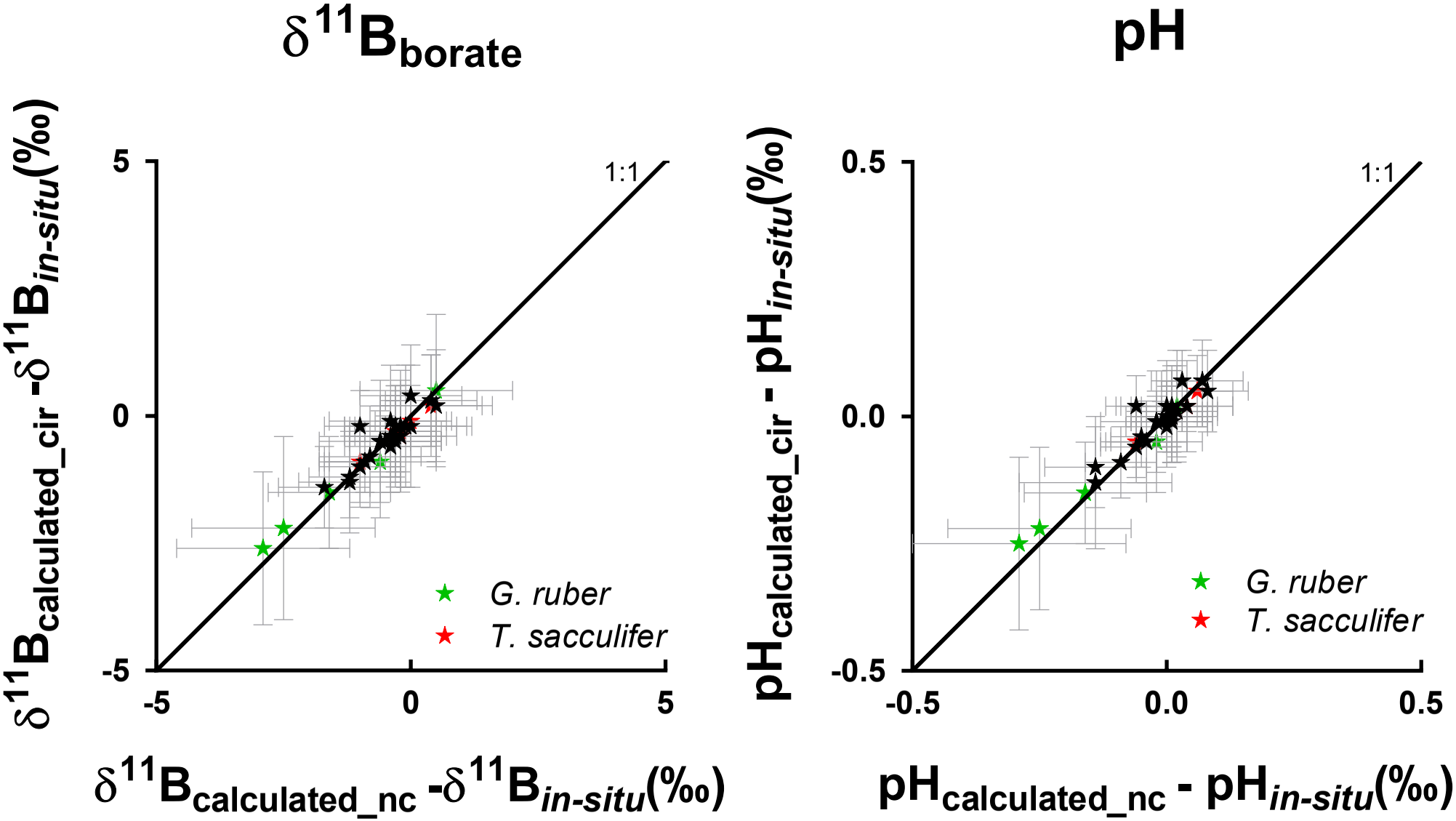
δ11Bborate
pH
1:1
1:1
G. ruber
T. sacculifer
G. ruber
T. sacculifer
δ11Bcalculated_cir -δ11Bin-situ(‰)
δ11Bcalculated_nc -δ11Bin-situ(‰)
pHcalculated_cir - pHin-situ(‰)
pHcalculated_nc - pHin-situ(‰)
5
0
-5
0.5
0.0
-0.5

Figure S5

Table S1

Elemental ratios	**Li/Ca**	**B/Ca**	**Mg/Ca**	**Al/Ca**	**Sr/Ca**	**Cd/Ca**	**Ba/Ca**	**U/Ca**	**Mn/Ca**	**Fe/Ca**
	µmol/mol	µmol/mol	mmol/mol	mmol/mol	mmol/mol	µmol/mol	µmol/mol	nmol/mol	µmol/mol	mmol/mol
Standard solution 0	0.8	9	0.10	0.131	0.00	0.03	0.6	31	1	0.01
Standard solution 1	2.3	38	0.31	0.112	0.49	0.05	1.9	38	12	0.02
Standard solution 3	6.8	108	1.31	0.177	1.06	0.13	3.0	53	39	0.04
Standard solution 5	14.6	216	3.17	0.223	1.57	0.23	5.1	62	129	0.08
Standard solution 6	19.0	278	5.23	0.352	1.97	0.28	5.5	74	196	0.11
Standard solution 8	25.0	281	6.07	0.602	2.99	0.50	20.1	390	501	0.50
Standard solution 9		408			4.89					
Standard solution 10		519			8.01					
Standard solution 11		607			9.93					

Table S2

Standard	$\delta^{11}B_1$ (‰)	$2SD_{AE121}$	n_{AE121}	$\delta^{11}B_2$ (‰)	$2SD_{AE121}$	n_{AE121}	Reference
NEP1	25.21	0.25	11	25.22	0.25	11	This study
NEP2	25.00	0.30	12				This study
NEP3	24.70	0.30	12				This study
NEP4	25.40	0.21	11				This study
NEP5	25.32	0.21	11	25.33	0.21	11	This study
NEP6	25.22	0.21	11				This study
NEP7	25.26	0.26	15				This study
NEP8	25.39	0.26	15				This study
NEP9	26.15	0.26	15				This study
NEP10	25.97	0.26	15				This study
NEP11	26.09	0.26	15	26.09	0.26	15	This study
NEP12	26.22	0.26	15	26.29	0.26	15	This study
NEP13	26.19	0.26	15	26.21	0.26	15	This study
NEP14	26.12	0.26	15	26.13	0.26	15	This study
NEP15	26.00	0.26	15				This study
NEP16	26.04	0.26	15				This study
NEP17	26.02	0.29	12				This study
NEP18	25.86	0.29	12	25.86	0.26	14	This study
NEP19	25.78	0.26	14				This study
NEP20	25.42	0.15	3	25.32	0.15	3	This study
NEP21	25.54	0.22	6	26.16	0.22	6	This study
NEP22	26.42	0.22	6				This study
JCP-1-1	24.07	0.10					This study
JCP-1-2	24.17	0.11		24.17	0.10		This study
JCP-1-3	24.01	0.11					This study
JCP-1-4	23.92	0.26					This study
JCP-1-5	24.03	0.26		24.05	0.39		This study
JCP-1-6	24.18	0.36		24.16	0.36		This study

Standard	Average $\delta^{11}B$	*2SD*	n	Reference
NEP	25.70	*0.93*	22	This study
NEP	26.20	0.88	27	Holcomb et al., 2015
NEP	25.80	0.89	6	Sutton et al., 2018
JCP-1	24.06	0.20	6	This study
JCP-1	24.37	*0.32*	57	Holcomb et al., 2015
JCP-1	24.42	*0.28*	7	Sutton et al., 2018

Table S3

Date of analysis	Standard	Li/Ca µmol/mol	B/Ca µmol/mol	Mg/Ca mmol/mol	Sr/Ca mmol/mol	Cd/Ca µmol/mol	Ba/Ca µmol/mol	U/Ca nmol/mol	Mn/Ca µmol/mol	Fe/Ca mmol/mol	Reference
10/7/17	CamWuel 1	16.0	204	1.22	1.31	0.26	4.6	43	67	0.04	This study
10/7/17	CamWuel 2	16.3	209	1.24	1.32	0.28	4.6	45	69	0.04	This study
10/7/17	CamWuel 3	16.3	209	1.23	1.31	0.26	4.6	44	77	0.04	This study
10/7/17	CamWuel 4	16.0	207	1.23	1.32	0.28	4.6	44	74	0.04	This study
10/7/17	CamWuel 5	16.4	210	1.23	1.32	0.27	4.6	42	74	0.04	This study
10/7/17	CamWuel 6	16.0	208	1.24	1.31	0.26	4.6	42	74	0.04	This study
10/7/17	CamWuel 7	16.6	213	1.23	1.32	0.28	4.6	44	74	0.04	This study
11/7/17	CamWuel 1	16.0	203	1.22	1.32	0.26	4.6	41	72	0.04	This study
11/7/17	CamWuel 2	16.1	205	1.22	1.32	0.27	4.6	42	76	0.04	This study
11/7/17	CamWuel 3	16.2	204	1.22	1.32	0.27	4.6	41	72	0.04	This study
11/7/17	CamWuel 4	16.1	205	1.22	1.32	0.27	4.5	41	71	0.04	This study
11/7/17	CamWuel 5	15.8	204	1.21	1.32	0.27	4.6	42	73	0.04	This study
11/7/17	CamWuel 6	16.1	206	1.22	1.32	0.27	4.6	42	68	0.04	This study
11/7/17	CamWuel 7	16.0	207	1.22	1.32	0.26	4.6	43	66	0.04	This study
11/7/17	CamWuel 8	15.9	203	1.21	1.32	0.27	4.6	42	68	0.04	This study
12/7/17	CamWuel 1	16.3	201	1.22	1.31	0.22	4.6	41	66	0.03	This study
12/7/17	CamWuel 2	16.1	203	1.22	1.32	0.23	4.6	42	67	0.03	This study
12/7/17	CamWuel 3	16.4	202	1.22	1.32	0.23	4.6	42	69	0.04	This study
12/7/17	CamWuel 4	16.3	202	1.22	1.31	0.22	4.6	41	68	0.04	This study
12/7/17	CamWuel 5	16.6	202	1.22	1.31	0.23	4.6	44	67	0.03	This study
12/7/17	CamWuel 6	16.6	205	1.22	1.31	0.24	4.5	42	66	0.03	This study
12/7/17	CamWuel 7	16.1	204	1.22	1.31	0.22	4.6	40	67	0.03	This study
12/7/17	CamWuel 8	16.4	204	1.22	1.31	0.23	4.6	43	67	0.03	This study
12/7/17	CamWuel 9	16.4	202	1.22	1.32	0.23	4.6	43	64	0.03	This study
13/7/2017	CamWuel 1	16.2	198	1.22	1.31	0.31	4.6	42	74	0.04	This study
13/7/2017	CamWuel 2	16.4	200	1.22	1.30	0.30	4.6	43	73	0.04	This study
13/7/2017	CamWuel 3	16.2	201	1.23	1.31	0.31	4.7	43	74	0.04	This study
13/7/2017	CamWuel 4	16.3	198	1.22	1.31	0.30	4.6	42	73	0.04	This study
13/7/2017	CamWuel 5	16.6	200	1.23	1.30	0.30	4.6	42	73	0.04	This study
13/7/2017	CamWuel 6	16.5	198	1.22	1.31	0.31	4.6	44	74	0.04	This study
13/7/2017	CamWuel 7	16.1	201	1.22	1.30	0.32	4.7	43	74	0.04	This study
	Average CamWuel	**16.2**	**204**	**1.22**	**1.31**	**0.27**	**4.6**	**42**	**71**	**0.04**	**This study**
	2SD	*0.4*	*7*	*0.01*	*0.01*	*0.06*	*0.1*	*2*	*7*	*0.01*	
	n	31	31	31	31	31	31	31	31	31	
	Published CamWuel	**16.4**	**202**	**1.23**	**1.30**	**0.29**	**4.8**	**44**	**71**		**Misra et al., 2014**
	2SD	*0.8*	*7*	*0.06*	*0.02*	*0.02*	*0.2*	*2*	*2*		
	n	180	180	180	180	180	180	180	180		

Table S4

Specie	Seasonality
T. sacculifer (sacc)	Spring
T. sacculifer (w/o sacc)	Spring
G. ruber (white)	Summer
N. dutertrei	Winter
G. tumida	Annual average
G. menardii	Annual average
O. universa	Annual average
P. obliquiloculata	Winter

Table S5

Species	B	A	Reference
T. sacculifer (sacc)	0.377	0.090	Anand et al., 2003
T. sacculifer (w/o sacc)	0.347	0.090	Anand et al., 2003
G. ruber (white)	0.300	0.089	Dekens et al., 2002
N. dutertrei	0.600	0.008	Dekens et al., 2002
G. tumida	0.380	0.090	Anand et al., 2003
G. menardii	0.360	0.091	Regenberg et al., 2009
O. universa	0.595	0.090	Anand et al., 2003
P. obliquiloculata	0.328	0.090	Anand et al., 2003

Species	A	B	C	dw correction	Condition	Reference	Equation
O. universa	16.500	4.800		-0.27	LL	Bemis et al., 1998	T=A-B* (δ18Oc-δ18Ow)
O. universa	15.700	4.460	0.35	-0.27	ML	Bemis et al., 2002	T=A-B* (δ18Oc-δ18Ow)+C*(δ18Oc-δ18Ow)^2
O. universa	14.900	4.800		-0.27	HL	Bemis et al., 1998	T=A-B* (δ18Oc-δ18Ow)
T. sacculifer	14.910	4.350		-0.27		Mulitza et al., 2003	T=A-B* (δ18Oc-δ18Ow)
G. ruber	14.200	4.440		-0.27		Mulitza et al., 2003	T=A-B* (δ18Oc-δ18Ow)
All	16.900	4.380	0.1	-0.2		Shackleton et al., 1974	T=A-B* (δ18Oc-δ18Ow)+C*(δ18Oc-δ18Ow)^2
All	17.000	4.520	0.03	-0.22		Erez and Luz, 1983	T=A-B* (δ18Oc-δ18Ow)+C*(δ18Oc-δ18Ow)^2
All	16.100	4.640	0.09	-0.27		Kim and O'Neil 1997	T=A-B* (δ18Oc-δ18Ow)+C*(δ18Oc-δ18Ow)^3

Table S6

Core	Species	CD_1	CD_2	CD_3	Reference
FC-01a	*G. ruber (white ss)*	83 ± 20	30 ± 10	50 ± 20	Sime thesis 2006
FC-02a	*G. ruber (white ss)*	56 ± 10	15 ± 10	60 ± 20	Sime thesis 2006
FC-12b	*G. ruber (white ss)*	Surface ± 10	0-30	60 ± 10	Peeters and Brumer, 2012 (non upwelling station Arabian sea)
FC-13a	*G. ruber (white ss)*	Surface ± 10	20 ± 20	60 ± 10	Peeters and Brumer, 2012 (non upwelling station Arabian sea)
WP7-01	*G. ruber (white ss)*			100±20	Elderfield and Ganssen, 2000
A14	*G. ruber (white ss)*		60 ± 10	100±20	Elderfield and Ganssen, 2000
FC-01a	*T. sacculifer (sacc)*	48 ± 10	50 ± 10	60 ± 10	Sime et al., 2005
FC-02a	*T. sacculifer (sacc)*	7 ± 10	30 ± 10	80 ± 20	Sime et al., 2006
FC-12b	*T. sacculifer (sacc)*	15 ± 10	40 ± 10		
WP7-01	*T. sacculifer (sacc)*		80 ± 20	125 ± 15	Rickaby et al., 2005
A14	*T. sacculifer (sacc)*		60 ± 10	125 ± 15	
FC-01a	*T. sacculifer (w/o sacc)*	88 ± 20	50 ± 10	60 ± 10	Sime thesis 2006 (Wind22-b)
FC-02a	*T. sacculifer (w/o sacc)*	32 ± 10	10 ± 10	80 ± 20	Sime thesis 2006
FC-12b	*T. sacculifer (w/o sacc)*	0-15 ± 10	30 ± 10	45 ± 20	Peeters and Brumer, 2012 (non upwelling station Arabian sea)
WP7-01	*T. sacculifer (w/o sacc)*		80 ± 20	125 ± 15	Rickaby et al., 2005
A14	*T. sacculifer (w/o sacc)*		60 ± 10	125 ± 15	Rickaby et al., 2005
CD107a	*O. universa*	80 ± 20	50 ± 20	0-50	Farmer et al., 2007
FC-01a	*O. universa*	45 ± 10	60 ± 10	90 ± 20	Sime et al., 2005
FC-02a	*O. universa*	127 ± 20	45 ± 15	65 ± 10	Birshe et al., 2013
FC-12b	*O. universa*	35 ± 10	30 ± 20		
WP7-01	*O. universa*		75 ± 25		
A14	*O. universa*		55 ± 15		
FC-01a	*P. obliquiloculata*	70 ± 20	75 ± 15	106 ± 20	Sime et al., 2005
FC-02a	*P. obliquiloculata*	226 ± 20	60 ± 10		
FC-12b	*P. obliquiloculata*	40 ± 10	50 ± 10		
FC-13a	*P. obliquiloculata*	65 ± 10	50 ± 10		
WP7-01	*P. obliquiloculata*		125 ± 25		
FC-01a	*N. dutertrei*	95 ± 20	90 ± 20	93 ± 20	Sime et al., 2005
FC-02a	*N. dutertrei*	65 ± 10	100 ± 20	146 ± 20	Sime et al., 2005
FC-12b	*N. dutertrei*	40 ± 10	50 ± 10		
FC-13a	*N. dutertrei*	45 ± 10	150 ± 20		
WP7-01	*N. dutertrei*		125 ± 25	165	Rickaby et al., 2005
A14	*N. dutertrei*		110 ± 20	165	Rickaby et al., 2005
FC-01a	*G. menardii*	135 ± 20	70 ± 20		
FC-02a	*G. menardii*	60 ± 10	60 ± 10		
FC-12b	*G. menardii*	65 ± 10	55 ± 15	60 ± 10	Peeters and Brumer, 2012 (non upwelling station Arabian sea)
FC-13a	*G. menardii*	55 ± 10	70 ± 10	60 ± 10	Peeters and Brumer, 2012 (non upwelling station Arabian sea)
WP7-01	*G. menardii*		180 ± 20		
FC-01a	*G. tumida*	70 ± 20	100 ± 10	160 ± 20	Birshe et al., 2013
FC-02a	*G. tumida*	70 ± 20	130 ± 20	160 ± 20	Birshe et al., 2013
WP7-01	*G. tumida*		180 ± 20	210 - 240	Rickaby et al., 2005

CD_1: Depth habitat estimated from $\delta^{18}O_c$

CD_2: Depth habitat estimated from Mg/Ca derived temperature

CD_3: Depth habitat from literature

Table S7

		PRE INDUSTRIAL IN-SITU PARAMETERS																		CALCULATED PARAMETERS										
Core	**Species**	**Depth habitat (m)**	**Temperature (°C)**	***2sd****	**Salinity**	***2sd****	**pH (pre-ind)**	***2sd****	**pCO_2**	***2sd****	**HCO_3^-**	***2sd****	**CO_3^{2-}**	***2sd****	**DIC**	***2sd****	**ALK**	***2sd****	**$\delta^{11}B_{borate}$**	***2sd****	**$T_{Mg/Ca}$**	***2sd***	**$pH_{\delta 11B}$**	***2sd***	**pCO_2**	***2sd****	***Calibration***	**$pH_{\delta 11B}$**	***2sd****	**pCO_2**	***2sd****	***Calibration***
Atlantic Ocean																															
CD107a	*O. universa*	80 ± 20	12.0	0.3	35.6	0.01	8.19	0.03	274	21	1856	29	192	12	2059	18	2333	1	17.86	0.31	20.0	1.4	8.19	0.06	285	*39*	[8]					
Indian Ocean																															
FC-01a	*G. ruber (white ss)*	50 ± 20	23.4	5.9	35.0	0.4	8.10	0.04	338	41	1743	138	226	48	1979	93	2299	22	18.40	0.90	26.1	1.4	8.07	0.05	387	29	[1]	7.88	0.16	630	42	[2]
FC-01a	*T. sacculifer (sacc)*	60 ± 10	21.9	5.7	35.1	0.3	8.09	0.03	346	38	1773	126	215	45	1998	84	2303	18	18.15	0.81	24.5	1.4	8.06	0.04	400	79	[3]	8.04	0.06	417	82	[4]
FC-01a	*T. sacculifer (w/o sacc)*	60 ± 10	21.9	5.7	35.1	0.3	8.09	0.03	346	38	1773	126	215	45	1998	84	2303	18	18.16	0.82	25.3	1.4	8.10	0.04	357	49	[3]	8.10	0.05	356	49	[4]
FC-01a	*O. universa*	90 ± 20	18.2	4.0	35.2	0.0	8.07	0.04	374	43	1856	94	184	35	2053	62	2311	9	17.42	0.61			7.98	0.06	499	63	[8]					
FC-01a	*P. obliquiloculata*	106 ± 20	20.5	4.6	35.2	0.1	8.09	0.03	353	32	1802	99	204	36	2018	65	2306	11	17.91	0.66	20.3	1.4	8.10	0.08	356	48	[11]					
FC-01a	*G. menardii*	70 ± 20	20.5	4.6	35.2	0.1	8.09	0.03	353	32	1802	99	204	36	2018	65	2306	11	17.93	0.68	20.2	1.4	8.16	0.05	304	43	[13]					
FC-01a	*N. dutertrei*	95 ± 20	17.7	4.0	35.1	0.0	8.06	0.04	380	43	1868	94	180	35	2061	62	2313	9	17.26	0.62	18.5	1.4	8.09	0.06	373	49	[13]					
FC-01a	*G. tumida*	100 ± 20	17.1	1.6	35.1	0.0	8.06	0.02	386	22	1881	41	175	15	2070	27	2314	3	17.21	0.27	17.2	1.4	8.06	0.07	400	52	[13]					
FC-02a	*G. ruber (white ss)*	60 ± 20	20.4	2.4	35.5	0.0	8.19	0.01	268	10	1724	26	246	10	1979	17	2332	2	19.06	0.34	24.6	1.4	8.13	0.04	332	26	[1]	8.03	0.10	428	31	[2]
FC-02a	*T. sacculifer (sacc)*	80 ± 20	19.3	1.9	35.6	0.1	8.19	0.01	268	7	1741	38	240	15	1989	24	2333	3	18.89	0.30	24.0	1.4	8.18	0.03	286	57	[3]	8.21	0.05	267	54	[4]
FC-02a	*T. sacculifer (w/o sacc)*	80 ± 20	19.3	1.9	35.6	0.1	8.19	0.01	268	7	1741	38	240	15	1989	24	2333	3	18.90	0.30	25.1	1.4										
FC-02a	*O. universa*	65 ± 10	20.1	1.1	35.5	0.0	8.19	0.00	268	2	1728	15	245	6	1981	9	2332	1	19.00	0.17	22.2	1.4	8.18	0.04	287	42	[8]					
FC-02a	*P. obliquiloculata*	60 ± 10	18.3	0.5	35.6	0.0	8.18	0.01	277	8	1769	17	228	7	2007	10	2334	1	18.64	0.14	21.7	1.4	8.16	0.08	302	43	[11]					
FC-02a	*G. menardii*	60 ± 10	20.4	1.9	35.5	0.0	8.19	0.01	268	10	1724	19	246	7	1979	12	2332	2	19.05	0.30	19.9	1.4	8.17	0.05	293	42	[13]					
FC-02a	*N. dutertrei*	146 ± 20	17.5	1.0	35.6	0.1	8.16	0.02	292	14	1798	31	216	13	2024	18	2333	2	18.33	0.27	20.3	1.4	8.12	0.06	339	46	[13]					
FC-02a	*G. tumida*	130 ± 20	17.8	0.8	35.6	0.0	8.17	0.02	284	17	1784	32	222	14	2015	19	2334	1	18.47	0.25	17.9	1.4	8.12	0.05	339	46	[13]					
Arabian Sea																															
FC-12b	*G. ruber (white ss)*	0-30	25.9	0.3	36.6	0.1	8.18	0.05	271	39	1655	53	292	23	1954	31	2374	8	19.81	0.65	30.2	1.4	8.15	0.04	305	28	[1]	8.20	0.10	265	26	[2]
FC-12b	*T. sacculifer (sacc)*	40 ± 10	25.3	0.6	36.5	0.0	8.10	0.06	350	64	1756	75	249	31	2015	46	2369	2	18.71	0.77	26.9	1.4	8.09	0.04	374	54	[3]	8.10	0.06	366	53	[4]
FC-12b	*T. sacculifer (w/o sacc)*	15 ± 10	25.9	0.0	36.5	0.1	8.16	0.04	290	34	1681	45	281	19	1970	28	2374	8	19.54	0.50	29.3	1.4	8.13	0.04	332	50	[3]	8.16	0.06	302	47	[4]
FC-12b	*O. universa*	35 ± 10	25.5	0.6	36.5	0.0	8.11	0.06	334	56	1738	68	257	28	2004	41	2369	1	18.90	0.69	27.2	1.4	8.13	0.03	336	50	[8]					
FC-12b	*P. obliquiloculata*	50 ± 10	25.0	0.9	36.5	0.1	8.06	0.06	382	69	1794	75	233	32	2038	45	2368	3	18.24	0.67	26.6	1.4	8.05	0.08	415	58	[11]					
FC-12b	*G. menardii*	65 ± 10	24.1	1.1	36.4	0.1	8.02	0.06	438	72	1850	75	209	32	2072	45	2365	4	17.69	0.62	24.8	1.4	7.97	0.06	514	68	[13]					
FC-12b	*N. dutertrei*	40 ± 10	25.3	0.6	36.5	0.0	8.10	0.06	350	64	1756	75	249	31	2015	46	2369	2	18.75	0.71	25.0	1.4	8.11	0.04	350	52	[13]					
FC-13a	*G. ruber (white ss)*	20 ± 20	27.1	1.1	36.7	0.1	8.10	0.03	343	27	1724	43	263	17	1996	26	2371	2	19.00	0.37	27.5	1.4	8.11	0.04	351	29	[1]	8.05	0.09	417	32	[2]
FC-13a	*T. sacculifer (w/o sacc)*	45 ± 20	25.7	0.7	36.6	0.0	8.07	0.03	380	34	1782	38	239	16	2032	23	2371	2	18.86	0.45	30.6	1.4										
FC-13a	*P. obliquiloculata*	50 ± 10	25.4	1.2	36.6	0.1	8.06	0.05	391	59	1797	66	233	29	2041	40	2370	4	18.31	0.57	28.9	1.4	8.08	0.08	385	55	[11]					
FC-13a	*G. menardii*	55 ± 10	25.1	1.3	36.6	0.1	8.04	0.05	409	65	1815	69	225	30	2052	41	2369	5	18.04	0.56	18.8	1.4	7.98	0.04	503	68	[13]					
FC-13a	*N. dutertrei*	150 ± 20	19.4	2.3	36.0	0.1	7.80	0.03	766	45	2056	37	118	15	2199	25	2348	1	15.37	0.27	19.5	1.4	7.79	0.08	811	101	[13]					
Pacific Ocean																															
WP07-a	*G. ruber (white ss)*	100±20	26.1	2.4	35.2	0.4	8.05	0.05	387	51	1753	81	224	31	1988	52	2305	7	18.21	0.64	27.0	1.4	8.03	0.05	426	32	[1]	7.80	0.16	778	52	[2]
WP07-a	*T. sacculifer (sacc)*	80 ± 20	27.4	2.2	35.0	0.5	8.08	0.05	357	56	1708	89	242	33	1960	58	2303	10	18.68	0.65	27.3	1.4	7.99	0.04	478	63	[3]	8.13	0.04	324	49	[4]
WP07-a	*T.sacculifer (w/o sacc)*	125 ± 20	24.7	1.8	35.4	0.2	8.03	0.00	413	30	1797	31	209	9	2017	23	2311	10	17.80	0.23	28.4	1.4	8.03	0.05	427	58	[3]	7.92	0.08	573	73	[4]
WP07-a	*O. universa*	75 ± 25	27.7	2.6	34.9	0.6	8.09	0.07	349	68	1696	110	247	39	1953	73	2303	15	18.78	0.83	28.2	1.4	8.10	0.04	352	52	[8]					
WP07-a	*P. obliquiloculata*	125 ± 25	24.7	3.6	35.4	0.4	8.03	0.02	413	30	1797	80	209	26	2017	56	2311	18	17.82	0.48	24.6	1.4	8.03	0.08	430	58	[11]					
WP07-a	*N. dutertrei*	165 ± 20	20.6	3.8	35.5	0.2	8.03	0.01	408	10	1855	44	189	18	2057	26	2322	0	17.34	0.45	26.4	1.4	8.09	0.06	369	50	[13]					
WP07-a	*G. tumida*	180 ± 20	18.7	5.0	35.4	0.2	8.04	0.01	403	13	1877	58	180	24	2070	35	2322	0	17.23	0.56	21.2	1.4	8.05	0.06	406	53	[13]					

* uncertainties calculated using Henehan's 2016 R code

** propagated uncertainty on pH including d11B, temperature, salinity uncertainties

*** propagated uncertainty on pCO2 including d11B, temperature, salinity, Alk uncertainties